

THE STRUCTURE OF EXTENSIVE AIR SHOWERS

A Thesis submitted by

STEPHEN CLAUDE LILLCRAP

for the degree of

DOCTOR OF PHILOSOPHY

in the

UNIVERSITY OF LONDON

September, 1963

(i)

ABSTRACT

An experiment to study cosmic ray extensive air showers of size exceeding $3 \cdot 10^7$ particles has been constructed on the Yorkshire Moors at Haverah Park, near Harrogate. The preliminary operation and results from this experiment are described. The extensive air showers are recorded by a triangular array of water Cerenkov detectors spaced at distances of 500m from a central detector.

During the setting up of the main array, the prototype Cerenkov detector units were employed in two subsidiary experiments. The first of these, described in Chapters 2 and 3, consisted of a small array of single basic detector units (single water-tanks). This array was the same shape as the large array but had an array spacing of 6m, and was used to study the distribution of energy in the electron-photon component of extensive air showers at distances within 12m of the shower axis.

The second experiment, which is described in Chapter 4, employed different combinations of the basic detector unit to investigate the density spectrum at very low densities. The results yielded information on the character of very small air showers, and indicated the manner in which the transition in density spectrum contributions from single particles to extensive air showers takes place.

Finally, the preliminary results of the main 500m array are

(ii)

presented and discussed, particularly with relation to determining the lateral distribution of the Cerenkov detector response and the problem of ascertaining the absolute shower size. A possible normalisation procedure applicable to all zenith angles is suggested. The initial results on the shower absorption, size spectrum and shower front curvature are given and compared with those of other workers. A number of suggestions for future work have been listed and the feasibility of an array to study even larger showers has been investigated.

(iii)

CONTENTS

<u>CHAPTER I</u>	<u>THE STRUCTURE OF EXTENSIVE AIR SHOWERS</u>	<u>Page</u>
I.1	Introduction	1
I.2	The Structure Function	3
I.3	The Absorption of Large Showers	6
I.4	Attenuation Length of Shower Particles	9
I.5	The Structure of the Shower Front	11
I.6	The Muon Component	12
I.7	Scope of the Present Work	13
<u>CHAPTER 2</u>	<u>THE 6-METRE ARRAY - PART I</u>	
2.1	Design of an Experiment	15
2.2	Arrangement of Apparatus	16
2.3	Calibration of Detectors	21
2.4	Operation of Array	23
2.5	Single Particle Calibration	24
2.6	Analysis	26
	2.6.1 Shape of the Cerenkov detector structure Functions	26
	2.6.2 Normalisation of Structure Functions	30
	2.6.3 Response Function	33
2.7	Comparison with Previous Work	33

<u>CHAPTER 3</u>	<u>THE 6-METRE ARRAY - PART 2</u>	
3.1	Interpretation of $n(\mathbf{r})$	38
3.2	Electron Track Length	40
3.3	Particle Multiplicity	41
3.4	Previous Interpretation	47
3.5	Relation of Track Length to Incident Particle Energy	50
3.6	Trial Energy Spectra	52
3.7	Radial Distribution of Energy	57
3.8	Partition of Energy between Electrons and Photons	60
3.9	Conclusions	67
<u>CHAPTER 4</u>	<u>THE DENSITY SPECTRUM</u>	
4.1	Introduction	68
4.2	Apparatus	74
4.3	Calibration	74
4.4	Experimental Details	76
4.5	Results	76
4.6	Muon Component	81
4.7	Local Showers	82
	4.7.1 Electrons arising from Muons	82
	4.7.2 Decay Electrons	83
	4.7.3 Knock-on Electrons	86
	4.7.4 Nuclear-Active Particles	89
	4.7.5 Barometer Coefficient	95
	4.7.6 Distribution of Energy	96

CHAPTER 3 (continued)

	4.7.7	Altitude Variation	97
	4.7.8	Discussion	100
4.8		Small Young EAS	101
4.9		Conclusions	106

CHAPTER 5 THE 500-METRE ARRAY - PART I

5.1		Introduction	108
5.2		Apparatus	108
5.3		Amplitude Display and Timing Systems	114
5.4		Calibration	116
5.5		Analysis	118
5.6		Comparison with Previous Work	125
5.7		Normalisation of Structure Functions	127

CHAPTER 6 THE 500-METRE ARRAY - PART 2

6.1		Introduction	135
6.2		Absorption Length of Showers	135
6.3		Size Spectrum	140
6.4		Curvature of the Shower Front	145
6.5		Future Programme	152
6.6		Conclusion	159

<u>APPENDIX 1</u>	Detector Response to Muon Flux	160
<u>APPENDIX 2</u>	Muon Decay	162
<u>APPENDIX 3</u>	Shower Arrival Directions	164
<u>APPENDIX 4</u>	Curvature of the Shower Front	168
ACKNOWLEDGMENTS		170
REFERENCES		171

CHAPTER I

THE STRUCTURE OF EXTENSIVE AIR SHOWERS

I.1 Introduction

An Extensive Air Shower (EAS) is the secondary product of a chain of nuclear interactions initiated by a primary cosmic ray particle of energy greater than about 10^{14} eV. The shower particles observed near sea level may be divided into three main components: the shower core, consisting of a highly collimated nucleon cascade; the electron-photon or soft component; and the muon (penetrating) component.

Since the discovery of EAS (Schmeiser and Bothe 1938, Auger et al. 1938, Kohlhorster et al. 1938) much work has been done to investigate the general features of shower structure; and the basic processes of shower production are now well understood. The data accumulated for the shower size range 10^4 to 10^7 particles have been reviewed by Greisen (1956) and have established the importance of the nucleon cascade in determining the shower characteristics. This central cascade is dominated by a few high energy nucleons which, on collision with the air nuclei, generate high energy pions and other particles. The neutral pions subsequently decay into high energy photon pairs which then develop into electron-photon cascades to form the soft component; while the charged pions with energy below about 10 GeV have a high probability of decay into muons.

Compared with the nucleon cascade, the individual photon-induced

cascades have a relatively short attenuation length and the soft component is maintained by being replenished after each nuclear collision. As the number of nuclear interactions in the atmosphere is only about 12, then fluctuations in the height of the first interaction and the rate of shower growth are very large. Much work has been performed recently in correlating the fluctuations in the experimentally observed shower parameters (Fukui et al. 1960, Miura and Hasegawa 1962, Gorjunov et al. 1962, Turkish and Nikolskij 1962, Chatterjee et al. 1962). It would appear from these results that the simple picture of a unique, smooth shower development through the atmosphere is insufficient, and that fluctuations at the various stages of shower growth must be considered. A number of authors have already examined the problem in some detail, including Miyake (1958), Grigorov and Shestoporov (1958), Ueda (1960), Cranshaw and Hillas (1960), Zatsepin (1960), Dedenko (1961), Clark et al. (1961). They have been mainly concerned with statistical fluctuations in the depth of the first and subsequent interactions in the atmosphere, and the statistical variations in the behaviour of the particles produced in these interactions. Also considered has been the dependence of the depth of the first interaction on the nature of the primary particle. A survey of many of these models together with those to describe the nuclear interactions at these superhigh energies has been made by Glencross (1962).

For large showers ($N \geq 10^7$ particles), less information is available. In general their character is not dissimilar to that of smaller showers, although there are indications that suggest that the fluctuations become less as the size increases (Linsley and Scarsi 1962a). These large showers

have a special astrophysical interest because it is difficult to understand why the primary particles producing them should be distributed isotropically, as the present evidence indicates (Linsley, Scarsi, Eccles and Rossi 1962). As much information as possible is therefore sought regarding the nature and behaviour of these primaries. The phenomena observed at sea level, however, are determined by the intermediate mechanisms of shower development as well as by the properties of the primary cosmic rays. A thorough investigation of the structure and evolution of EAS is therefore of great importance in trying to differentiate between the two processes.

Because of the low flux of large EAS, most of the information about them must be obtained from their soft and penetrating components, which, at sea level, have spread laterally over several hundred metres. The normal mode of observation, and that which is used in the experiment described in the following chapters, is to sample the shower fronts at intervals across their surfaces, using detecting arrays of particle counters. To investigate EAS of size 10^9 to 10^{10} particles, it has been necessary, in recent years, to construct giant arrays with collecting areas of up to 10 km^2 . The maximum shower size which has been recorded by such techniques is $5 \cdot 10^{10}$ particles (Linsley 1963).

In the following sections the information available on large showers is reviewed, and the scope of the present research indicated.

I.2 The Structure Function

The lateral distribution of particle density in a shower (commonly

called the structure function) has been measured by many workers both at sea level and mountain altitudes. At distances within 200 m from the shower axis the electron component contributes more than 90% to the recorded densities, and the distribution in this range is effectively that of the electrons; while the structure further from the axis than 1 km is strongly influenced by the predominant muon component. The experimental structure function shows little variation with either shower size, zenith angle or altitude. Greisen (1960) has combined the results of many workers into a single empirical function which is claimed to be indistinguishable from the average experimental distributions for shower sizes ranging from $2 \cdot 10^3$ to $2 \cdot 10^9$ particles, at atmospheric depths varying from 537 g cm^{-2} to 1800 g cm^{-2} , and at distances running from 5 cm to 1500 m. This function is

$$\rho(N, r) = \frac{0.4N}{r_1^2} \left(\frac{r_1}{r} \right)^{0.75} \left(\frac{r_1}{r + r_1} \right)^{3.25} \left(1 + \frac{r}{11.4r_1} \right)$$

where ρ is the density at distance, r , from the shower axis, and r_1 is the Molière unit (79 m at sea level). For $r \ll 100$ m this expression is a close approximation to that derived by Kamata and Nishimura (1958) for electron-photon cascades having an age parameter, $s = 1.25$. There have, nevertheless, been slight, but observable, deviations from the above distribution such that the parameter s appears to decrease slowly with increase in both shower size and altitude. The M.I.T. and Cornell groups (Clark et al. 1961, Delvaille et al. 1960, 1962) have found that for $N > 10^9$ particles their distributions are best fitted by a value of s between 1.0 and 1.1. The latter group have also shown that this decrease is small: of the

order of 0.06 ± 0.09 for a factor 10^3 in shower size (Delvaillle et al. 1960). A similar, low value of s has been obtained at an altitude of 4100 m (Rossi 1960, Hersil et al. 1961, 1962) for showers of size greater than 10^7 particles. Both these steep distributions have been obtained with large arrays and are applicable to distances which extend to well over 200 m from the shower axis. With regard to the altitude variation, other experimenters working at similar altitudes but studying smaller showers with smaller arrays have found results fitting to $s = 1.2$ to 1.3 (Dobrovolski et al. 1956); and at sea level no variation has been observed with increasing zenith angle (Clark et al. 1961, Fukui et al. 1960, Miura et al. 1962, Brennan et al. 1958). Apart from Clark's array, the distributions were for distances within 200 m of the axis.

At great distances from the shower axis, $r \gg r_1$, the recent results of Linsley et al. (1962) have shown that, for showers of size, $N \sim 2 \cdot 10^7$, at an altitude of 1800 m, the structure function can be represented by a power law of the form r^{-n} with n decreasing from 3.5 to 2.0 as the atmospheric depth increases from 800 g cm^{-2} to 2000 g cm^{-2} .

Thus, it would appear that between the radial distances 20 m and 200 m, the lateral distribution of electrons is independent of shower size and atmospheric depth, although a slight steepening with increasing altitude and size cannot be ruled out. At great distances from the shower axis there is evidence of a flattening of the function

With increasing atmospheric depth, which may be attributed to the influence of the flatter muon distribution.

I.3 The Absorption of Large Showers

The absorption properties of large showers are studied by observing the change in shower intensity with varying altitude, barometric pressure and zenith angle. The altitude variation is the most direct method but with large EAS is extremely impracticable.

The absorption length, Λ , for vertical showers may be defined as,

$$\frac{dI}{I} = - \frac{dt}{\Lambda} \quad (1.1)$$

where dI is the change in the intensity of vertical showers for a difference, dt , in altitude.

If the thickness of the atmosphere at the point of observation is t g cm^{-2} ; then the intensity at an angle θ may be expressed as,

$$I(\theta) = I(0) \cos \theta \exp \frac{t(1 - \sec \theta)}{\Lambda} \quad (1.2)$$

where $\cos \theta$ gives the projection onto the plane normal to the shower axis.

For small zenith angles ($\theta \ll 40^\circ$), the expansion of the

exponential term may be approximated to

$$I(\theta) \simeq I(0) \cos \theta \left[1 - \frac{t}{\Lambda} (\sec \theta - 1) \right]$$

which by Taylor's theorem

$$\simeq I(0) \cos \theta \left[1 + (\sec \theta - 1) \right]^{-t/\Lambda}$$

$$\simeq I(0) \cos^{1+t/\Lambda} \theta$$

Thus, if the measured zenith angle distribution is fitted to a $\cos^n \theta$ power law, then

$$n \simeq \frac{t}{\Lambda} + 1 \quad (1.3)$$

The barometer coefficient for vertical showers, B_v , is defined as the fractional change in intensity with pressure. Thus

$$B_v = \frac{dI}{I dt} = - \frac{13.6}{\Lambda} \% \text{ cm Hg}^{-1}$$

where dt is now measured in cm Hg.

If the average zenith angle is θ_{av} , then the barometer coefficient for all showers is

$$B \simeq - \frac{13.6 \sec \theta_{av}}{\Lambda} \quad (1.4)$$

The values of Λ obtained for large showers ($N \gg 10^7$ particles) appear to depend on both the shower size and altitude of observation.

At sea level the Cornell group (Delvaille et al. 1960, Bennett et al. 1962) report a gradual increase from 110 g cm^{-2} to about 200 g cm^{-2} as the shower size increases from 10^7 particles to 10^9 particles. Clark et al. (1961), also working at sea level, obtained a value of $113 \pm 9 \text{ g cm}^{-2}$ for all showers between the size $5 \cdot 10^5$ and $5 \cdot 10^7$ particles.

The trend found by the Cornell group at sea level has also been observed at higher altitudes. The M.I.T. results (Linsley et al. 1962) indicate that, at an altitude of 1800 m, there is an increase from a value of 140 g cm^{-2} to 210 g cm^{-2} as the shower size goes from $5 \cdot 10^7$ particles to $2 \cdot 10^8$ particles. At 4200 m (atmospheric depth, 630 g cm^{-2}), Hersil et al. (1961, 1962) have found that the zenith angle distribution for the range $10^7 < N < 3 \cdot 10^7$ is much broader than at sea level; and for showers of size $N > 2 \cdot 10^8$ particles the **distribution** actually goes through a minimum at $\theta = 0$, - a negative absorption. They conclude that showers with $3 \cdot 10^7$ particles and $2 \cdot 10^8$ particles reach their maximum development near a depth of 600 g cm^{-2} and 800 g cm^{-2} respectively; and the attenuation of these showers beyond their maximum is approximately exponential with an attenuation length of $160 \pm 20 \text{ g cm}^{-2}$. These conclusions agree with those of Linsley et al. at the lower altitude, and together they form a consistent picture in which the region of maximum development occurs at a depth which increases with increasing shower size. The Cornell results indicate that a shower of size 10^{10} particles is near its maximum development at sea level.

I.4 Attenuation Length of Shower Particles

Closely related to the absorption length of showers, Λ , is the attenuation length of shower particles, λ . This is defined as the mean distance in which the number of particles of greater than a given energy is reduced by a factor e , when the shower is beyond maximum development. Thus,

$$\frac{dN}{N} = - \frac{dt}{\lambda} \quad (1.5)$$

Direct observations on individual showers in different stages of growth have been rare. Chudakov et al. (1960) compared the amount of Cerenkov light from the sky with the total number of particles in the shower for different zenith angles; and for showers of size $N \sim 10^6$ particles they obtained a value of $\lambda \sim 220 \text{ g cm}^{-2}$. Bennett et al. (1962) observed the development of individual inclined showers at different stages as they crossed their array. For showers with $\sim 2 \cdot 10^7$ particles, this procedure yielded an average value of $\lambda = 400 \text{ g cm}^{-2}$.

The average attenuation length of shower particles is usually derived indirectly from separate measurements of the absorption length and the exponent of the integral shower size spectrum, γ . The spectrum may be written.

$$I (> N_0) = K N_0^{-\gamma} \quad (1.6)$$

where $I (> N_0)$ is the intensity of showers of size greater than N_0

particles at the level of observation, and K is a constant. If the depth is increased by $t \text{ g cm}^{-2}$, the shower size is reduced to N , where

$$N = N_0 e^{-t/\lambda}$$

Since these are the same showers the intensities must be the same,

thus

$$I_t (> N) = K N_0^{-\gamma} = K N^{-\gamma} e^{-\gamma t/\lambda}$$
$$\frac{d I_t}{dt} = \frac{-\gamma}{\lambda} K N^{-\gamma} e^{-\gamma t/\lambda} = \frac{-\gamma}{\lambda} I_t$$

Comparing this equation with equation (1.1)

$$\gamma \lambda = \lambda \tag{1.7}$$

This relation only holds if the fluctuations in shower growth are not extreme and the observations at different atmospheric depths are of similar showers in different stages of development.

Bennett et al. have reviewed the results for sea-level showers and have suggested that in showers of $N < 10^7$ particles the electronic component is comparatively soft, and the progress of the shower is dominated by the rate of exhaustion of nucleonic energy ($\lambda \sim 200 \text{ g cm}^{-2}$). For the larger showers the value increases rapidly as the region of maximum development is approached, and here the average attenuation length of the electronic component becomes greater than that of the nuclear energy in the shower.

I.5 The Structure of the Shower Front

Another parameter which contributes to the understanding of shower development is the shape of the shower front. Although delayed shower particles had previously been observed by Jelley and Whitehouse (1953), the first attempt to measure the radius of curvature of the shower front was made by Bassi et al. (1953). These authors measured the relative time delays for several configurations of an array of three scintillation counters, with counter separations up to 30 m. They found that, near the axis, most of the shower electrons lie within a band of thickness between 1 and 2 m, and the muons in a slightly broader band. A lower limit of 1300 m was found for the radius of curvature of the shower front. These conclusions were later confirmed by an experiment by Sugarman and De Benedetti (1956). More recently, groups at both M.I.T. (Linsley and Scarsi 1962b) and Cornell (Bennett et al. 1962) have extended the measurements out to greater distances. The Cornell group used scintillation counters in an array of diameter 1 km and timed the arrival of the first detectable particles in the shower. They found that the average curvature corresponds to a radius of 2.8 km, but that individual values fluctuate considerably from this. By a similar technique, the M.I.T. group determined that the average median surface for the electrons has a radius of curvature which increases from about 1 km to 3 km as the distance from the shower axis varies from 400 m to 1200 m. A shielded detector was incorporated in their array to give data on the muons; these were found to lie in a band, the median surface of which is spherical, having a centre at an atmospheric depth of

300 g cm^{-2} . From measurements on individual delayed particles they found that, at about 1 km from the axis, these could arrive several microseconds late.

I.6 The Muon Component

Investigations on the muon component yield more direct information on the processes occurring in the showers. Although less abundant than the electrons, their average energy is much higher (about $5 \cdot 10^9$ eV per muon); and, in general, they carry more total energy than the electron-photon component.

The lateral distribution of muons of energy above 1 GeV has been measured by Clark et al. (1958), and for sea-level showers with zenith angles less than 25° is of the form $r^{-2.1}$ in the region $100 \text{ m} < r < 1 \text{ km}$. Between the shower sizes $10^6 < N < 10^8$ particles, the shape of the distribution appears to remain constant; but the total number of muons is estimated to increase as $N^{\frac{3}{4}}$.

The relative proportion of muons to all charged particles has been investigated using lead shielded particle counters. A number of measurements have been made near the shower axis (Kraushaar 1958, Fujioka 1953, Cocconi 1949, Cranshaw et al. 1958, Eidus et al. 1952) and the proportion appears to increase from 1% at 10 m to 7% at 100 m. At greater distances the evidence is much slimmer: Eidus et al. give $40 \pm 20\%$ at 600 m while Cranshaw et al. give about 30% at 700 m.

More recent results at mountain altitudes by Linsley, Scarsi and Rossi (1962) indicate that there is an increase in the proportion from 6% at 100 m from the axis (80 m, sea-level equivalent) to 35% at 1km (800 m, sea-level equivalent). These proportions seem to remain constant out to zenith angles which correspond to vertical sea-level showers.

The energy spectrum of the muons depends on the distance from the shower axis at which they are detected, the spectrum becoming steeper with increasing distance from the shower axis. From their measurements with a shielded magnetic spectrometer, run in conjunction with their array, Bennett et al. (1962) deduced a mean energy for muons in EAS of 7 GeV.

I.7 Scope of the Present Work

The work which is reported in the following chapters was primarily designed to study EAS in the size region above 10^7 particles. A large detecting array (collecting area, 0.32 km^2) has been constructed at Haverah Park, in Yorkshire, and has been in operation since December 1962. Preliminary results from this experiment are presented in the later chapters. During the early stages of the development of the main array, the prototype detector units were used to investigate the structure of small air showers near the shower axis. To this end two subsidiary experiments were operated; the first to examine the energy distribution of the electron-photon component within 12 m of the shower

axis, and the second to explore the particle density spectrum at very low densities.

CHAPTER 2

THE 6-METRE ARRAY - PART I

2.1 Design of an Experiment

The experiment described in the following sections is a continuation of the work carried out by the Imperial College group using similar apparatus at the Silwood Park Field Station. In that experiment, which has been reported by Allan et al. (1962) and Wills (1961), a triangular array of four water Cerenkov detectors was used to locate the core position and determine the size of EAS, as well as to study the energy distribution of the shower particles. Estimates about this distribution were made by comparing the lateral structure function for the Cerenkov response with the particle density structure function found by other workers. The difference between these lateral structure functions was interpreted as being due to the variation with distance from the shower axis of the electron track length associated with the incident particles as they formed cascades of differing sizes in the water of the detector. The cascades result from the energy distribution of the incident particles which was assumed to be a differential spectrum of the form $E^{-(s+1)} dE$. Values of the parameter, s , which gave the observed track lengths were calculated under Approximation A, and found to vary from 0.58 at distances less than 3 m from the shower axis to about 1.7 at distances greater than 30 m. For such approximations, the number of particles should increase exponentially with depth for values of $s < 1$, and decrease exponentially for $s > 1$.

The present experiment was designed to follow up this earlier work: in particular to investigate further the nature of the electron-photon component near the shower axis. To do this the depth of the present detectors was made variable to enable the cascade in the water to be sampled at intermediate stages of development. The maximum depth available was 3.4 radiation lengths, which allowed the cascade to be followed to later stages of development than in the earlier work, when the depth was 2.05 radiation lengths. In addition, an examination of the particle multiplicities was made using Geiger counters placed above and below one of the tanks.

2.2 Arrangement of Apparatus

A diagram of a detector is shown in figure 2.1. The container was a galvanised iron tank, 4 ft x 6 ft in horizontal cross section and 4 ft deep, the inside of which was lined with white diffusing sheets of P.V.C. (Darvic). Water from a nearby bore-hole was chosen as the Cerenkov medium because of its low acid content and good transmission properties. The tank was covered by a 10-gauge aluminium lid which was clamped on to rubber strips and sealed with a black adhesive (Lassotape) to render the interior light-proof. A singly charged relativistic particle in water emits about 200 photons per cm of path in the visible region. To convert this light yield into a proportionate electrical pulse, a 5 inch photomultiplier (E.M.I. type 9618 YB) was mounted in the centre of the aluminium lid with its photocathode dipping into the water. A rubber annulus which gripped the photomultiplier

stem protected the associated electronics from the water vapour.

In later stages of the experiment, the photomultiplier and top Darvic sheet were supported on a Dexion framework which could be lowered into the tank to change the depth of the detector.

The four detectors were housed in two adjacent wooden huts at 220 m altitude. Their positions are given in figure 2.2 where the distance, d , was 6 m; the centres of the outer detectors form the vertices of an equilateral triangle.

A block diagram of the recording system is shown in figure 2.3. The photomultiplier outputs were passed through emitter follower circuits and into a central recording system which consisted of a pulse-mixer unit, non-linear amplifier and oscilloscope (Tektronix type 515A). Non-linear amplification permitted a total range of pulse amplitude of about 50 : 1 to be measured with an accuracy of 10% from the recording oscilloscope screen. Relative delays between the pulses were achieved by interposing different lengths of co-axial cable (Uniradio 39) between the photomultipliers and mixer unit. The longest delay used was 7.5 microseconds (1500 m of cable). To prevent any overlapping of pulses (decay time ~ 8 microseconds), 70 m lengths of shorted cable were used to shape, by reflection, all but the final pulse to widths of 0.7 microsecond.

FIGURE 2.1 Cross-section of Cerenkov detector. The broken lines indicate the lower levels of the top Darvic sheet.

FIGURE 2.2 Plan of the detector array.

FIGURE 2.3 Block diagram of the recording system.

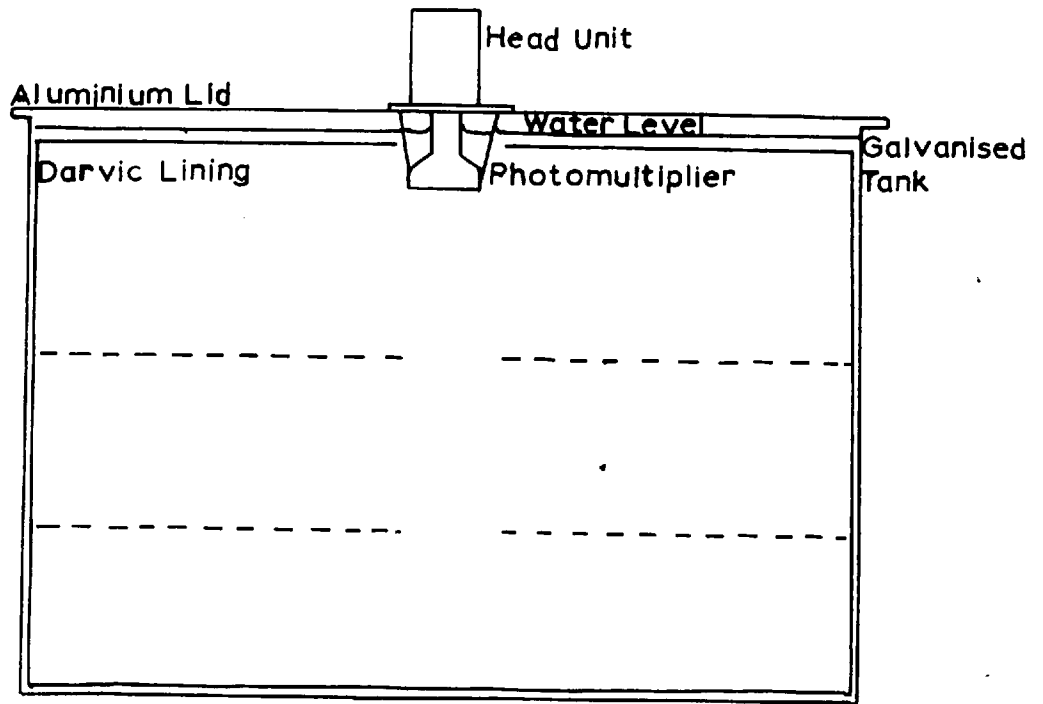


Figure 2.1

0.5m

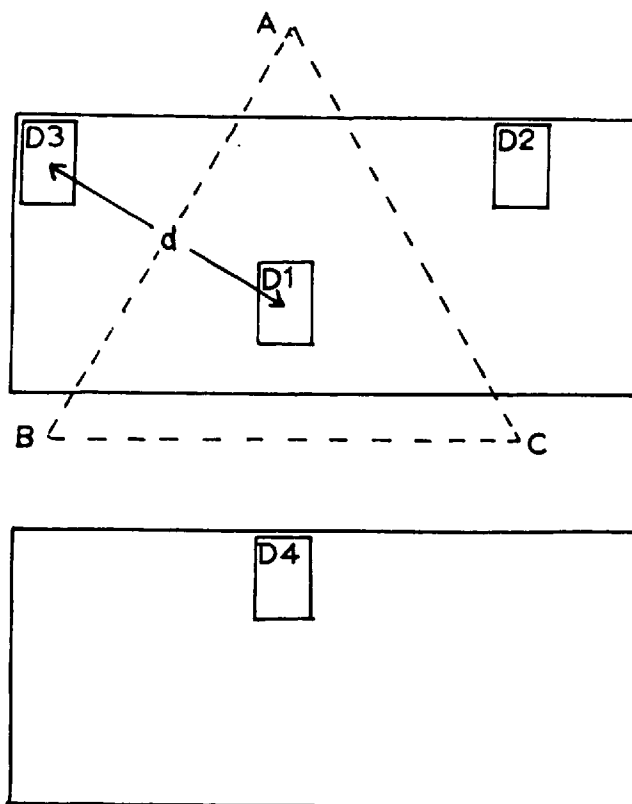


Figure 2.2

5m

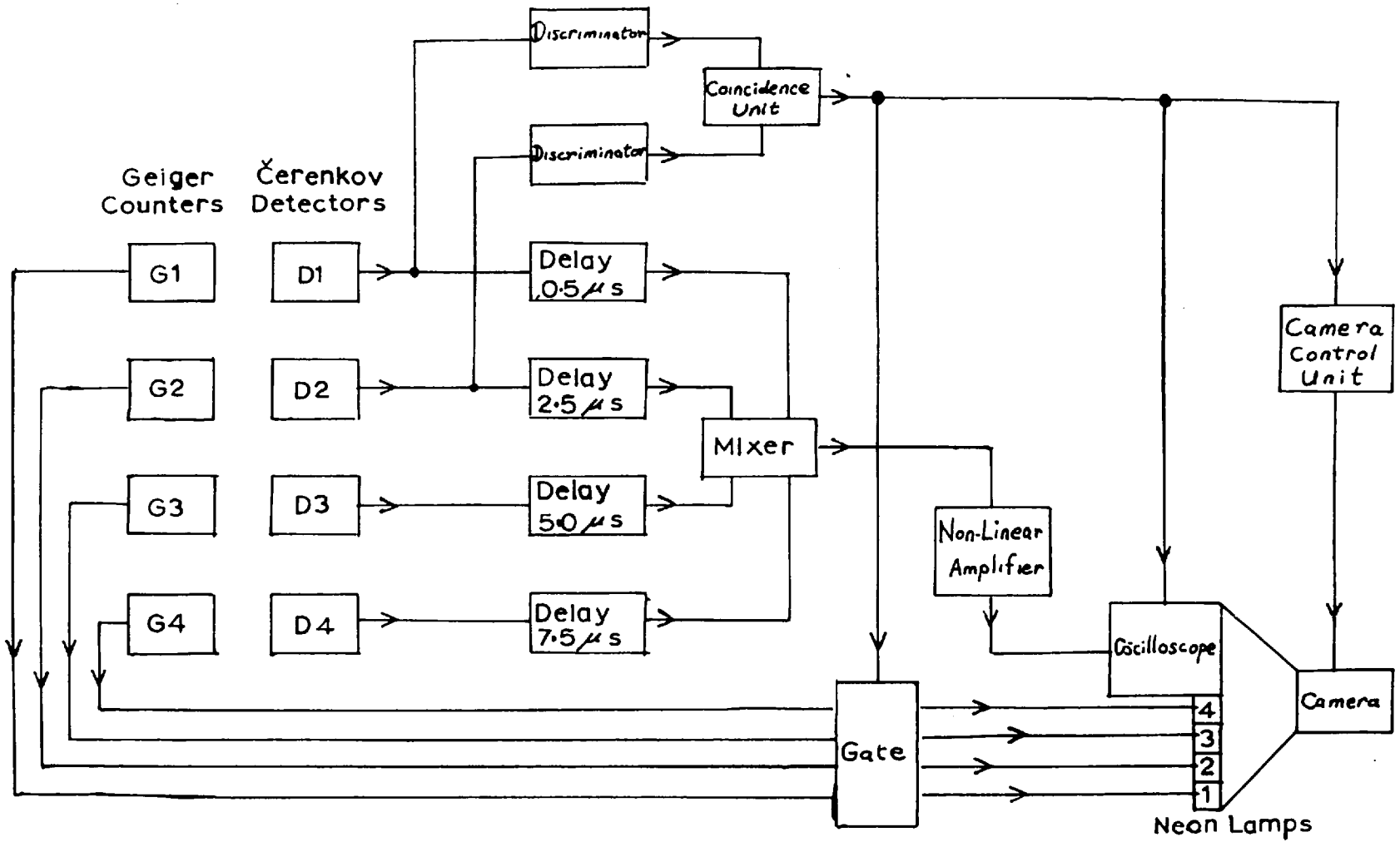


Figure 2.3

For purposes of calibration two trays of three halogen quenched Geiger counters, each of area 570 cm^2 , were placed on top of each detector. Whenever a coincidence occurred between the two trays simultaneously with an extensive shower, an associated neon lamp attached to the perimeter of the recording oscilloscope screen was illuminated. This method of calibration is identical to that used at Silwood Park, and detailed descriptions of the electronic circuits and Geiger counter characteristics are given by Bryant (1958) and Wills (1961).

In order to select air showers from the incident radiation, events were only recorded if densities greater than $25 \text{ particles m}^{-2}$ fell in coincidence on the central and one selected outer detector. This was done using standard coincidence and gating circuits to trigger the oscilloscope time base and pass the calibration data to the neon lamps.

All the necessary shower information was photographed on single 35 mm film which was subsequently read by projection onto a calibrated scale.

2.3 Calibration of Detectors

The purpose of the Geiger counter calibration was two-fold. In the first place it allowed a continual check to be maintained on the overall gain of each detector channel; and secondly, when used in conjunction with the single particle calibration (section 2.5) in

the subsequent analysis, it enabled the actual electron track length per incident particle to be calculated (section 3.1).

The probability of recording a coincidence between two Geiger counter trays of area, A , when a uniform particle density, Δ , falls upon them is

$$P(\Delta) = (1 - e^{-\eta \Delta A})^2$$

The term, η , is included to allow for the Geiger efficiency, which in this case was about 80%. About 500 shower events were required for an independent calibration to be made, which when the array was running normally was equivalent to two or three days data. For these events the Cerenkov outputs from each detector were grouped into intervals of pulse height and, for every interval, the probability of an associated Geiger counter tray coincidence was found. The expression above was then used to correlate the average pulse height of the interval, x , with the particle density, Δ , that gave the observed probability. In this way a value for the quantity, Δ/x , was obtained for each interval from which an average value was calculated, suitably weighted according to the number of events in each interval. Thus a multiplying factor was obtained for each detector by which the pulse heights were converted to 'nominal densities', D . Since the detector response is energy dependent, the nominal density is related to the true density by a factor which varies with distance from the shower axis. The true and nominal densities are only equal at the 'calibration distance', r' , the determination of which is described in

2.4. Operation of Array

Between October 1961 and April 1962 a total of 1700 showers were recorded by the array. In order to investigate the cascade development in the tank, data was obtained from detector depths of 3.4, 2.05 and 1.0 radiation lengths (125 cm, 76 cm and 38 cm respectively). The second depth was chosen to be equal to that of the Silwood Park detectors to allow the results of both experiments to be combined.

The gains of the four detector channels were first adjusted to give approximately the same integral count rate above a bias level of 5 particles per tank (100 counts per min). To do this the signal inputs to the mixer unit were disconnected and fed separately into a discriminator and scaler circuit and the E.H.T. supplied to each photomultiplier adjusted accordingly.

At the start of each run several independent Geiger counter calibrations were made for each detector; after which the counter trays were repositioned in order to investigate the distribution of particle multiplicities through the different depths of water. Two sets of calibration trays were placed beneath one of the outer detectors, D3, which was raised on girders, and two above. During these periods only D3 was calibrated. The constancy of the gains of the other detectors was checked by comparing their integral count rates with that of D3, using the method outlined above. Throughout the duration of the individual run, the stability of the detectors was

such that, within the calibration accuracy of 10%, no evidence was found for drifts in gain.

2.5 Single Particle Calibration

In order to determine the pulse height produced by a singly charged relativistic particle traversing a known distance in the water, vertical muons which penetrated the total detector depth were selected by a scintillator telescope, and the related electrical output measured. The telescope consisted of three counter units: 7 inch diameter scintillators viewed by 2 inch photomultipliers (E.M.I. type 9514 B) encased in light-tight aluminium boxes. Each unit was mounted one above the other in a metal framework, separated by two 3 inch layers of lead bricks. Pulse height distributions obtained with this 'ordinary' configuration were compared with those obtained with the upper unit placed beneath one of the tanks. As anticipated, the distribution in the latter case was much sharper due to the increased resolution of the telescope (maximum angle accepted = 5°); the average values, however, were identical. Hence the single particle pulse heights could be determined without bias for the tanks that were not supported on girders; - an important consideration in the calibration of the 500 m array (see section 5.3).

For an accurate calibration, the variation in the response of the detector across its area must be known. Accordingly, pulse height distributions were obtained for five different positions in a rectangular area, the diagonal of which stretched from the centre to the corner of the

tank. Contours of equal response were drawn for this area and extended by consideration of symmetry to cover the whole detector. Comparison of the calculated mean pulse height with the observed response contours enabled a convenient calibration position for the telescope to be selected. This was on a contour corresponding to the mean pulse height, - about midway between the centre and the middle of a shorter side. The mean response across the detector area varied by about 30% between the central and corner positions. From the shape of the distribution, assuming it to be Poissonian, a mean of about 7 photoelectrons produced at the photocathode per incident muon was calculated. A full description of this method of derivation is given by Wills (1961).

The above investigations were performed on the largest depth of 3.4 radiation lengths. Further comparative information was acquired by maintaining a constant photomultiplier gain as the depth of water was altered. Both the related quantities, mean pulse height and the associated number of photoelectrons liberated, were found to be proportional to the depth of the detector. It follows that the attenuation path of the light in the water was long compared with the detector depth. Similar conclusions may be drawn from the results of the theoretical treatment of the optical problem by Porter (reported by Jelley 1958). This author has extended the calculations of Mandò (1954), relating to non-focussing counters, to include the effect of light absorption in the medium. He shows that the optical efficiency of

the counter can be expressed as

$$\eta = \frac{\rho}{\rho + \mu + \rho\mu + \left[\exp(\bar{x}/\lambda - 1) \right]}$$

where μ is the coefficient of reflection of the Darvic, ρ is the ratio of the area receiving light to that scattering light, \bar{x} is the average distance between successive reflections, and λ is the mean free path for the absorption of photons in the medium. If the manufacturers' figures for the coefficient of reflection and photomultiplier efficiency are taken, then $\lambda \sim 8$ m.

2.6 Analysis

The experiments described in this and following chapters, using triangular arrays of detectors, depend for their analyses on similar procedures. In this section the general principles of analysis which apply to both experiments are discussed, but applied in particular to the 6 m array.

2.6.1. Shape of the Cerenkov Detector Structure Functions

In section 2.3 a multiplying factor was calculated by which the observed pulse heights could be converted to nominal density, D . The variation of this nominal density with distance from the axis of a shower of size, N , for a detector of depth, i , may be defined by the equation

$$D_i = C_i N j_i(r) \quad (2.1)$$

where $j_i(r)$ is the structure function appropriate to depth, i , and C_i is a constant depending for its value on the units of $j_i(r)$.

The form of $j_i(r)$ was arrived at by using a series of trial functions of the form

$$j_i(r) \propto r^{-mi}$$

and determining the value of m which best fitted the experimental data.

The method of intersecting loci (Allan et al. 1960) was used to locate the shower axes with an accuracy of 0.5 m. It is clear from equation 2.1 that for a given ratio of nominal densities between a pair of detectors, there existed a locus on which the shower axis must have fallen. This locus satisfied the condition that the values of the structure functions at the detectors were in the same ratio as the nominal densities. Loci for different ratios were plotted on a scale drawing of the array and sets of loci prepared for different values of m . To locate the axis of a particular shower the points of intersection of the loci relevant to the three larger densities were determined; and the ambiguity of location removed by reference to the fourth density. The resulting unnormalised shower size, $C_i N$, was then used to predict the value of the nominal density recorded at the fourth detector. The 'best' value of m was simply that with which this predicted value was greater or less than that observed with equal frequency. For the three detector depths, 3.4, 2.05 and 1.0 radiation lengths, these

values of m were 1.48 ± 0.02 , 1.39 ± 0.02 and 1.33 ± 0.02 respectively. To assess the errors on these values, three values of the exponent, m , were tried at each depth.

The distances over which these exponents are applicable extend from 1.5 m to 12 m from the shower axis. Later, it will be shown that the calibration procedure required these measurements to be extended out to the calibration distance of 16 m (section 2.6.2). In order to do this, the data obtained in the previous experiment (Allan et al. 1962) for detectors of depth 2.05 radiation lengths in arrays of spacing $d = 5$ m and 15 m were combined with the present results. For the 5m array (range: 1.5m to 10m) the best value of m was found to be 1.42 ± 0.04 - in agreement with the present results, - increasing to 1.83 ± 0.03 for the 15m spacing (range; 5m to 30m). These two trial functions were joined by a smooth curve which was then adopted as the best structure function over the total range. The showers were then re-analysed to confirm its accuracy. Minor adjustments were now made to this combined function by using it to analyse the whole of the data obtained from both experiments for the depth of 2.05 radiation lengths. The resulting function $j_{2.05}(r)$ is appropriate to the range $1.5\text{m} < r < 30\text{m}$.

Another function obtained in the previous work was that for 0.61 radiation lengths depth. This function and the one just constructed were used to indicate the shape of the functions for the two other depths, which were thereby extrapolated to the calibration distance, $r' = 16\text{m}$.

The three modified structure functions were tested by the original method of density prediction and small empirical adjustments were made.

In order to avoid bias and unnecessary errors, several selection criteria had to be imposed on the showers used in the above determination of the structure functions. As these have been comprehensively discussed by previous authors (Glencross 1962, Wills 1961) only a brief summary of the main restrictions is given. Showers in which the central detector did not record the largest nominal density were not used in the subsequent analysis. The reason was that outside the triangular collecting area ABC (figure 2.2) thus defined, the accuracy of location of the shower axes deteriorated rapidly. Once a structure function had been assumed, three shower density measurements sufficed to locate its core position. For this reason it was important for these densities to be statistically reliable; a level of at least 55 particles per tank was therefore demanded for three of the four detectors. Normally the array was biased strongly towards showers having a relatively flat lateral distribution of particles. To eliminate this bias two further criteria were imposed. The showers were required to be able to trigger the array irrespective of where they fell within the collecting triangle, i.e. a minimum, or critical size was introduced; also, the central detector was required to register a density significantly larger than the outer three. This latter condition ensured that large showers falling at great distances were not included as a result of

possible statistical fluctuations of the central density.

As a result of these, and other less important criteria, the total number of about 1700 recorded showers were reduced to 558 'efficient' showers.

2.6.2 Normalisation of the Structure Functions

The procedure so far gave only the shapes of the Cerenkov detector structure functions. Their absolute values were found by normalising to the particle density distribution. This was done so that the value of each Cerenkov function equalled that of the density function at the distance at which the average track length per shower particle was equal to the appropriate detector depth. The recorded pulse height $\bar{\mu}_i$ corresponding to this track length was obtained from the muon calibration. In section 2.3 a multiplying factor, $(\frac{\bar{\Delta}}{x})_{r'}$, was obtained for each detector, by means of which the pulse heights were converted to nominal densities, D . It was also pointed out that this nominal density is only equal to the true density, Δ , at the calibration distance, r' .

Now, for Cerenkov detectors, the variation of nominal density is described by the function, $j_i(r)$,

$$D_i = C_i N j_i(r) \quad (2.1)$$

while for the same shower, the density follows the distribution function $f(r)$.

$$\Delta = N f(r) \quad (2.2)$$

At r , when $D_i = \Delta$

$$C_i = \frac{f(r')}{j_i(r')}$$

where $f(r')$ is proportional to the incident density at r' , and $j_i(r')$ is proportional to the track length per unit area produced by this density. From the statement of normalisation, at the beginning of this section, it follows that the constants of proportionality are equal provided that the track length is measured in units of detector depth. Thus,

$$j_i(r) = \frac{f(r)}{\left(\frac{\Delta}{x}\right)_{r'} \cdot S \cdot \bar{\mu}_i}$$

from which $C_i = \bar{\mu}_i \cdot S \left(\frac{\Delta}{x}\right)_{r'}$

where S = area of a single detector.

The values of the parameters involved in the derivation of the constant of normalisation C_i , together with their estimated errors are summarised in Table 2.1.

TABLE 2.1 : Calibration Data

Depth i	$\left(\frac{\Delta}{x}\right)_{r'}$	μ_i	$n(r') = 1/C_i$
1.0 rl.	0.87 ± 0.04	0.53 ± 0.03	0.96 ± 0.07
2.05 rl.	1.48 ± 0.07	0.45 ± 0.02	0.66 ± 0.05
3.4 rl.	1.00 ± 0.05	0.74 ± 0.04	0.59 ± 0.04

rl = radiation length

Finally, it was necessary to calculate the calibration distance, r' . It is evident from equations (2.1) and (2.2) that the multiplying factor which converts pulse height (proportional to D) to particle density, Δ , is proportional to the ratio, $f(r) / j(r)$, at the distance of observation. Thus r' is the distance at which this ratio, in arbitrary units, is equal to its mean value averaged over the showers used in the calibration. The mathematical derivation of r' is basically similar to that performed by Wills (1961) for the previous array spacings of 5 m and 15 m, with slight modifications to allow for the different triggering conditions. In performing the computation it was necessary to assume that at large distances $j(r)$ becomes parallel to $f(r)$; which, because of the small contributions from these distances, introduces a negligible error in r' .

The value of r' was found to be 16 ± 1 m, independent of the detector depth. Since the structure functions appropriate to the deeper detectors are steeper it might be expected that the array of these detectors would select more showers at smaller distances than would the array of shallow detectors. However, the densities registered at these distances were such that the probability of a Geiger counter discharge was generally too high to be used in the calibration, with the result that the value of r' did not vary by more than a metre between the detectors of 1.0 and 3.4 radiation lengths depth.

The lateral distribution function of particle density used in

these calculations is a combined function which was taken to represent the mean distribution of those obtained by Abrosimov et al. (1960) and Fukui et al. (1960). The Russian function was measured with an array of Geiger counters and agrees with that given by Fukui et al. at distances greater than about 10m, but is slightly flatter nearer the shower axis. The Japanese results were obtained with an array of scintillators (4.5 cm deep) which were corrected for their slight energy sensitivity with a neon hodoscope.

In figure 2.4 the Cerenkov detector structure functions, $j_i(r)$, are normalised to the combined particle density structure function, $f(r)$, using the value of r' determined above. The absolute shower sizes are based on these functions. In this experiment the minimum critical size (see section 2.6.1) for efficient showers was $9 \cdot 10^4$ particles.

2.6.3 Response Function

A convenient quantity to be used later is the Cerenkov detector response function $n_i(r)$, defined as the ratio $j_i(r)$ to $f(r)$. The response functions for the three detector depths used in this experiment are presented in figure 2.5.

2.7 Comparison with Previous Work

It is of interest to compare the results of this experiment with those of the earlier Silwood Park experiment (Allan et al. 1962). As has been noted already (section 2.6.1), the structure functions

FIGURE 2.4 The Cerenkov detector lateral structure function, $j_i(r)$, for detectors of depth 1.0, 2.05 and 3.4 radiation lengths compared with the particle density structure function, $f(r)$, determined by Fukui et al. (1960) and Abrosimov et al. (1960).

A - $j_i(r)$ (1.0 radiation lengths)

B - $j_{2.05}(r)$ (2.05 radiation lengths)

C - $j_{3.4}(r)$ (3.4 radiation lengths)

D - $f(r)$ (particle density)


 - Normalisation points

FIGURE 2.5 The detector response function, $n_i(r) = j_i(r) / f(r)$.

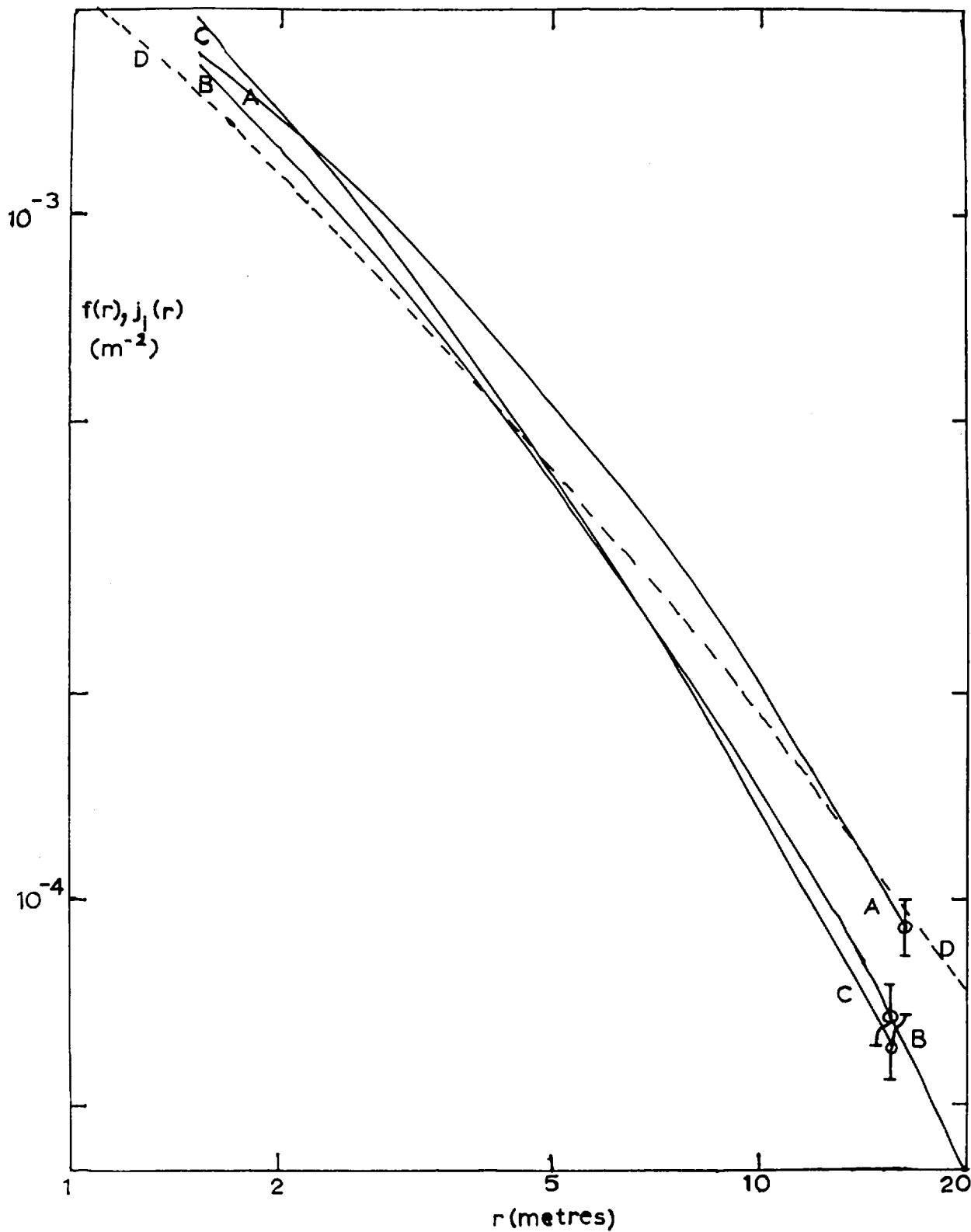


Figure 2.4

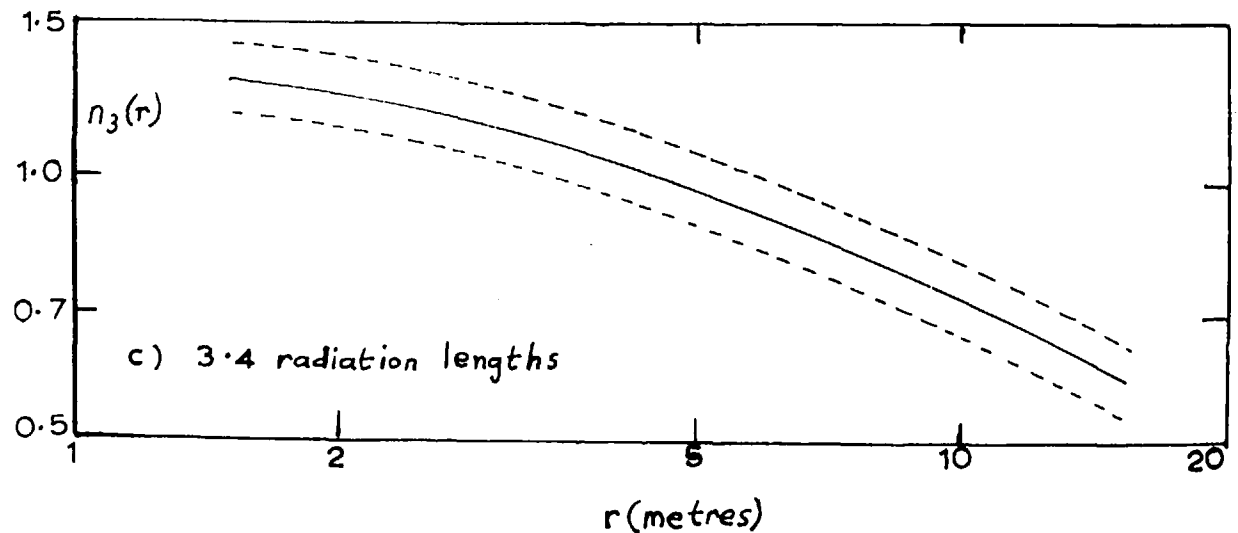
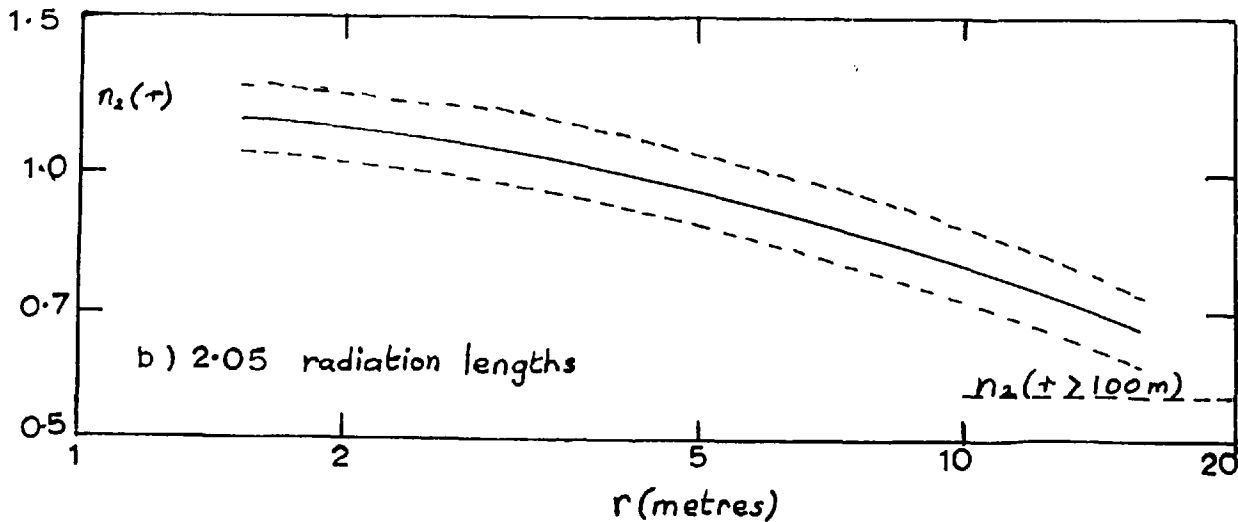
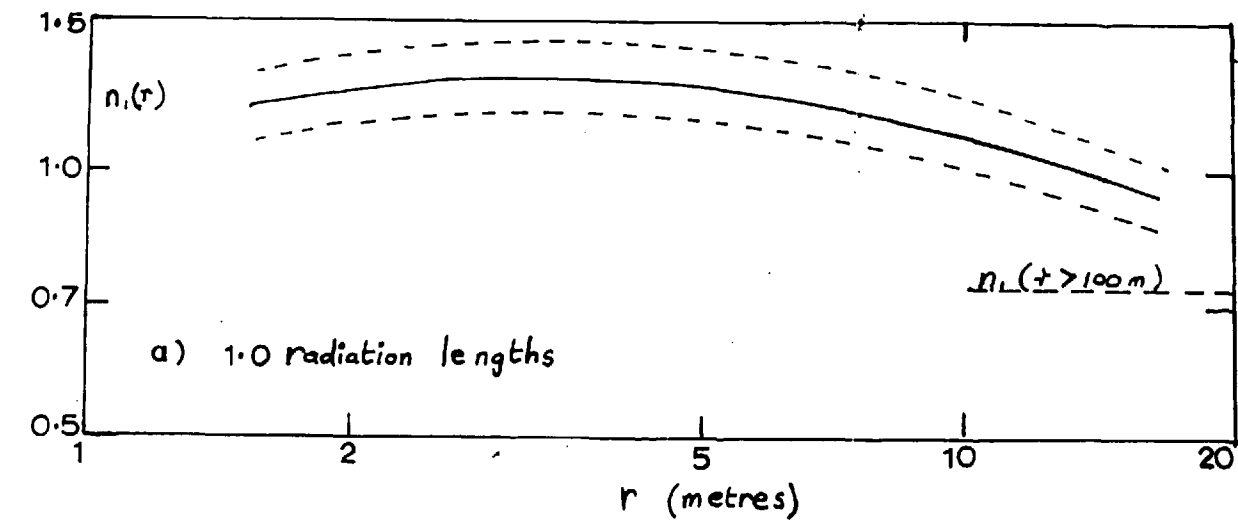


Figure 2.5

obtained at the common depth of 2.05 radiation lengths do not differ in form, within the limits of error; consequently the shape of the response functions $n_{2.05}(r)$ are also similar. Their absolute magnitudes after normalisation, however, differ appreciably, the values in the present experiment being about 30-35% lower than previously. Obviously the source of the discrepancy must lie with either the Geiger counter calibration or, more probably, the single particle calibration. Since in the earlier work it was not possible to place one element of the telescope below a detector, some of the muons selected may not have penetrated the full depth of the detector. In this case the amount of Cerenkov light radiated would be less than appropriate to a muon track-length of one detector-depth. On the basis of the results described in section 2.5, however, this is unlikely. The most credible explanation lies in the variation of mean response across the detector. Compared with the 5 photo-electrons liberated at the photocathode for the passage of a single particle in the present experiment, the corresponding figures at Silwood Park was 2. Thus the collection efficiency was much poorer, and hence the mean response would be expected to have had a greater variation across the detector, i.e. greater than 30%. In such a case the single particle pulse height would be very sensitive to the position of the telescope and would easily account for the above 30% difference in the absolute values of $n_{2.05}(r)$.

CHAPTER 3

THE 6-METRE ARRAY - PART 2

The Distribution of Energy in the Electron-Photon Component

3.1 Interpretation of $n(r)$

In section 2.6.2 it was shown how the Cerenkov structure functions were normalised so that they were equal to the density function at the distance at which the average track length per shower particle was equal to the appropriate detector depth. The difference between the functions are a result of the cascade development in the water. For values of $j_i(r) > f(r)$ there is an increase in the average track length compared with the detector depth, and for $j_i(r) < f(r)$ a corresponding decrease. Thus the response functions $n_i(r)$ ($= j_i(r) / f(r)$) represent the mean track length per incident particle, measured in units of detector depth. In figure 2.5 these are plotted for the three detector depths out to a radius of 15 m.

At greater distances from the shower axis the values may be estimated from the cascade predictions of Kamata and Nishimura (1958). These authors have suggested that at large distances from the shower axis (~ 100 m) the electron component is produced from relatively low energy photons which have travelled out from near the shower core. Unlike the photons, the low energy electrons can travel only a short distance because they lose their energy by ionisation processes. As a result, although the particle density falls steeply at these distances, the average energy per electron tends to remain constant and the shower

reflects the absorption properties of the photon component. Over a fairly wide range of energies (between 10 MeV and 200 MeV) the absorption length, λ_a , of photons in air and water remains near a maximum value of about 60 g cm^{-2} . If the total energy falling on the tank is E , then the energy absorbed in a small depth, dt , at the top of the detector is

$$\frac{E \, dt}{\lambda_a}$$

In order to produce this energy loss by ionisation, the number of electrons which must traverse this depth is

$$\frac{E}{k \lambda_a}$$

where k = the ionisation loss per g cm^{-2} . The total energy lost in a detector of depth, t , is

$$E (1 - e^{-t/\lambda_a})$$

which corresponds to a track length of

$$\frac{E}{k} (1 - e^{-t/\lambda_a})$$

Thus the total track length per incident particle is

$$\lambda_a (1 - e^{-t/\lambda_a})$$

$$\text{and } n(r) = \frac{\lambda_a}{t} (1 - e^{-t/\lambda_a})$$

Hence, for any depth, t , the value of $n(r)$ depends entirely on the absorption length of the incident photons. As the distance from the shower core increases, the individual energies of the photons would be expected to approach that corresponding to minimum absorption. This would lead to a limiting value of $n(r)$ from this source of 0.42, 0.57 and 0.73 for the three detector depths 3.4, 2.05 and 1.0 radiation lengths respectively. The actual region of minimum absorption covers a fairly broad energy band between 20 MeV and 30 MeV, and these photons would produce Compton recoil electrons of average energy between 10 MeV and 20 MeV which would have a range of about 10 cm in water.

At distances greater than about 1 km from the shower axis the muon component is predominant, and here the value of $n(r)$ for each depth would approach unity.

For comparison, the values which $n(r)$ are expected to approach at $r \gtrsim 100\text{m}$ are plotted on the same graph as the values obtained close to the shower axis (figure 2.5).

3.2 Electron Track Length

From the curves of figure 2.5 it is possible to determine the track length per incident particle, z , measured in radiation lengths, as a function of absorber depth, t , for any distance, r , from the shower axis. Graphs of z against t for $r = 2, 4, 8$ and 12m are shown

in figure 3.1. The broken line, $z = t$, represents the track length of a particle which passes through the detector without undergoing either multiplication or attenuation. It is seen that for distances less than 2m from the shower axis there is a net multiplication for all depths, at least up to 3 radiation lengths. As the distance, r , is increased the multiplication gives way to attenuation at large depths, and for distances greater than about 10m the effect is one of attenuation for all depths over 1 radiation length.

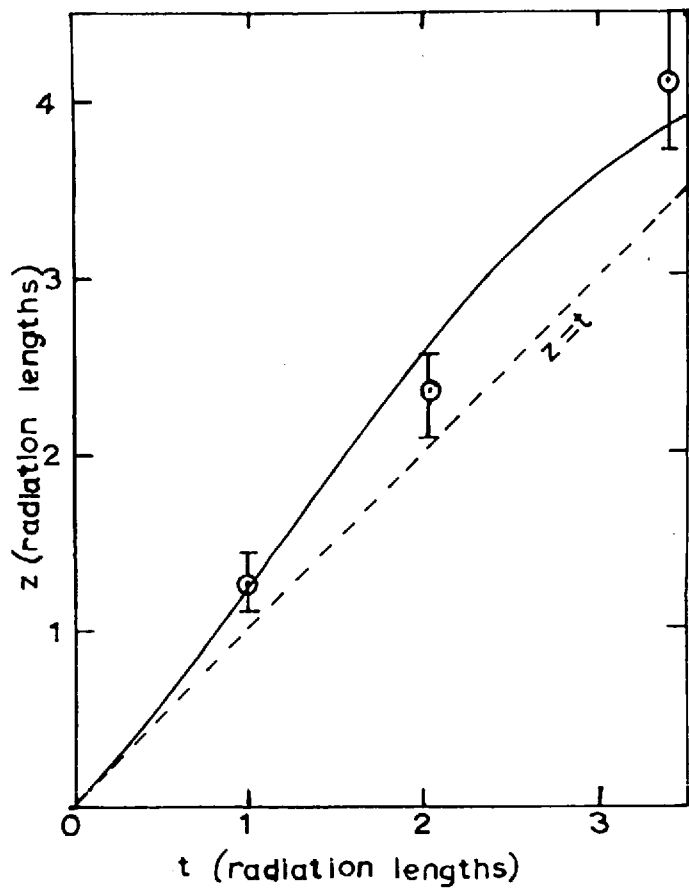
3.3 Particle Multiplicity

The multiplicity of shower particles may be defined as the ratio of the number of particles leaving the bottom of the detector to that incident on the top. Multiplicities were derived from the results of the Geiger counter trays above and below the detector, though the statistical nature of these results, averaged over a wide range of incident density, prevented any detailed quantitative conclusions from being reached. Also, the situation of the counter trays at one of the outer detectors limited measurements to a narrow range of distance from the shower axis. The results for the three depths were grouped into two intervals (3m to 6m and 6m to 10m) and the mean distance of the shower axis from the detector for each interval was determined. Using the probability expression given in section 2.3 the average probability of coincidence for each group was related to the density, and the associated multiplicity was calculated. These values, for mean distances of 5.0m and 7.5m, are presented in figure 3.2. The

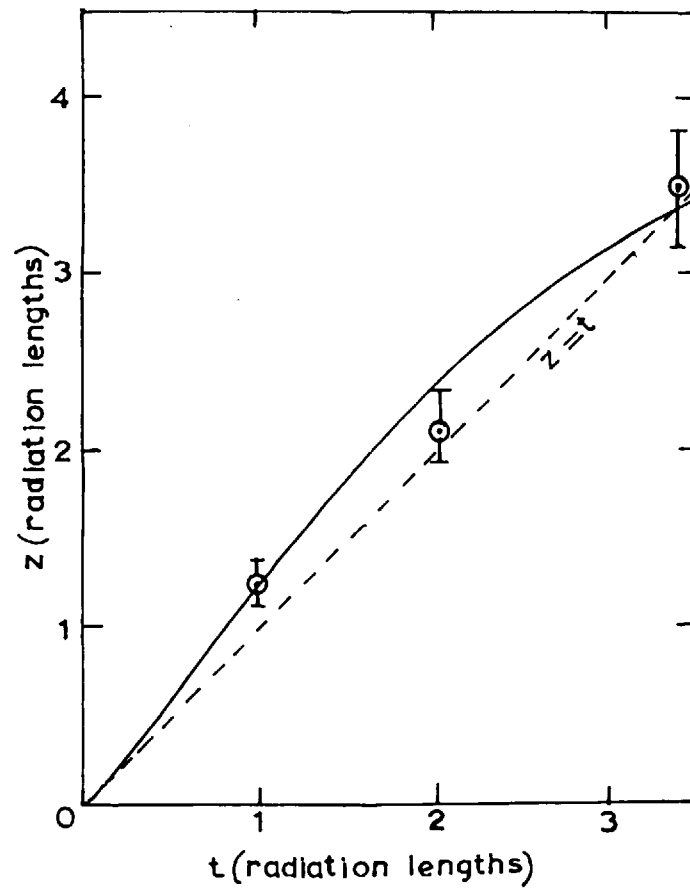
FIGURE 3.1 The average track length per incident electron, z , as a function of the detector depth, t , for different values of the distance, r , from the shower axis. The points are experimental, while the curves represent the track lengths calculated from the results of Butcher and Messel (1960) for the energy values shown, assuming $n \gamma = 1$.

FIGURE 3.2 Particle multiplicities as determined using Geiger counter trays.

FIGURE 3.3 Average track lengths per electron, derived from the particle multiplicities, compared with those derived from the Cerenkov detector response functions.

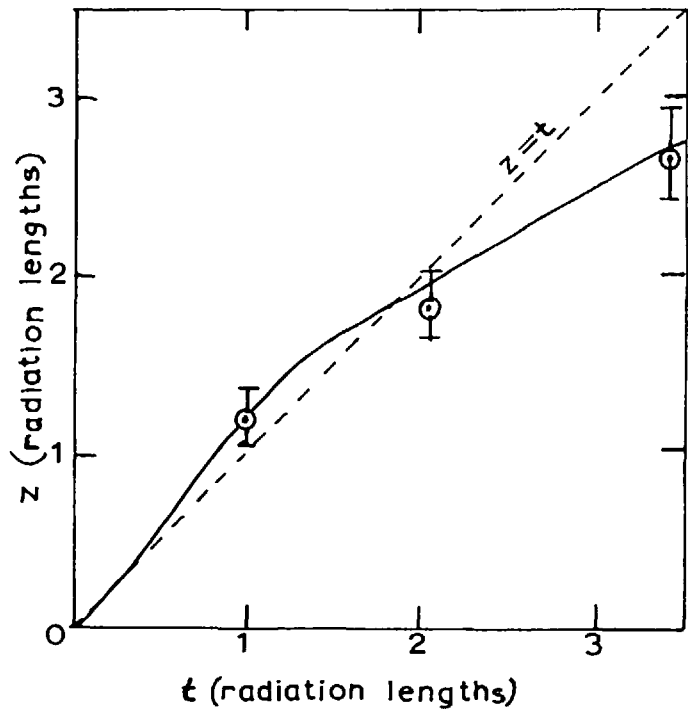


a) $r=2m$ $E_e=105\text{ MeV}$ $\bar{E}=440\text{ MeV}$

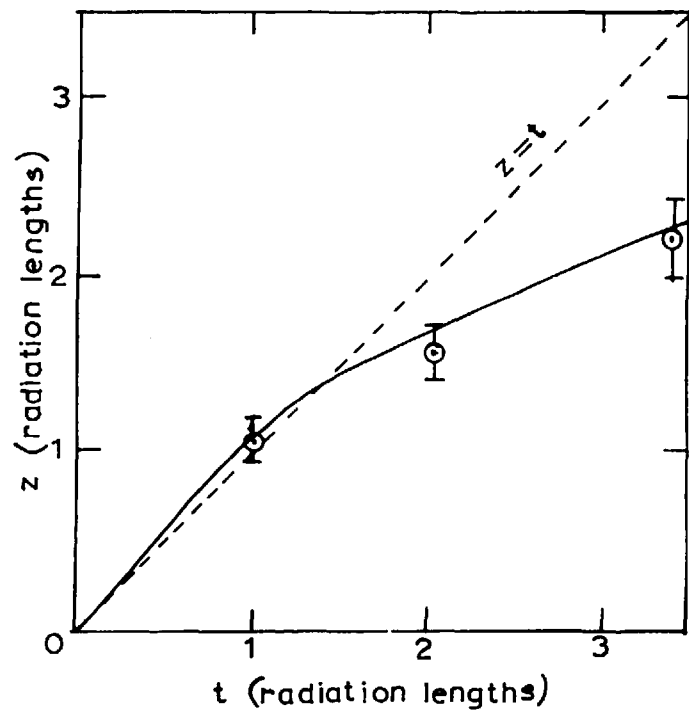


b) $r=4m$ $E_e=120\text{ MeV}$ $\bar{E}=350\text{ MeV}$

Figure 3.1

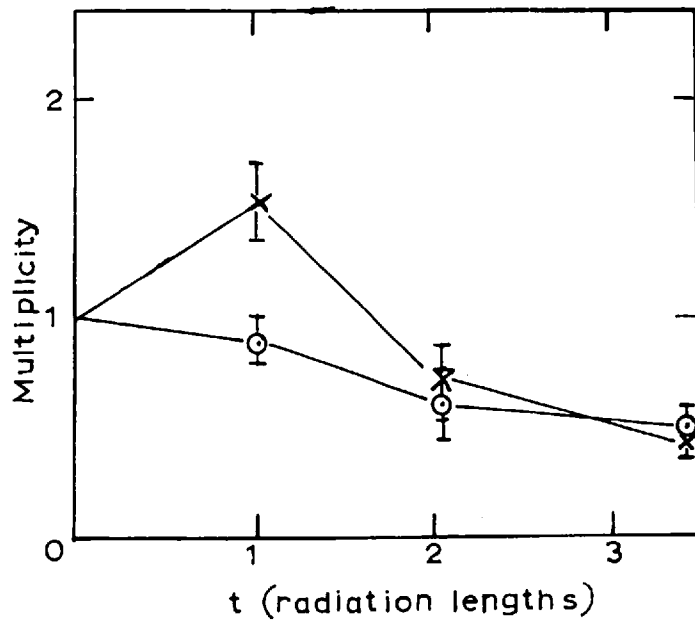


c) $r=8m$ $E_e=130\text{MeV}$ $\bar{E}=240\text{MeV}$



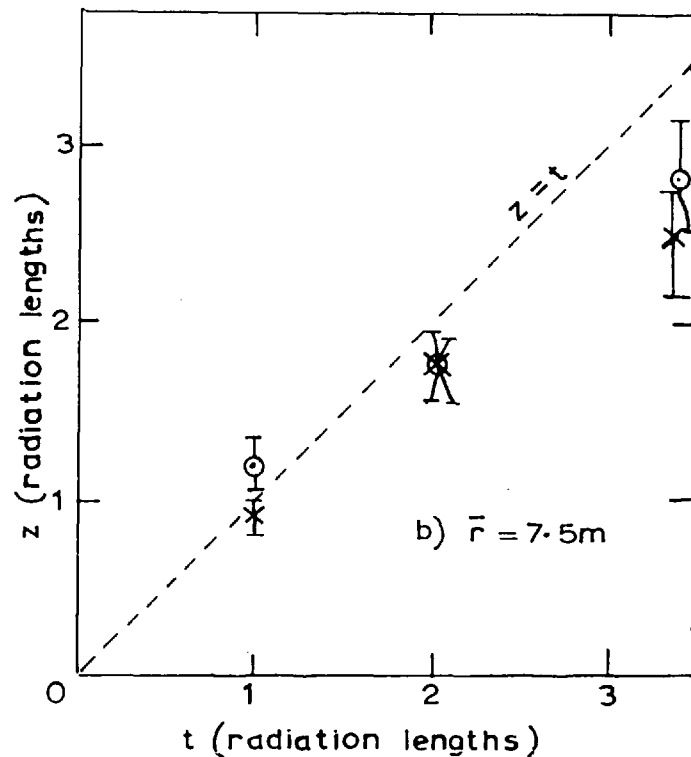
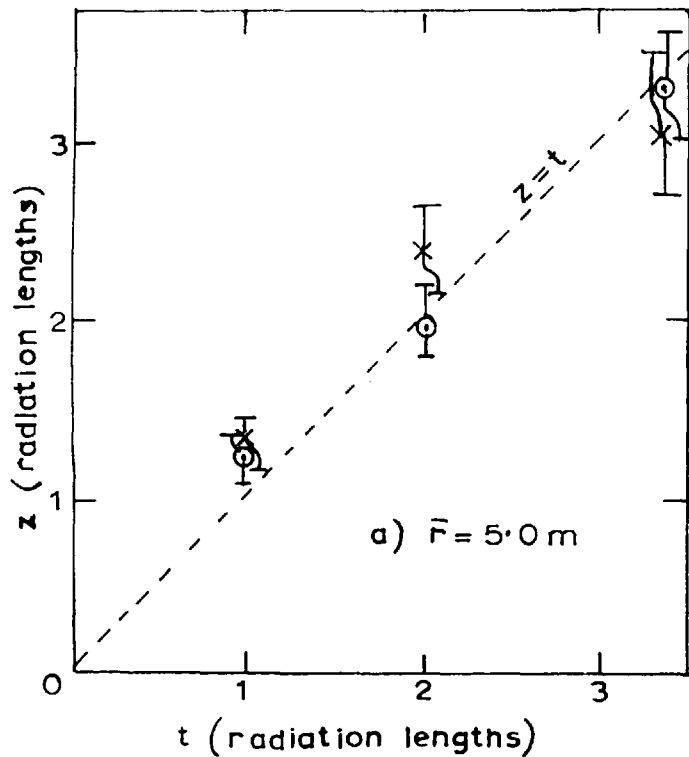
d) $r=12m$ $E_e=120\text{MeV}$ $\bar{E}=195\text{MeV}$

Figure 3.1



\times $\bar{r} = 5.0m$ \circ $\bar{r} = 7.5m$

Figure 3.2



⊙ derived from Cerenkov response functions (figure 3.1)

⊗ derived from particle multiplicities (figure 3.2)

Figure 3.3

track lengths in the detectors are given by the integrals with respect to depth of these multiplicities; and are compared in figure 3.3 with the track lengths derived from the Cerenkov response functions, $n_i(r)$.

Despite the large errors, the multiplicities at 5.0m from the axis are in fair agreement with those found at 1575m above sea level by Green and Barcus (1962) who used scintillation detectors above and below a water absorber of variable depth. However, their results for smaller distances would predict greater track lengths in the Cerenkov detectors than were in fact observed. This could be a consequence of the fact that the energy spectrum of shower electrons is harder at mountain altitudes than at sea level (Toyoda 1962).

Although the estimates of the absolute multiplicities are somewhat rough, it should be possible to determine the radius at which the value is unity quite accurately. Unfortunately this position only lay within the range of observation for the shallow detector, for which the radius was $7 \pm 1m$. For the other depths there was still a marked attenuation even as close as 3m from the shower axis.

3.4 Previous Interpretation

The cascade processes occurring in the detectors reflect the energy distributions of the incident electrons and photons, the form of which varies with distance from the shower axis. If assumptions are made about the form of the energy spectrum, and the relative numbers of

electrons and photons, it is possible to interpret the detector responses in terms of the parameters describing the spectrum. In the earlier experiment, described by Wills (see section 2.1), a differential energy spectrum of the form $E^{-(s+1)} dE$ was assumed and values of the parameter, s , were found which produced the observed distribution of $n(r)$. Spectra of this form appear in 'stationary solutions' of the diffusion equations of shower theory if the latter are derived under Approximation A (Rossi 1952). These solutions are ones in which the shape of the energy spectra and the relative numbers of the electrons and photons do not vary as the cascade develops. They are of the form

$$N_e(E, t) = F_e(E) e^{\lambda t}$$

$$N_\gamma(E, t) = F_\gamma(E) e^{\lambda t}$$

where e refers to electrons and γ to photons.

If, now, it is assumed that the assumptions of Approximation A are valid, the general diffusion equations may be simplified, and the above solutions reduced to the form

$$N_e(E, t) = a E^{-(s+1)} e^{\lambda t}$$

$$N_\gamma(E, t) = b E^{-(s+1)} e^{\lambda t}$$

and similarly for Approximation B;

$$N_e(E, t) = a E^{-(s+1)} P_e\left(s, \frac{E}{\epsilon}\right) e^{\lambda t}$$

$$N_\gamma(E, t) = b E^{-(s+1)} P_\gamma\left(s, \frac{E}{\epsilon}\right) e^{\lambda t}$$

where the functions p_e , p_γ tend to unity for energies large compared with the critical energy, ϵ .

All stationary solutions predict an exponential variation of particle number with depth, and thus for a particular depth of detector, the value of the response function, $n(r)$, depends solely on the value of λ applicable to that radius. The distance at which $\lambda = 0$ is most interesting; here the cascade remains unchanged as it propagates through the absorber; consequently, the values of the response function, $n(r)$, and the multiplicity remain at unity for all depths of detector. Comparison of these predictions with the present experimental results show that the assumptions that lead to them are obviously not valid: the distance at which $n(r) = 1$ varies between 14m for the depth of 1.0 radiation lengths and 2m for that of 3.4 radiation lengths; and likewise, for a multiplicity of unity, the variation in distance is from 7m to less than 3m. Again, if the particle numbers vary exponentially, then the rate of track length production must always increase or decrease with depth - a condition which, from figure 3.1, can be seen to apply only to the distance of 2m from the shower axis. At this distance the experimental track length points may be fitted for a value of $\lambda = 0.2$, which under Approximations A and B corresponds to the spectrum parameter of $s = 0.8$.

It is clear from purely physical considerations that any model which demands an exponential increase of the number of electrons with

depth must break down if the depth is large enough, otherwise the total energy dissipated through ionisation would diverge for an infinitely deep detector. By similar reasoning a spectrum with $s < 1$ is not physically realizable for all E , since the energy integral diverges.

It may be concluded that, for the range of distances $2m < r < 12m$, the stationary solution of the diffusion equations are not sufficient to describe the shower development in detectors of these depths. An alternative approach, which is described in the following sections, is to consider the separate cascade contributions from individual particles in the incident spectrum.

3.5 Relation of Track Length to Incident Particle Energy

In order to compute the separate track length contributions from individual incident particles it is necessary to know the manner in which the resulting cascades develop in the water. The principal physical processes which occur at shower energies are Bremsstrahlung and pair production, with secondary effects such as Compton interactions and ionisation losses becoming significant at energies below about 100 MeV. In the cascade calculations of Butcher and Messel (1960) the accurate Bethe-Heitler cross sections for Bremsstrahlung and pair production have been used, and Compton and collision losses allowed for. Monte Carlo methods were used to determine the average number of secondary electrons above certain energies at selected depths in air and aluminium absorbers; and the results tabulated for secondary energies above a minimum of 5 MeV.

They also showed that, in common with the cascade results of Approximations A and B, if the depth is measured in radiation lengths and the energy in terms of the critical energy of the electrons in the medium, then there is close agreement between the results for both absorbers. Thus these results may be scaled to describe showers in other media; and since the critical energy for water (65 MeV) lies between the values used by Butcher and Messel (95 MeV for air and 52 MeV for aluminium) the cascade figures for water could be obtained quite accurately. Before these results could be applied to the present detectors it was necessary to extrapolate the individual energy spectra of secondary electrons obtained at various absorber depths from 3.3 MeV (the lower limit after scaling) to 0.8 MeV, the Cerenkov threshold. The probable error in this extrapolation was estimated to be not greater than 20% and in most cases less than 10%. Curves of the average number of secondary particles, $N(E_0, t)$, for different depths, t , were plotted as functions of the energy of the initiating electron or photon, E_0 . Figure 3.4 is a plot of such curves and illustrates the measure of agreement obtained for a water radiator from the two independent sets of data. Finally, the quantities of figure 3.4 are replotted in figure 3.5 as $N(E_0, t)$ versus t for fixed values of E_0 .

The total electron track length, $z(E_0, t)$, due to an incident particle of energy, E_0 , is simply the integral

$$z(E_0, t) = \int_0^t N(E_0, t') dt'$$

These integrals are plotted in figure 3.6 from which it is seen that the deep detectors are capable of absorbing almost completely the cascades initiated by electrons with energies below 200 MeV and photons with energies below 100 MeV. It is interesting to note, as confirmation of their accuracy, that these curves asymptotically approach the maximum electron track length which would be expected from a very deep detector in which the whole of the primary energy would be dissipated by ionisation (2 MeV/ g cm^{-2}).

3.6 Track Energy Spectra

The total track length, z , due to a differential spectrum of incident electrons or photons, $n(E) dE$, is given by integrating over the whole energy spectrum. Thus

$$z(t) = \int_0^{\infty} n(E) \int_0^t N(E, t') dt' dE$$

For any such spectrum it is possible to find the average energy per incident electron, \bar{E} , which is the ratio of the energy density of the electron-photon component to the associated electron density. If the mean energies of the electrons and photons are E_e and E_γ respectively, and the number of photons per electron is n_γ , then

$$\bar{E} = E_e + n_\gamma E_\gamma$$

The spectra considered in the present calculations were of the

FIGURE 3.4 Average number of secondary electrons of energy greater than 0.8 MeV, $N(E_0, t)$, for different depths, t , as a function of the energy of the initiating electron (a) and photon (b), E_0 .

FIGURE 3.5 Figure 3.4 is replotted as the average number of secondary electrons of energy greater than 0.8 MeV, $N(E_0, t)$, as a function of depth, t , for cascades initiated by electrons (a) and photons (b) of energy E_0 .

FIGURE 3.6 The total track length of secondary electrons, z , as a function of depth, t , for different primary energy electrons (a) and photons (b); i.e. the integrals with respect to t of the curves of figure 3.5.

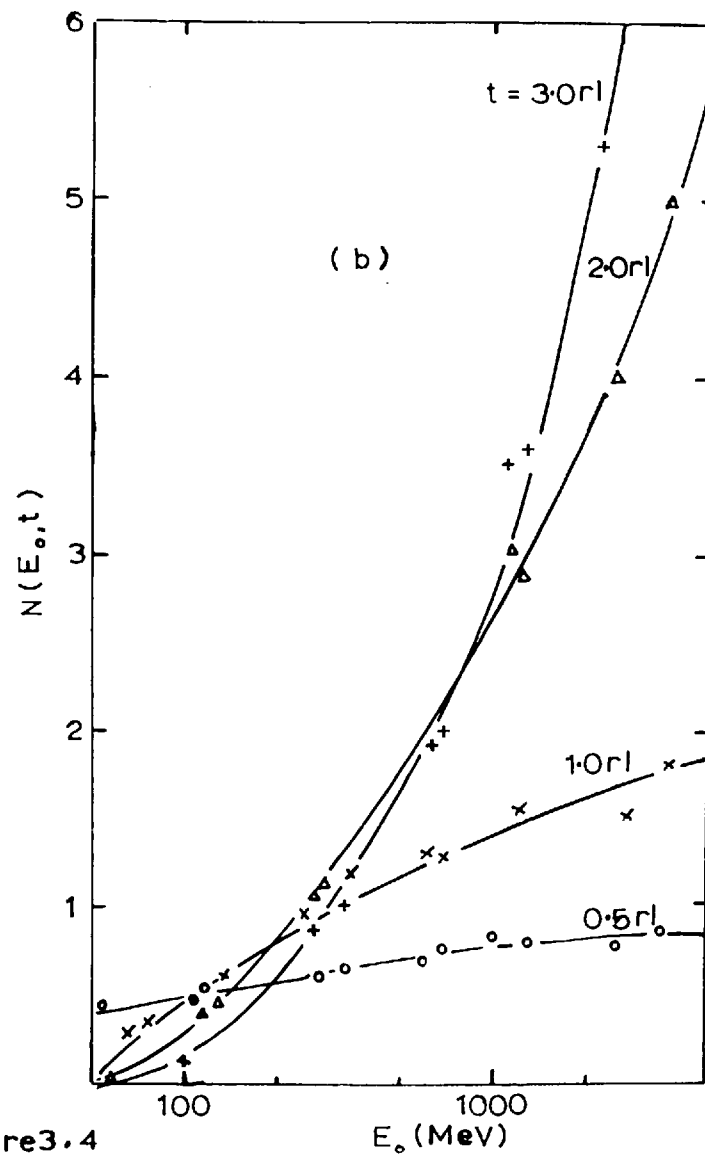
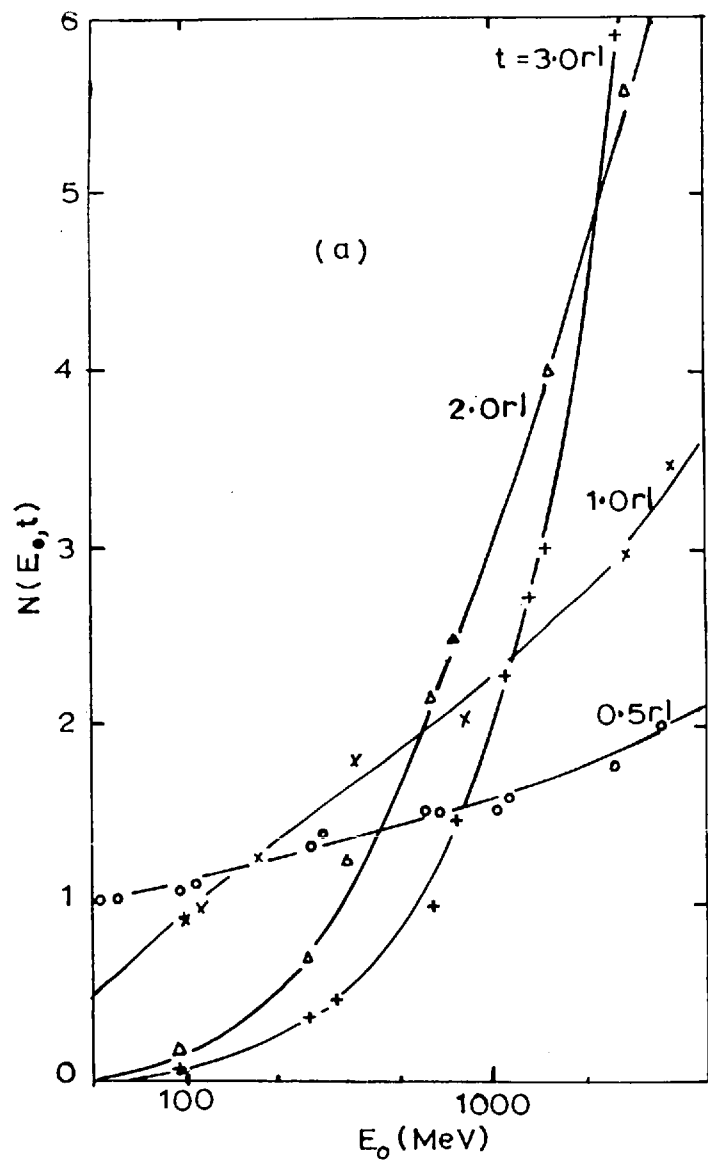


Figure 3.4

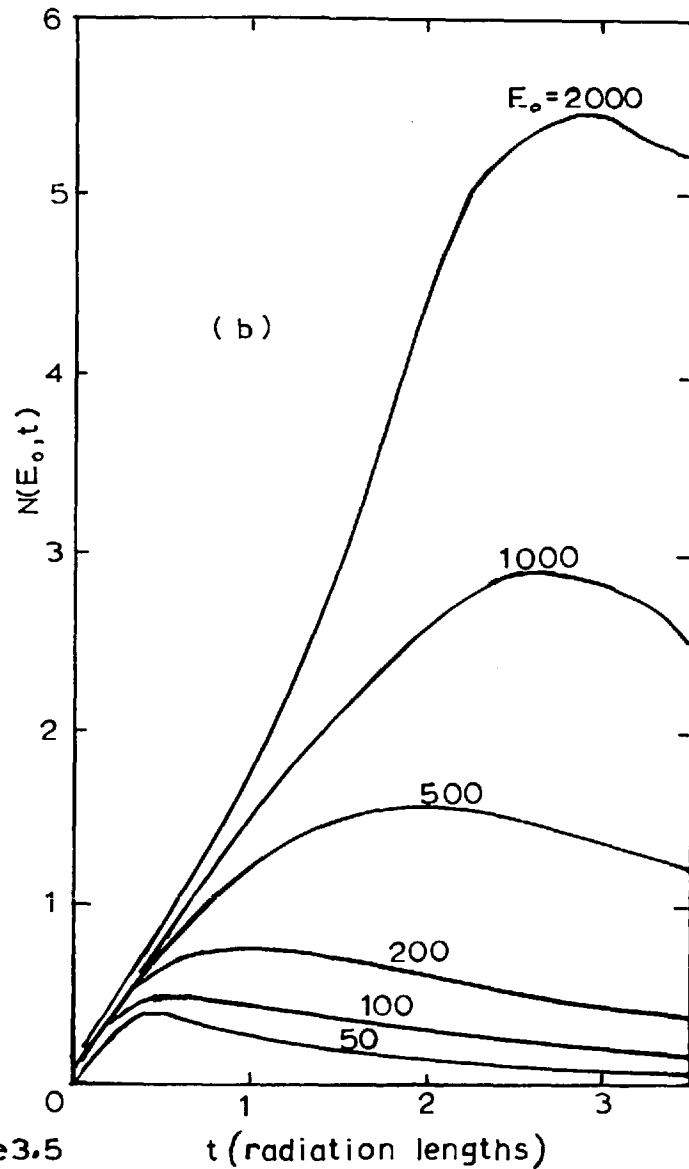
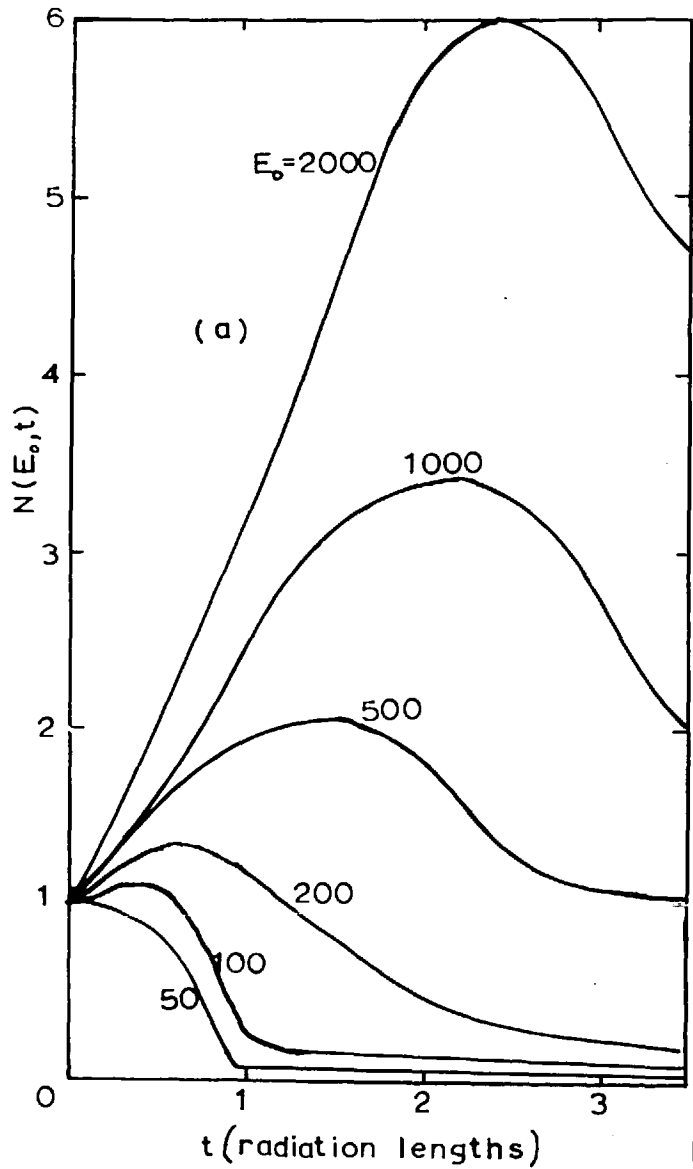


Figure 3.5

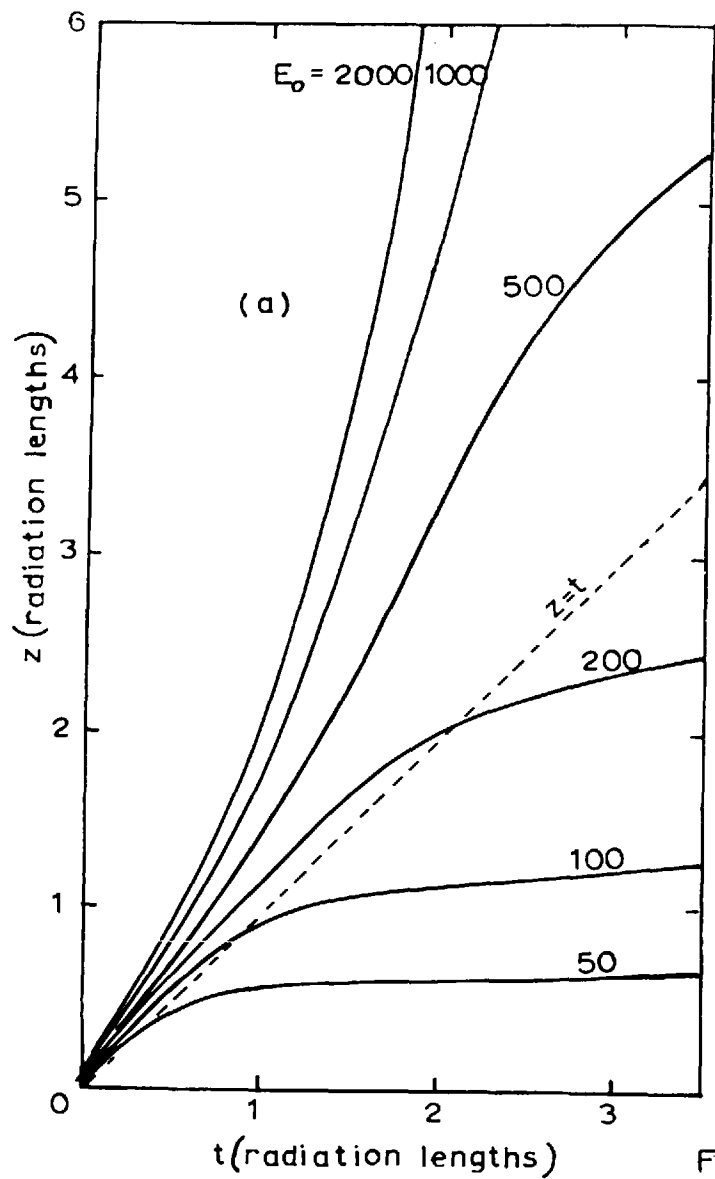
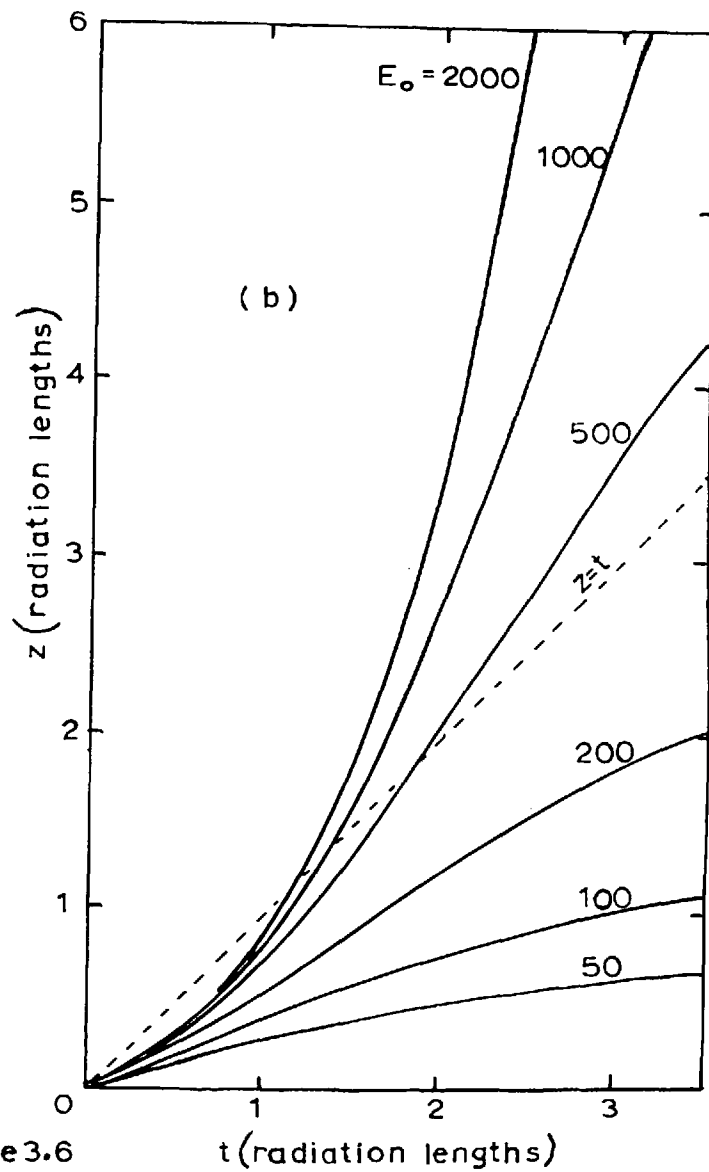


Figure 3.6



form

$$n(E) dE = 0 \quad E < E_{\min} \quad (3.1.a)$$

$$n(E) dE \propto E^{-(s+1)} dE \quad E \gg E_{\min} \quad (3.1.b)$$

Recent experimental evidence (Toyoda 1962, Ivanovskaia et al. 1957), obtained with cloud chambers at sea level, suggests values for the parameter s near 1.8. It was found that, over the relevant range of variables ($1.2 \leq s \leq 2.0$ and $7.5 \text{ MeV} \leq E_{\min} \leq 150 \text{ MeV}$) the computed values of $z(t)$ for $t = 1.0, 2.05$ and 3.4 radiation lengths depended only on the mean energy of the spectrum E_e or E_γ . Qualitatively, this is not altogether unexpected when it is considered that the majority of the energy is carried at the low energy end of the spectra, and consequently the greater part is absorbed within the first one or two radiation lengths.

For mean energies greater than about 200 MeV the track length was found not to differ from that which would be given by a single incident particle of energy E_e or E_γ . The track lengths for energies greater than 400 MeV were therefore calculated according to this approximation.

3.7 Radial Distribution of Energy

From the previous section it appears that the track length in the detectors due to a spectrum of electrons or photons is uniquely related to the mean energy of that spectrum, provided that the spectrum does not differ greatly from that given by equation 3.1. Thus, if the calculated

track lengths due to combinations of such spectra are compared with the experimental results for different depths, it should be possible to determine the mean energies of the electrons and of the photons. The variation of the track length, z , with detector depth, t , is given by

$$z(E_e, E_\gamma, n_\gamma, t) = z(E_e, t) + n_\gamma z(E_\gamma, t).$$

where $z(E_e, t)$ and $z(E_\gamma, t)$ are given by the procedure of section 3.5.

The manner in which z varies with the three unknowns E_e , E_γ and n_γ is such that only two of these may be determined uniquely, even though measurements were made for three values of t . It is clear from the shower curves of figure 3.6 that the cascade development will be concentrated in the top of the detector, either if the energy is carried more by electrons than by photons or if the photon energy is carried by a larger number of lower energy photons. The equivalence of these alternatives was shown by calculations in which n_γ was put equal to 1, 2 and 3 and in each case the values of E_e and E_γ which gave the best fit to the experimental results were found. The accuracy with which the experimental points could be fitted was independent of the value of n_γ selected. With the assumption of $n_\gamma = 1$, curves of z versus t , appropriate to the best values of E_e and E_γ , have been superimposed on the experimental points in figure 3.1.

Although the values of E_e and E_γ could not be found separately,

the value of the composite quantity \bar{E} was found to be independent of n_γ at each of the four selected distances from the shower axis. This is to be expected on the same qualitative grounds as were discussed in section 3.6 to explain the dependence of the track length on the average energy of the incident spectrum. \bar{E} is the sum of E_e , which decreases, and $n_\gamma E_\gamma$, which increases, as n_γ is increased. In this respect the data from 1.0 radiation length depth may be taken to be largely dependent on the composition of the incident radiation and that from 3.4 radiation lengths on the incident energy. From such considerations, the fairly rapid early production of electron track length in the detector for all distances out to 12 m from the shower axis rules out the possibility that the majority of the energy in this region is carried by single photons.

The variation of \bar{E} with distance, r , from the shower axis is shown in figure 3.7. Theoretical calculations of the variation with distance from the shower axis of the energy carried by the electrons and photons were made by Kamata and Nishimura (1958). Their results were applicable to the maximum of a pure electron-photon cascade initiated by a primary particle of infinite energy, and though they are said to be insensitive to the shower age it is not unreasonable to expect some measure of disagreement with experimental results for real showers. This expectation has been confirmed by measurements of the total energy per electron obtained with 'ionisation calorimeters' (Dmitriev et al. 1959, Vernov et al. 1959) and with total absorption

Cerenkov detectors (Hasegawa et al. 1962). These results are generally lower than the theoretical values, at least for distances less than about 20m from the shower axis, and the values of \bar{E} obtained in the present experiment are consistent with this observation (see figure 3.7). According to Fukui et al. (1960) the difference between the experimental and theoretical results may be removed by performing the calculations for a primary energy less than 10^{12} eV.

It has been shown in section 3.1 that the response function, $n(\mathbf{r})$, represents the mean track length per particle measured in units of detector depth. Since the energy lost by ionisation per cm of track length in water is about constant for relativistic particles at 2 MeV/cm, the function, $n(\mathbf{r})$, is also a measure of the energy absorbed by ionisation in the water. The broken curve plotted in figure 3.7 is the estimated energy lost by the incident shower particles passing through the tank. For distances greater than about 10m from the shower axis, the deep detectors effectively measure the total energy of the electron-photon component. At closer distances, as much as 30% of the incident energy escapes through the bottom of the tank.

3.8 Partition of Energy between Electrons and Photons

In addition to measuring the total energy per electron this experiment has given some indication of the division of energy between the electrons and photons. This is shown in figure 3.8, where the track length curve for 4m distance from the shower axis (figure 3.1.b)

FIGURE 3.7 The average energy carried by the electron-photon component per electron, \bar{E} , as a function of the distance, r , from the shower axis. The broken curve is the energy lost by the incident shower particles passing through the tank, estimated from the response function $n_{3.4}(r)$.

FIGURE 3.8 A comparison of track length curves for the same average energy divided in different proportions between electrons and photons, based on the results of figure 3.1.b.

FIGURE 3.9 The ratio of the energy carried by photons to that carried by electrons, as a function of the distance, r , from the shower axis. The apparent discrepancy between the experimental and the theoretical values is a function of the assumptions made in interpreting the results, as is discussed in section 3.8.

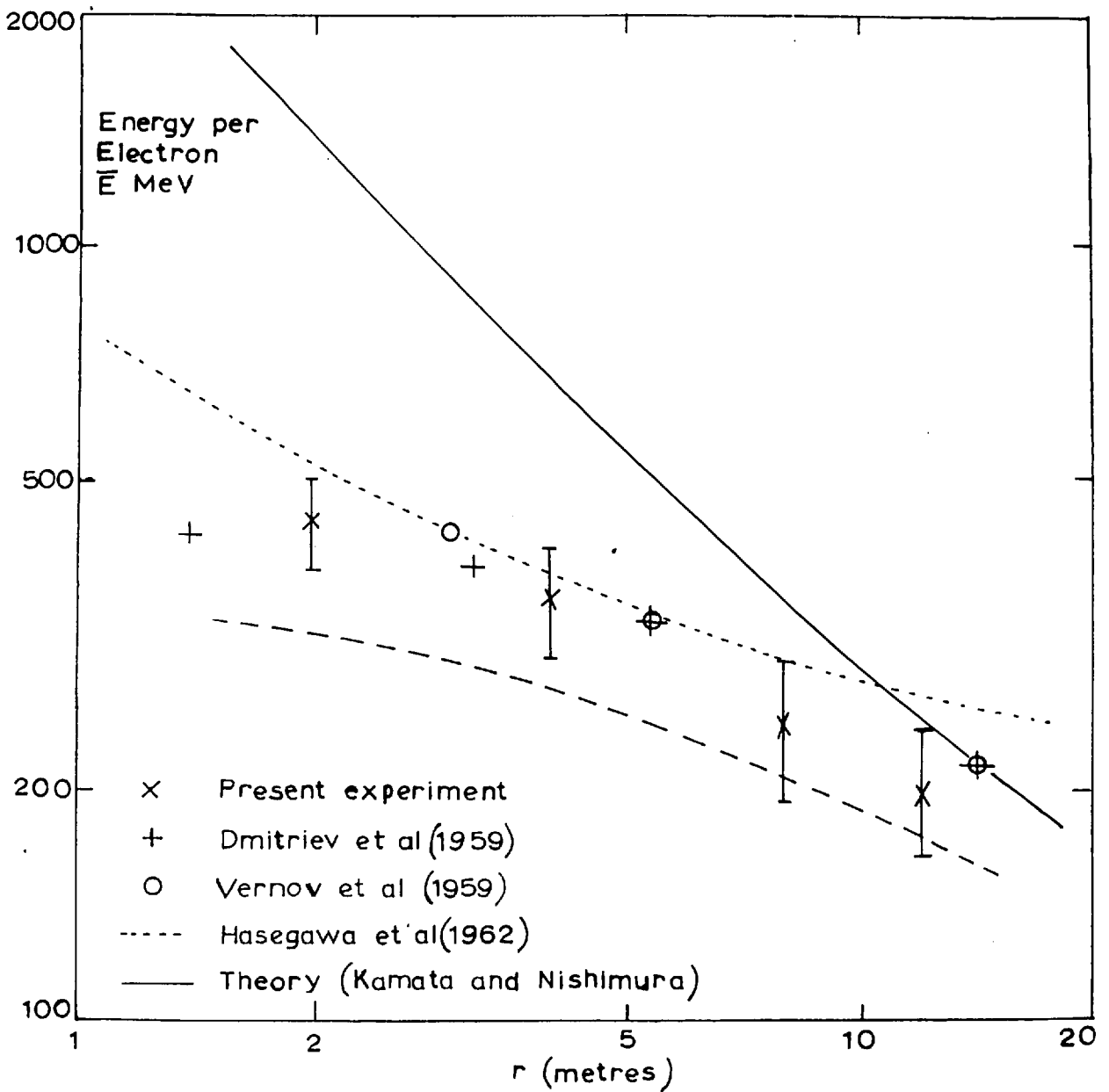


Figure 3.7

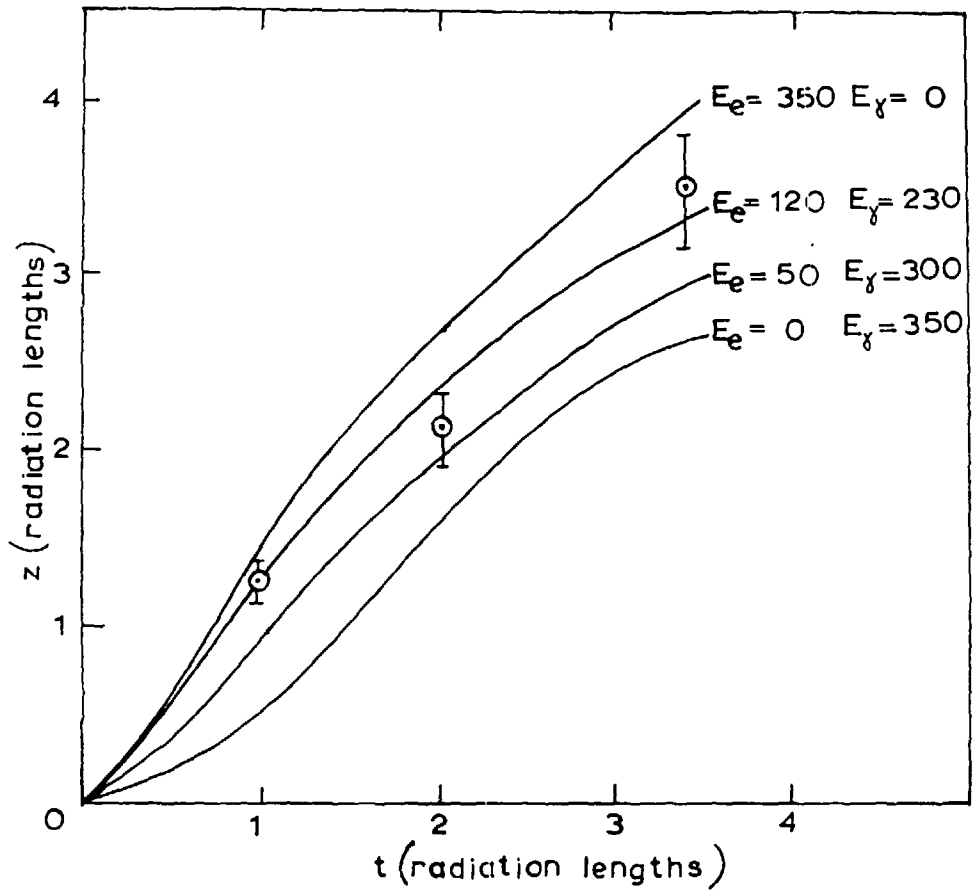
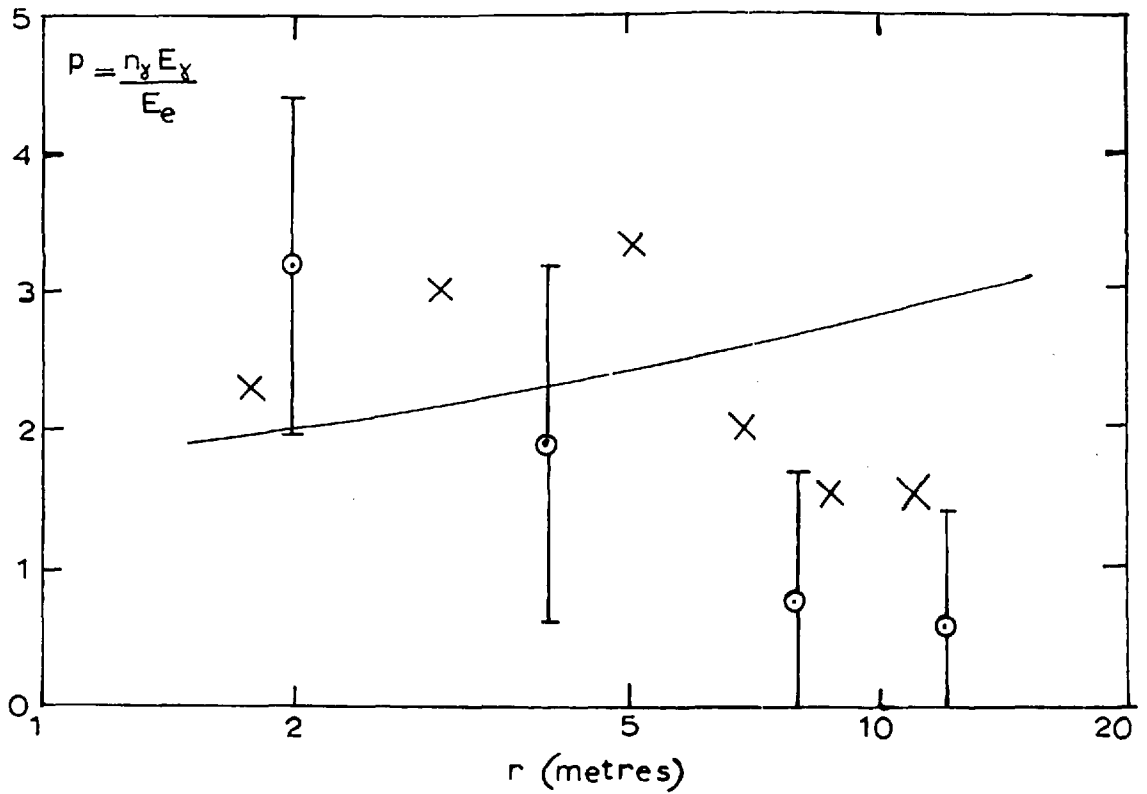


Figure 3.8



- Present experiment
- × Results of Green and Barcus
- Theory (Kamata and Nishimura)

Figure 3.9

is replotted with the superposition of the curves appropriate to cascades initiated by a single electron or a single photon of energy equal to the total energy \bar{E} . Neither of these curves is compatible with the experimental points, which are best fitted by the curve of figure 3.1.b.

Simple cascade theory (Approximation A) suggests that where the energies are high the division of energy between electrons and photons might be roughly equal, but this will not be so at large distances from the axis ($r \gg 100\text{m}$). Here, as discussed in section 3.1, the electrons are produced from relatively low energy photons which originate in the vicinity of the shower core. The individual electron energies do not differ greatly from those of the photons, but the numbers of electrons and photons (and hence also the total energy carried by them) are in the ratio of their characteristic absorption lengths. At minimum absorption the photon absorption length is 60 g cm^{-2} , and this applies over a fairly wide range of energy. The electrons, having energies of only $\sim 10 \text{ MeV}$, lose energy by ionisation and so penetrate less than 10 g cm^{-2} . It is thus expected that up to ten times more energy is carried by the photons than by the electrons. Quantitative confirmation of this is given by the calculations of Kamata and Nishimura (1958). Experimental evidence that at distances $\sim 100\text{m}$ from the axis the electrons are accompanied by many photons has been given by the smallness of the statistical fluctuations in the response of photon-sensitive detectors (Allan et al. 1960).

The ratio of the energy carried by the photons to that carried

by the electrons is given by

$$p = \frac{n_{\gamma} E_{\gamma}}{E_e}$$

As has already been pointed out (section 3.7) it is not possible to determine n_{γ} , E_{γ} and E_e separately from the experimental data, so this ratio cannot be measured unambiguously. One possible procedure, adopted by Green and Barcus (1962), is to assume that $n \approx 1$ at all distances from the shower axis. The values of p obtained in the present experiment under this assumption are shown in figure 3.9, together with those given by Green and Barcus, suitably scaled for the variation of the Molière unit with altitude. These measurements are in general agreement, but differ somewhat from the theoretical predictions of Kamata and Nishimura. For $r \gg 7$ metres the experimental values of p are significantly lower than the theoretical ones.

Green and Barcus suggest that the decrease in the ratio, p , at larger distances should be expected because at such distances the energies of both electrons and photons would eventually fall to the critical energy and remain there, so that p would approach unity. The arguments outlined above and given in detail by Kamata and Nishimura show that this is unlikely: it seems more reasonable that the assumption of $n \approx 1$ should be modified. A value of n which increases to 2 or 3 at $r \approx 10$ m does in fact lead to agreement between the theoretical and experimental values of p , without affecting the measured average energy, \bar{E} .

3.9 Conclusions

In addition to studying the energy distribution of the shower particles, the experiment just described has illustrated the potentiality of the deep detectors as energy sampling devices. In the following chapters two further experiments are described which utilise this property in the investigation of large and small scale air shower phenomena.

CHAPTER 4

THE DENSITY SPECTRUM

4.1 Introduction

The integral density spectrum of EAS is the frequency of occurrence of showers having a particle density greater than Δ at the place of measurement, irrespective of the sizes and axis locations of the showers. Experimentally, it has been found to follow a power law of the form

$$R (>\Delta) = R_0 \Delta^{-\gamma}$$

with γ increasing from 1.4 to 1.6 over the density interval 2 particles m^{-2} to 500 particles m^{-2} . Measurements, especially at low densities, have mainly been made using coincident Geiger counters, separated by one or two metres to select air showers. The results of most of these experiments, and others using proportional counters, ionisation chambers and cloud chambers have been summarised by Greisen (1956), and will not be discussed further, except to refer to the relevant results.

Another approach which has been used recently by several authors is to measure the integral pulse height spectrum from a single, flat, scintillation detector. This was first done at mountain altitudes by Green and Barcus (1959) who used a liquid scintillator of area $7.3 m^2$; and later by Delvaille et al. (1960) and Miyake et al. (1962) who used smaller plastic scintillators at sea level. Included in the latter experiment was a measurement of the energy content of the electrons

producing the observed densities. The altitude of these observations and the detector dimensions are given in table 4.1, and the resulting spectra presented in figure 4.1.

Table 4.1: DETAILS OF SCINTILLATOR EXPERIMENTS				
Authors	Detector		Altitude of observation	Position of 'link'
	Area m^{-2}	Thickness $g\ cm^{-2}$		
Green and Barcus (1959)	7.3	12	1575m	$6m^{-2}$
Delvaille et al. (1960)	0.86	thin	260m	$45m^{-2}$
Miyake et al. (1962)	0.36	2.5	Sea level	$60m^{-2}$
			2100m	$100m^{-2}$
Miyake, Hinotani et al. (1962)	0.25	thin	2770m	$100m^{-2}$

The higher density portions of these curves agree closely with the EAS density spectrum as found by the coincident Geiger counters technique; the lower portions, however, are considerably steeper than expected. Both Delvaille et al., and Miyake et al. have found that if, as a triggering condition, at least one particle is simultaneously recorded in a second scintillator placed a few metres away, the steep portions of the curves are no longer present. This behaviour suggests

that, in the case of a single detector, there is superimposed on the EAS density spectrum a steeper spectrum resulting from local, narrow showers which are almost wholly contained within a radius of perhaps 1m from the axis. Such showers would be automatically excluded if coincidences were demanded over distances greater than this. The point at which the integral pulse height spectrum begins to diverge from the EAS density spectrum occurs towards higher densities as the area of scintillator decreases; - a further indication of the presence of narrow showers which predominate at low densities.

The following sections describe an experiment designed to study in more detail the nature and possible causes of these local events. The large sensitive area of the Haverah Park detectors, up to a maximum of 34 m^2 , has allowed reliable statistical results to be obtained at densities below $1 \text{ particle m}^{-2}$; while their depth of 3.4 radiation lengths has enabled estimates to be made of the average energy associated with the incident flux.

Unlike scintillators, which measure essentially the ionisation loss of the intercepted particle in the scintillation medium, Cerenkov detectors are strongly biassed towards the detection of light, charged particles. The threshold energy for the production of Cerenkov light rises linearly with particle mass. Consequently, an electron in water requires only 265 KeV before it radiates, whereas a proton needs a kinetic energy near 500 MeV. The possible nature of the radiation has

FIGURE 4.1 Integral pulse height spectra obtained by various authors with scintillators of different areas.

FIGURE 4.2 Block diagram of recording systems.

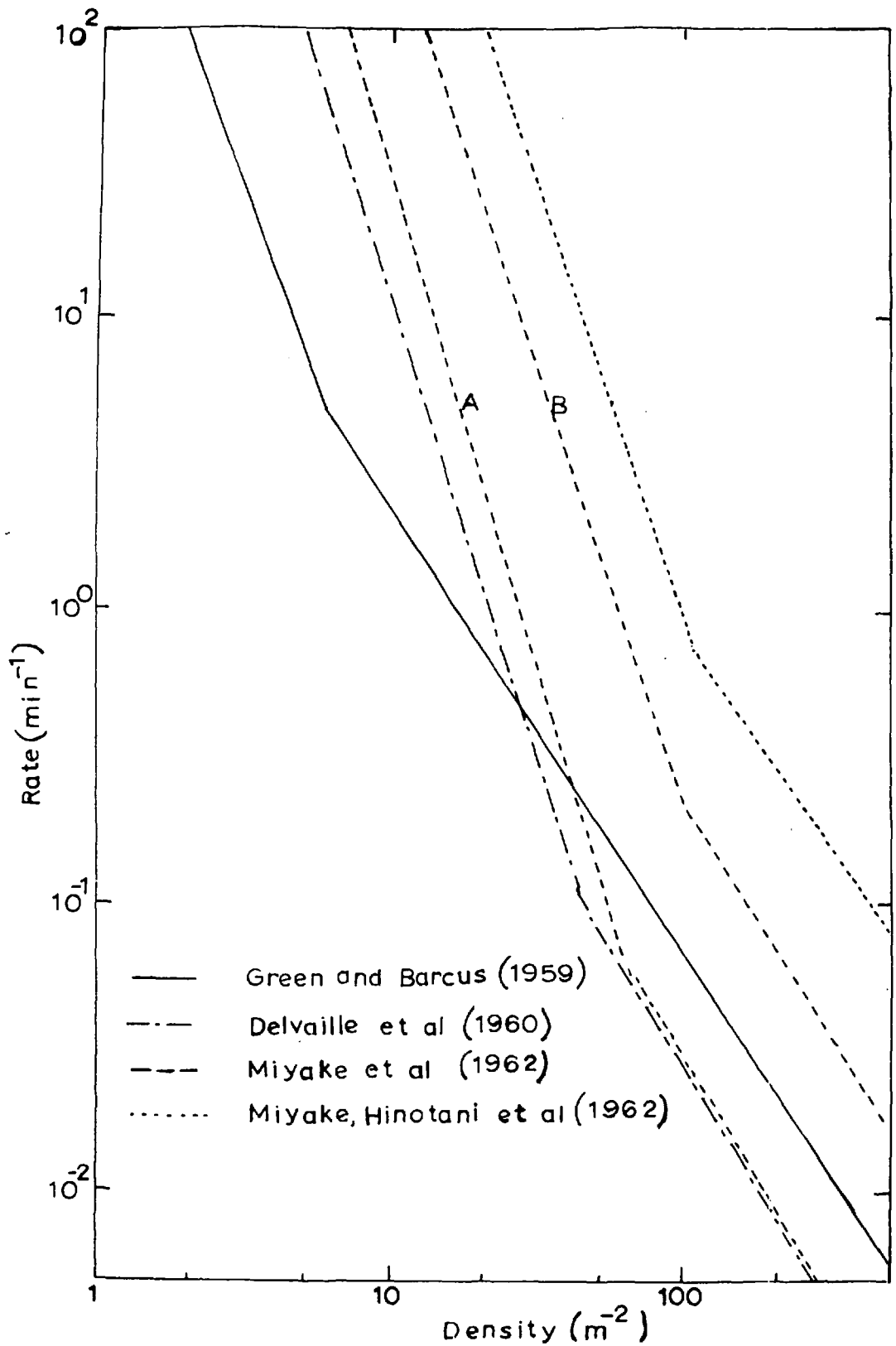


Figure 4.1

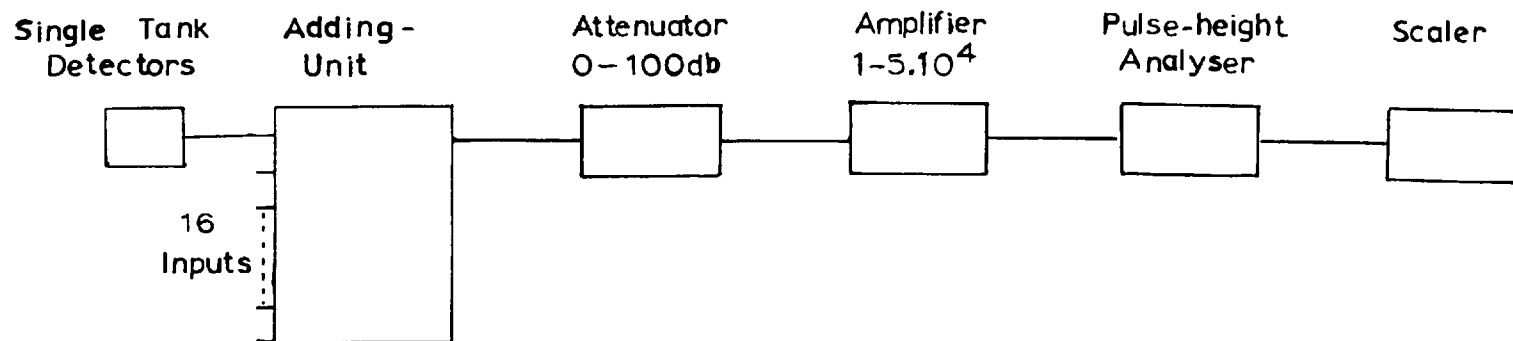


Figure 4.2

therefore been examined by comparing the responses of the two types of detector.

4.2 Apparatus

The single detector has been described in some detail in Section 2.2. It consists of a water-filled tank; 4 feet x 6 feet in surface area and 4 feet deep. The Cerenkov radiation emitted is sampled by a single 5-inch photomultiplier, the output of which is passed through an emitter follower and into an adding-unit. The latter adds the photomultiplier outputs of 16 such detectors. In order to examine the pulse height distribution from several combinations of detectors the added output was then fed into an analysing circuit consisting of a variable amplifier (Nuclear Enterprises, NE 5202) of maximum gain $5 \cdot 10^4$, followed by a single channel pulse height analyser (Nuclear Enterprises, NE 5103) and a scaler (Ekco No. 51459). An attenuator of total range 0-100 db, variable in 1 db steps, was also included as a means of checking selected points on the pulse height spectrum. A block diagram of the recording system is shown in figure 4.2.

4.3 Calibration

Section 2.5 has described the calibration of a single detector in connection with the 6m array. An identical procedure was employed here; briefly, a three-fold scintillator telescope selected near-vertical muons passing through the detector and the associated pulse outputs were recorded photographically from an oscilloscope. A mean single particle

pulse height of 6.7 ± 0.2 mV was obtained. A second estimate was made by feeding the photomultiplier output from a single tank into the analysing circuit, the output of which was gated by the telescope pulse. The differential pulse height spectrum for single particles was then plotted in 2 mV intervals and the mean pulse height found to agree with that above to within the accuracy quoted.

The gains of the remaining detectors were made equal to that of the calibrated one by adjusting the E.H.T. supplied to each photomultiplier until their integral count rates above a fixed discrimination level were the same. In order to obtain small statistical spreads, a level corresponding to two particles traversing the standard detector was selected; which produced an integral rate of 1000 counts in about 40 seconds. In this, and subsequent work when the maximum detector area was used as a station of the 500m array, it was found possible to maintain a uniform integral rate across the detectors to within $\pm 10\%$; which, because of the steepness of the exponent of the pulse height spectrum in this region ($\gamma < -3$), meant that each detector was kept within $\pm 2\%$ in relative response at the 2 particle level of the spectrum.

Calibration of the electronic recording equipment was effected using a General Radiological Pulse Generator that was itself set up using a Standard A.V.O. The combined errors allowed the final discrimination level to be ascertained with a 5% uncertainty.

4.4 Experimental Details

Integral pulse height spectra were measured for the three separate detector areas: 2.25 m², 9.0 m² and 34 m², corresponding to a single tank, 4 adjacent tanks, and a 15-fold addition. The major part of these spectra could be obtained within a few hours, in which time the barometric pressure remained relatively constant. For the days during which these measurements were performed the pressure was found to vary between 985 millibars and 995 millibars which, allowing for the altitude correction, is equivalent to a sea level mean of one standard atmosphere. A few high density points required overnight running for which no continuous monitoring of the pressure could be made; hence, the error on these points is uncertain. However, the maximum pressure difference between the beginning and end of individual runs was found to be 7 millibars, so that the required corrections can be assumed to be small.

To investigate the overall noise contribution from the several components, the photocathode of one of the photomultipliers with a high dark current rating was covered with a black adhesive and a bias curve plotted (figure 4.4).

4.5 Results

The resulting density spectra for the three detector areas are presented in figure 4.3, where the integral counting rates are plotted as a function of the 'equivalent density'. This quantity is simply the

observed pulse height per unit area divided by that produced by a single, vertically incident muon. For comparison, the EAS density spectrum given by Greisen (1956) for coincident Geiger counter measurements is also plotted. This latter curve is normalised using the data of Cocconi and Tongiorgi (1949) at 260m altitude, and includes a correction factor for the loss of counts owing to the separation of the counters.

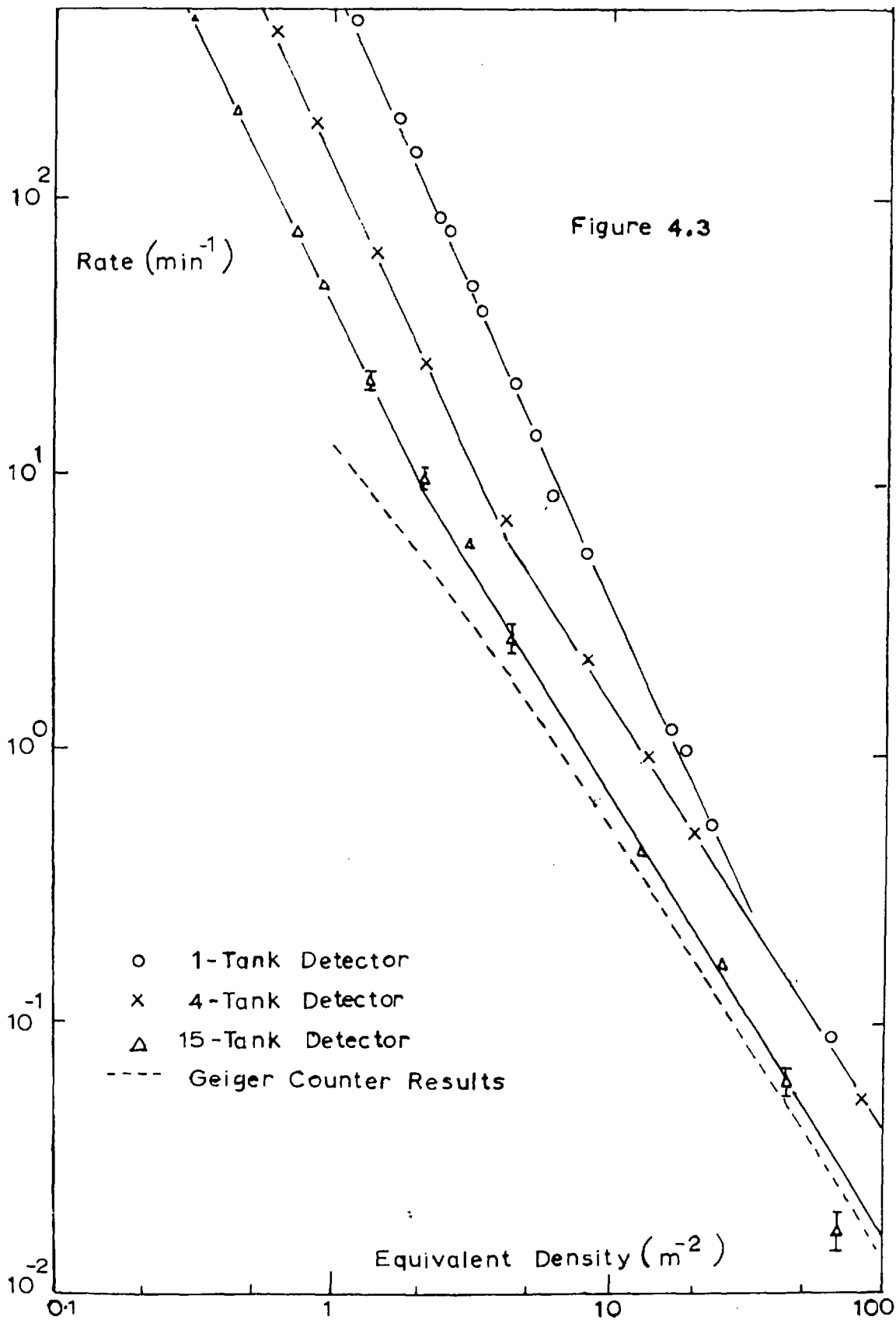
The general features of these curves are similar to those obtained using the smaller scintillation counters described in section 4.1; namely, a steep negative exponent at small densities which flattens and approaches that of the EAS density spectrum with increasing pulse amplitude. Although there is no evidence for a sharp change in slope, it is convenient to fit the best straight lines to the two portions of the curve.

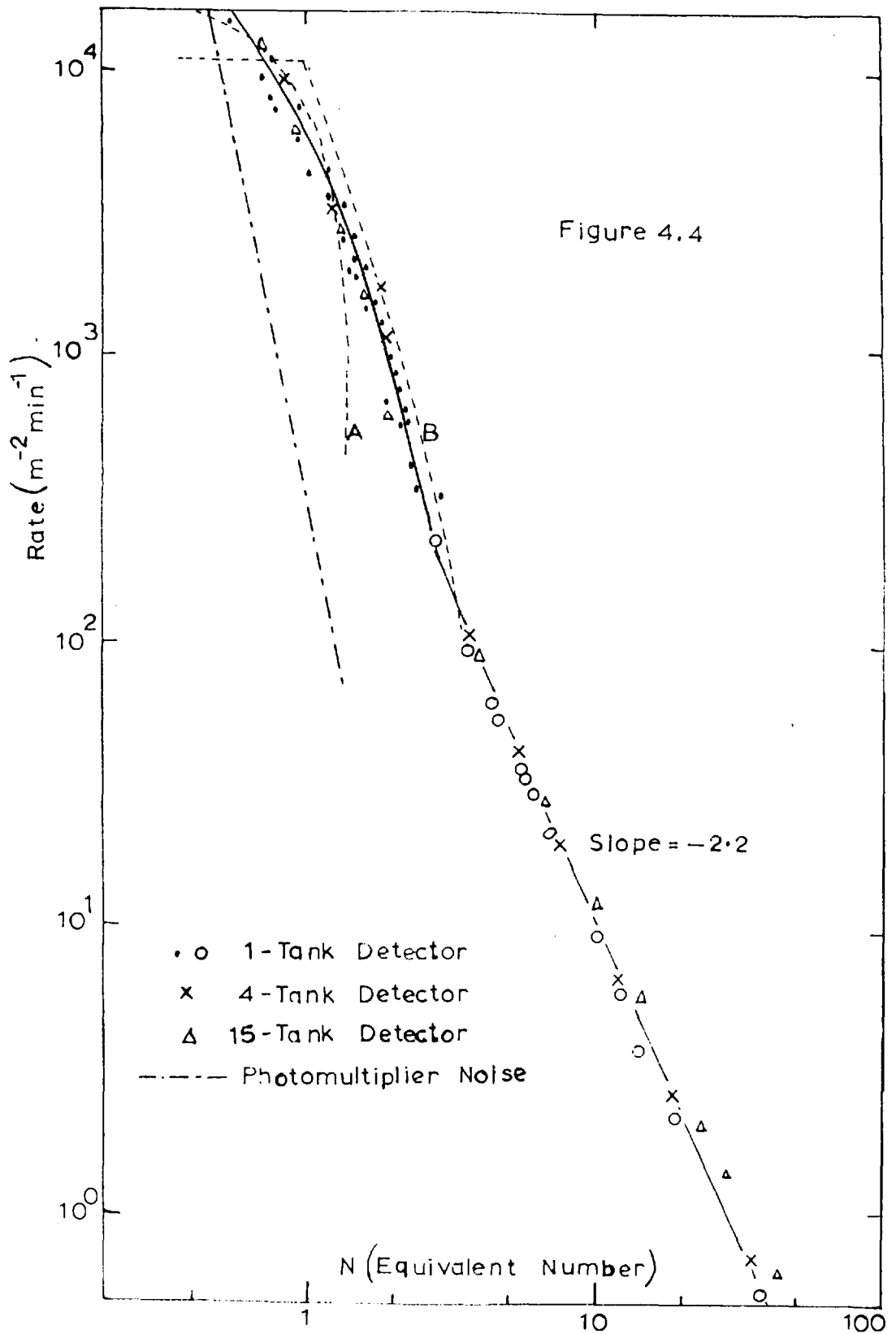
It is interesting to note that, although the spectra for the two smaller area detectors merge when the EAS density spectrum exponent is approached; they do not merge with the 15-tank measurements even at the higher densities, but remain parallel to it, displaced in density by about 50%. An explanation for this behaviour is offered in section 4.8.

In figure 4.4 the steep portions of the curves are plotted again with the integral rate per unit area plotted as a function of the equivalent number of recorded particles. The spectra are here extended back to near the noise level of the photomultipliers, and the noise spectrum of one of the poorer tubes is given. It is now possible to

FIGURE 4.3 Density spectra for three areas of Cerenkov detector.

FIGURE 4.4 Integral rate per unit area as a function of the 'equivalent' number of recorded particles, N . Curves A and B are the distributions expected from the muon flux calculated for a spherical, and flat detector respectively.





draw a single smooth curve through the combined points for all detector areas, which supports the evidence of section 4.1 that the steep portions of the spectra are in fact due to narrow, local showers. It also follows that the majority of these particles must fall within an area much less than $2m^2$; otherwise the single tank would lose a substantial fraction of the particles in the shower, causing these points to lie below those of the detectors of larger areas.

The complex form of the integral pulse height distribution in figures 4.3 and 4.4 arises from the superposition of a number of component spectra, each of which dominates in turn over a limited density interval. The possible sources of such spectra in the incident cosmic ray flux and their relative importance are discussed in the following section. An understanding of the processes present is important for work on the 500m array as it is proposed to maintain the stability of the large detectors by monitoring the integral rate above a discrimination level within this range.

4.6. Muon Component

The portion of the spectrum in figure 4.4 below the value $N = 2$ was obtained with a single tank and may be attributed to the muon component. Also shown (curve A) is the spectrum to be expected from the muon flux, calculated, as a convenient approximation, for the case of a spherical detector of the same volume as the tank. The separation of the curves at the larger values of N is a result of this approximation:

the maximum track length for the sphere is only 1.4 detector depths, whereas the diagonal of the tank corresponds to 2.1 depths. Curve B is that expected for an infinite area flat detector of finite thickness, and is a close approximation to the spectrum expected from the 15-tank detector. The derivation of these curves is outlined in Appendix 1.

4.7 Local Showers

The bursts producing the track lengths above $N = 2$ arise principally from electron-photon cascades. These may be initiated either by photons created by the decay of neutral pions, or electrons produced from muon decay and knock-on processes. Contributions, at sea level, from processes such as muon Bremsstrahlung and pion and proton knock-on are negligible (Puppi 1956). Also, such processes as star formation, which has been suggested by Green and Barcus (1959) to explain a similar effect in scintillators, remains unimportant with water Cerenkov detectors because of the high inherent threshold energies.

4.7.1 Electrons arising from Muons

If a high energy electron is produced in the atmosphere above the tank, the extent of the resulting cascade which develops in the water will depend on the height of the electron production. Consequently, an electron of energy, E_0 , will be able to produce a Cerenkov pulse of minimum size, N equivalent particles, provided it is produced between certain limits of atmospheric depth. In general, these limits define a region, $x \text{ g cm}^{-2}$ thick, which extends from inside the detector to a

point above.

The writer has calculated values of x for different values of minimum shower size, N , and electron energy, E_0 (figure 4.5). The modified Butcher and Messel tabulations for the electron track lengths in air and water (see section 3.5) were used for energies less than 5 GeV. For higher energies, the shower curves obtained by Rossi (1952) under Approximation B were used in conjunction with the same cascade predictions of Kamata and Nishimura (1958) as were applied in section 3.1 to determine the Cerenkov detector response functions at large distances from the shower axis. These authors suggested that at such distances the electrons are produced (mainly by the Compton process) from relatively low energy photons which, because of their long absorption length ($\sim 60 \text{ g cm}^{-2}$), have been able to penetrate considerable depths of atmosphere. For a detector of depth 3.4 radiation lengths, a limiting response of 0.42 equivalent particles per incident electron was obtained. These same arguments may be applied to the electrons in a shower well beyond its maximum development. In the calculation of x for high energy primaries, each electron in a shower remnant was therefore assumed to produce a track length equivalent to 0.4 detector depths.

4.7.2 Decay Electrons

In appendix 2 it is shown that in three body muon decay

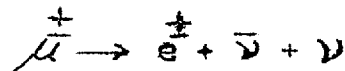


FIGURE 4.5. Values of the parameter x for different values of the minimum shower size, N , (the numbers attached to the curves) as a function of the energy of the initiating electron, E_0 .

The broken line is the average lateral displacement per radiation length, r , of an electron of energy E_0 .

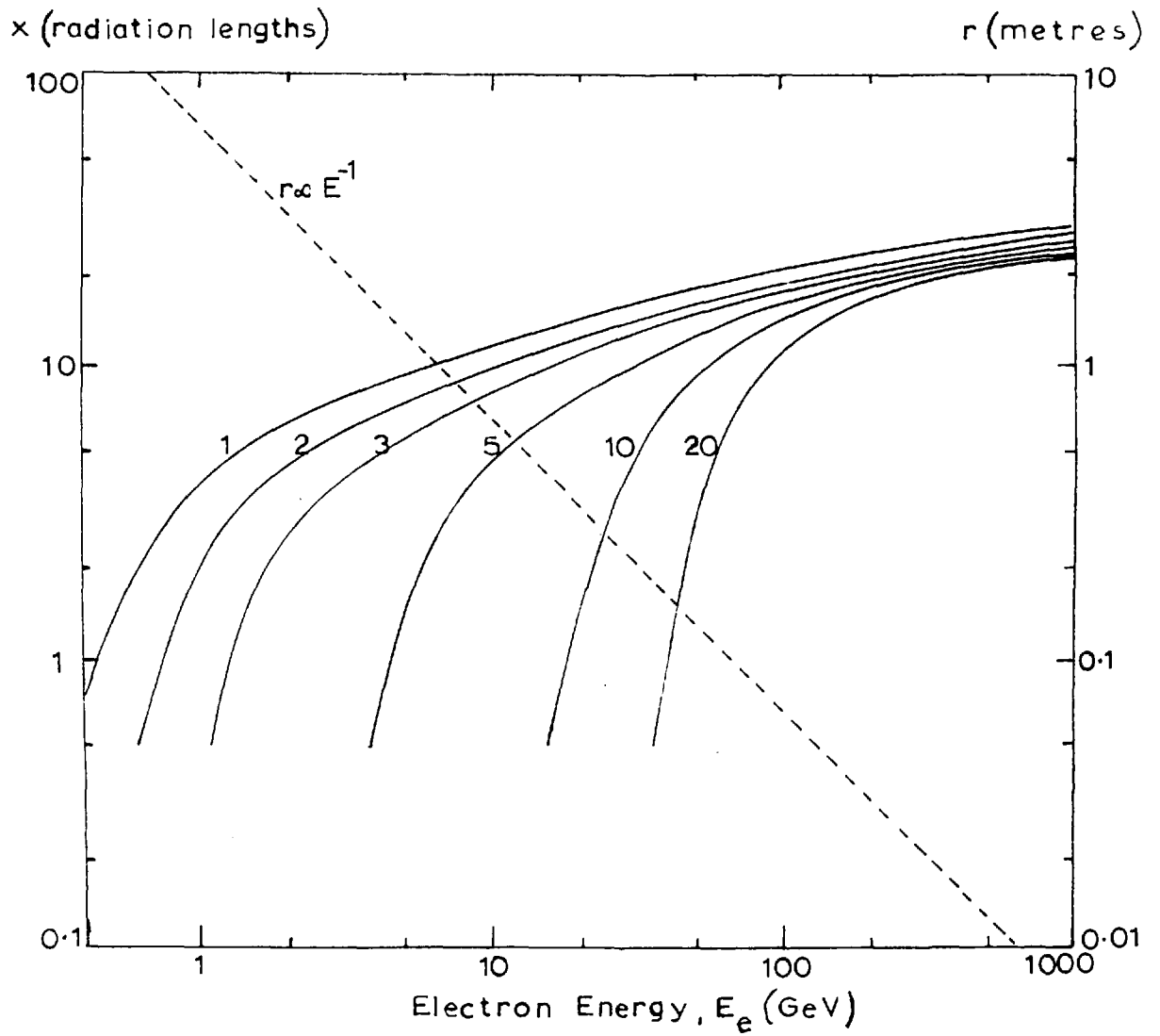


Figure 4.5

the electron, on average, takes a third of the muon energy.

The contribution to the integral rate for showers above a size, N_0 , was estimated by summing the contributions from roughly equal logarithmic intervals of the muon energy spectrum. The average energy for each interval was calculated and the decay electrons were assumed to possess one third of this energy. The contribution to the integral rate is simply $n_0 (1 - e^{-x/\lambda})$ where n_0 is the number of muons in the energy interval, λ is the calculated decay mean free path for the average energy muons, and x is the distance over which the decay electron is capable of producing more than N_0 equivalent particles in the tank. The separate contributions were found to converge rapidly with increasing muon energy, and the total contribution could therefore be estimated fairly accurately.

The calculation was performed for a number of points between $N = 2$ and $N = 20$, and yielded an estimated contribution which was typically of the order of $1/4$ of the observed rate.

4.7.3 Knock-on Electrons

The collision probability for a muon of kinetic energy, E , traversing a thickness of $dx \text{ g cm}^{-2}$, to release an electron with kinetic energy between E and $E + dE$, has been calculated by Bhabha (1938) and Massey and Corben (1939). It is

$$P(E, E) dE dx = \frac{0.3 m c^2}{\beta^2} \frac{Z}{\Lambda} \frac{dE}{E^2} \left(1 - \beta^2 \frac{E}{E_m} + \frac{1}{2} \frac{E}{E + N_0 c^2} \right)^{-2} \quad (4.1)$$

where E_m is the maximum energy transferable, and M and m are the masses of the muon and electron respectively. When E is small compared with E_m this expression reduces to the classical Rutherford formula for the probability of collision.

The value of E_m is obtained by the application of the conservation laws of energy and momentum to the collision of a muon with a free electron. The maximum energy transfer corresponds to a head-on collision.

$$E_m = \frac{2 (E + Mc^2 + mc^2)^2 mc^2}{M^2 c^4 + m^2 c^4 + 2 mc^2 (E + Mc^2)} - 2 mc^2 \quad (4.2)$$

The contribution to the counting rate from muon knock-on electron showers was estimated by a procedure similar to that used for the decay electrons. The muon energy spectrum was again divided into small, roughly equal logarithmic intervals, and the separate contributions calculated. The average energy muon in each interval is capable of knocking-on electrons up to a maximum energy given by equation 4.2. Thus the total contribution of the interval is made up of the separate contributions of many electrons; their energies being distributed according to equation 4.1. The probability of an electron of energy between E and $E + dE$ producing a pulse of size $> N$ is given by $P(E) dE x_E$: the probability of the electron being formed and the distance over which it is effective in producing the pulse. The total contribution is

$$n_o \int_0^{E_m} P(E) dE x_E .$$

Theoretically, it is possible to integrate such an expression, but, owing to the complex form of the quantities, a numerical summation had to be made.

The above process was repeated for each interval in the muon energy spectrum until the series had converged sufficiently to allow an accurate summation to be made. Once more the expected contributions to the integral count rates were calculated for different values of N between 2 and 20 and were found to be about half the amplitude expected from the decay electron source.

In the above calculations the muon flux appropriate to x_E was used. For this it was assumed that the energy spectrum does not change substantially with altitude up to a height of about 600 g cm^{-2} . The variation of the muon rate with altitude is relatively slow and has only a small effect on the computed sea level spectra.

On the basis of these two estimates it may be concluded that electron-photon showers secondary to muon processes would account for about half the observed rate of track length production; which, even allowing for rather large possible errors, would indicate that an appreciable contribution comes from a different origin.

The estimates just presented were made without reference to the lateral spreads of the contributing showers. This effect is

due principally to the multiple coulomb scattering of the shower electrons and may be approximately expressed as

$$r \simeq 0.67 E^{-1}$$

where r , in metres, is the average lateral displacement per radiation length of an electron of energy, E GeV. This function is plotted on the curves of figure 4.5 and gives an indication of the lateral spread expected from the various electron energies which make up the total contribution to showers of different sizes. It can be seen that for showers larger than $N = 5$, all the contributions should lie within about 2m radius. For smaller showers, however, some of the contributions may be expected to extend to considerably greater distances.

Although contributions from heights up to 15 radiation lengths were included in the estimates, the maximum contribution, at least up to shower sizes of $N = 10$, lay within 5 radiation lengths. It might be expected, therefore, that an appreciable part of the spectrum may result from single high energy electrons cascading in the tank.

Other knock-on contributions, such as the production of more than one high energy electron by a single muon, and knock-on electrons from the light wooden roof and aluminium tank cover were estimated and shown to be negligible in comparison with those above.

4.7.4 Nuclear-Active Particles

It has been pointed out at the beginning of this section that

the occurrence of nuclear stars, with the accompanying low energy evaporation products, would not be observed in a water Cerenkov detector which requires a relatively high threshold energy for light production. This consideration disposes of contributions from nuclear-active particles except in interactions with pion production and the formation of subsequent electron-photon cascades.

Various measurements have been made on the different components of the nuclear-active flux, but unfortunately the total sea level intensity is not well known. The absolute energy spectrum of the nuclear-active particles incident on the tank may be estimated from the measured primary cosmic ray flux if assumptions are made regarding the mean free path for collision, and the inelasticity, K .

A procedure was adopted similar to that developed by Cranshaw and Hillas (1960) to explain the constancy of the shower attenuation and age parameters (λ and s) at high primary energies. Briefly, they considered that showers consist of a chain of nuclear interactions, from each stage of which a relatively short range electron-photon cascade originates. It follows that what are observed at sea level are mostly the products of the last nuclear interaction. With this model the statistical fluctuations at every stage of the cascade become important and must be considered. Suppose a particle of energy, E_0 , is the product of i nuclear interactions, then the energy of the initiating particle must have been $E_0 \beta^{-i}$ where $\beta = 1 - K$ is the elasticity of the collisions. If the primary energy spectrum can be expressed in the form $R(> E) = A E^{-\gamma}$,

then the rate of particles of energy $> E_0$ at a depth t which have suffered i collisions is

$$A P(i) E_0^{-\gamma} \beta^{i\gamma},$$

where $P(i)$ is probability of i collisions and, assuming a Poisson distribution, may be written

$$e^{-m} \frac{m^i}{i!}$$

where m is the mean number of collisions, in this case t/L , where L is the nuclear interaction length.

The total count rate is now simply

$$R(> E_0) = \sum_{i=0}^{\infty} A e^{-m} \frac{m^i}{i!} E_0^{-\gamma} \beta^{i\gamma}$$

which, on summing, reduces to

$$R(> E_0) = A E_0^{-\gamma} \exp - \frac{t}{L} (1 - \beta^\gamma)$$

Consequently the calculated sea level integral energy spectrum depends on the values of the parameters, γ , β and L .

The primary cosmic ray energy spectrum for energies greater than 10^{10} eV has been fitted by Cocconi (1961) to the expression

$$R(> E) = 10^{13} E^{-1} (0.67 + 0.037 \log E) \text{ sec}^{-1} \text{ m}^{-2} \text{ st}^{-1}$$

In the region between 10^{10} eV and 10^{13} eV this is based largely on the results of Lal (1953) and Kaplon (1952) who observed the interactions of the primary radiation in photographic plates flown at balloon altitudes.

The energies of the primary particles which contribute to the local showers must, on account of the frequency requirement, lie between 10^{10} eV and 10^{14} eV. The values of the parameters γ and L in this region are fairly well known; $\gamma \sim 1.5$ and $L \sim 80 \text{ g cm}^{-2}$. The measured values of β , however, fluctuate considerably, although recent experimental evidence (Siddheswar Lal et al. 1962, Azimov et al. 1962, Guseva et al. 1962) suggest values which lie between 0.5 and 0.7. The curves plotted in figure 4.6 are the expected sea-level energy spectra of nuclear-active particles calculated for values of β between 0.5 and 0.7. A further assumption was made in that only the primary particle contribution within one steradian of the vertical was considered. That this assumption is applicable is shown by the strong vertical collimation of EAS, - which reflect the properties of the nuclear-active cascade, - by the atmosphere; such that about 75% of all sea level showers arrive within one steradian.

On this picture, the nuclear-active particles incident on a detector consist primarily of an energetic nucleon together with the remnants of the last interaction. If, now, it is assumed that a third of the energy released in this interaction goes into the production of neutral pions and subsequently into γ -rays; a γ -ray energy flow spectrum ($\sum E_\gamma$) can be constructed. Such a spectrum is presented in figure 4.6, taking a

FIGURE 4.6 A - the primary cosmic ray energy spectrum.

B, C, D - sea-level energy spectra of nuclear-active particles calculated for inelasticity values of 0.3, 0.4 and 0.5 respectively.

E - γ -ray energy flow spectrum at sea-level for $K = 0.4$.

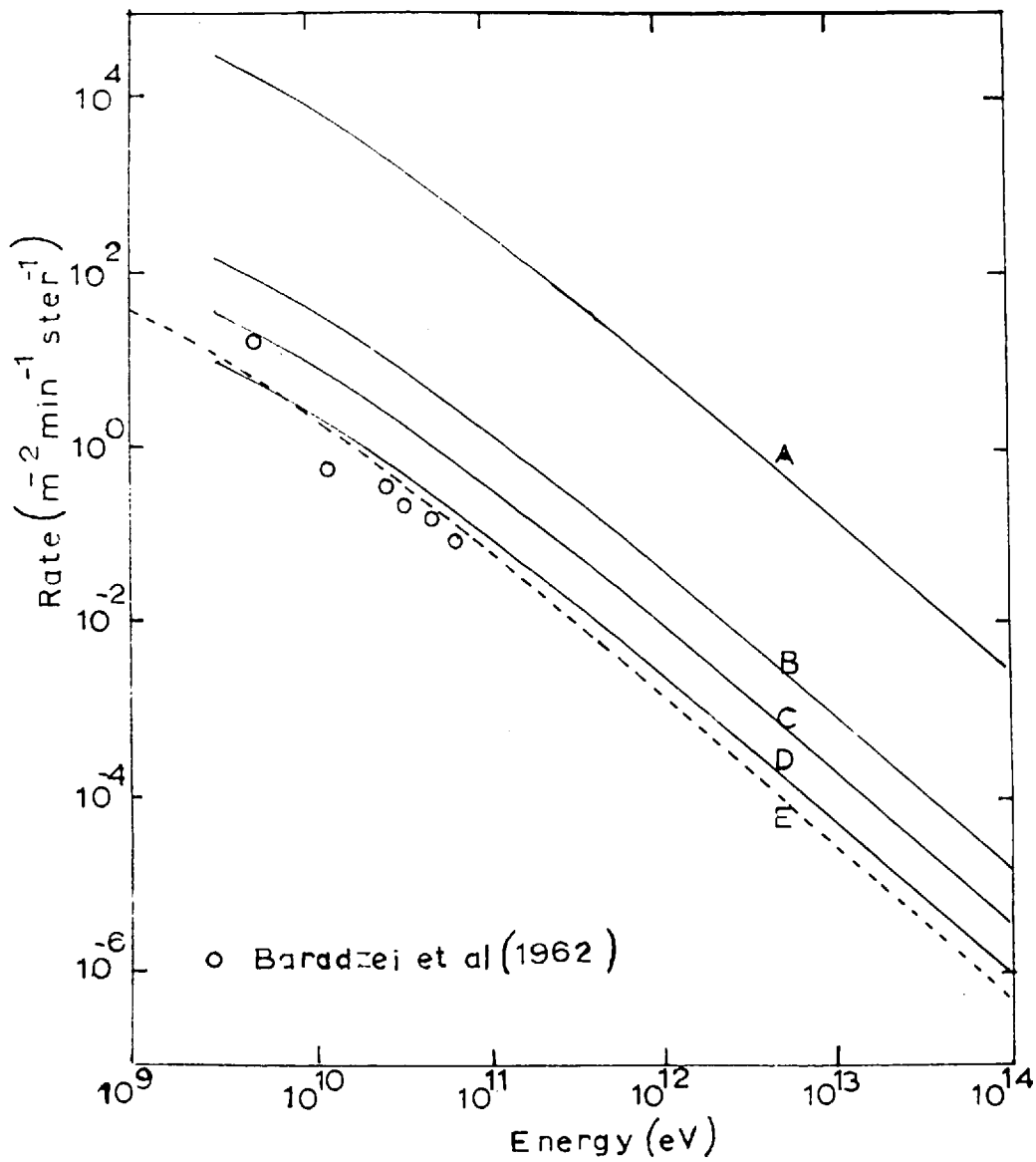


Figure 4.6

value of $\beta = 0.6$ as a representative average.

It is interesting to compare this latter curve with the results of Baradzei et al. (1962) who measured the quantity $\sum E_{e-\gamma}$ with ionisation chambers beneath carbon filters. The agreement between the experimental points and the calculated spectrum is very close. Unfortunately however, it is not known what proportion of their measured energy flux arises from the alternative processes of muon decay and knock-on.

The computed energy-flow spectrum in figure 4.6 may now be compared with the experimental results in figure 4.4 where each equivalent particle corresponds to an energy loss of 250 MeV by ionisation. It can be seen that the observed integral pulse height spectrum is capable of being produced entirely by the electron-photon cascades initiated by neutral pions, provided that at least half the estimated incident energy is dissipated in the tank.

It must be emphasized that these estimates are very dependent on the value of the constant of inelasticity used, as is clearly illustrated in figure 4.6. The value of $K = 0.4$ ($\beta = 0.6$) seems a reasonable average, but as yet the experimental evidence is very patchy.

4.7.5 Barometer Coefficient

Since the completion of this experiment the barometer coefficient at two bias levels on the pulse height spectrum have been obtained. These

are for size $N = 1.8$ and 10 equivalent particles. The former has a coefficient of less than 1% in rate per cm Hg change in pressure; a result which would be expected if that part of the distribution resulted primarily from the flux of muons. On the other hand, at $N = 10$ the coefficient is $6 \pm 2\%$ $(\text{cm Hg})^{-1}$; if these showers are composed wholly of cascades secondary to muon processes a similar barometer coefficient to the lower level would be anticipated. It is possible that EAS are beginning to contribute to the rate at this level; but if the curve given by Greisen in figure 4.3 for these densities is correct, this should amount to less than 20% of the total component. For neutral pions it has been shown that

$$R (> E_0) = A E_0 \exp - \frac{t}{L} (1 - \beta^Y)$$

Thus, the quantity, $\frac{L}{1 - \beta^Y}$, represents the absorption length of the nuclear cascade. When $\beta = 0.6$ it has a value of 150 g cm^{-2} which is equivalent to a barometer coefficient of about 10% $(\text{cm Hg})^{-1}$. A higher value of the elasticity, β , nearer 0.7, would produce the observed coefficient.

4.7.6 Distribution of Energy

An estimate of the energy associated with each incident shower particle as a function of the shower size can be made if the true particle number spectrum falling on the tank is known. Figure 4.7 is a plot of the sea level experimental results obtained by various authors, expressed in terms of particle number incident on their detectors. The 20% shift towards smaller numbers in the case of Miyake et al. can be understood if,

with his small detectors, he lost on average 20% of each event recorded, consistent with a lateral spread of ~ 1 m for local showers. Plotted also on this graph is the spectrum they obtained under 2.5 cm of lead. The multiplicity per particle is seen to increase with increasing shower size. Cerenkov detectors measure essentially the track length produced and hence the energy lost by relativistic charged particles crossing their volume. Comparison of the response of the Haverah Park detectors with that of thin scintillators shows that the average energy loss accompanying an incident particle more than doubles as the shower size increases from 3 particles to 10 particles. If the detectors of Delvaille et al. are assumed to collect most of the shower particles, then this energy loss increases from 200 MeV/particle at 3 particles to about 440 MeV/particle at 10 particles. This behaviour infers that the cascades can be considered as young, i.e. $s < 1$, increasing in age as they become smaller; and suggests an origin within a few radiation lengths of the top of the detector. The above energy estimations are lower limits for the total energy per electron; at lower energies - 200 MeV/particle - most of the energy is absorbed, while at 400 MeV/particle as much as half the energy may pass out through the bottom of the tank, depending on how many photons share the energy.

4.7.7 Altitude Variation

The results of Green and Barcus (who performed their experiment at 1575 m), when normalised in the above manner, yield a rate which is about four times higher than that found at sea level; such an increase

FIGURE 4.7 Integral pulse height spectra obtained by various authors expressed in terms of particle number incident in their detectors.

A - spectrum obtained with no absorber.

B - spectrum obtained beneath 2.5 cm of lead.

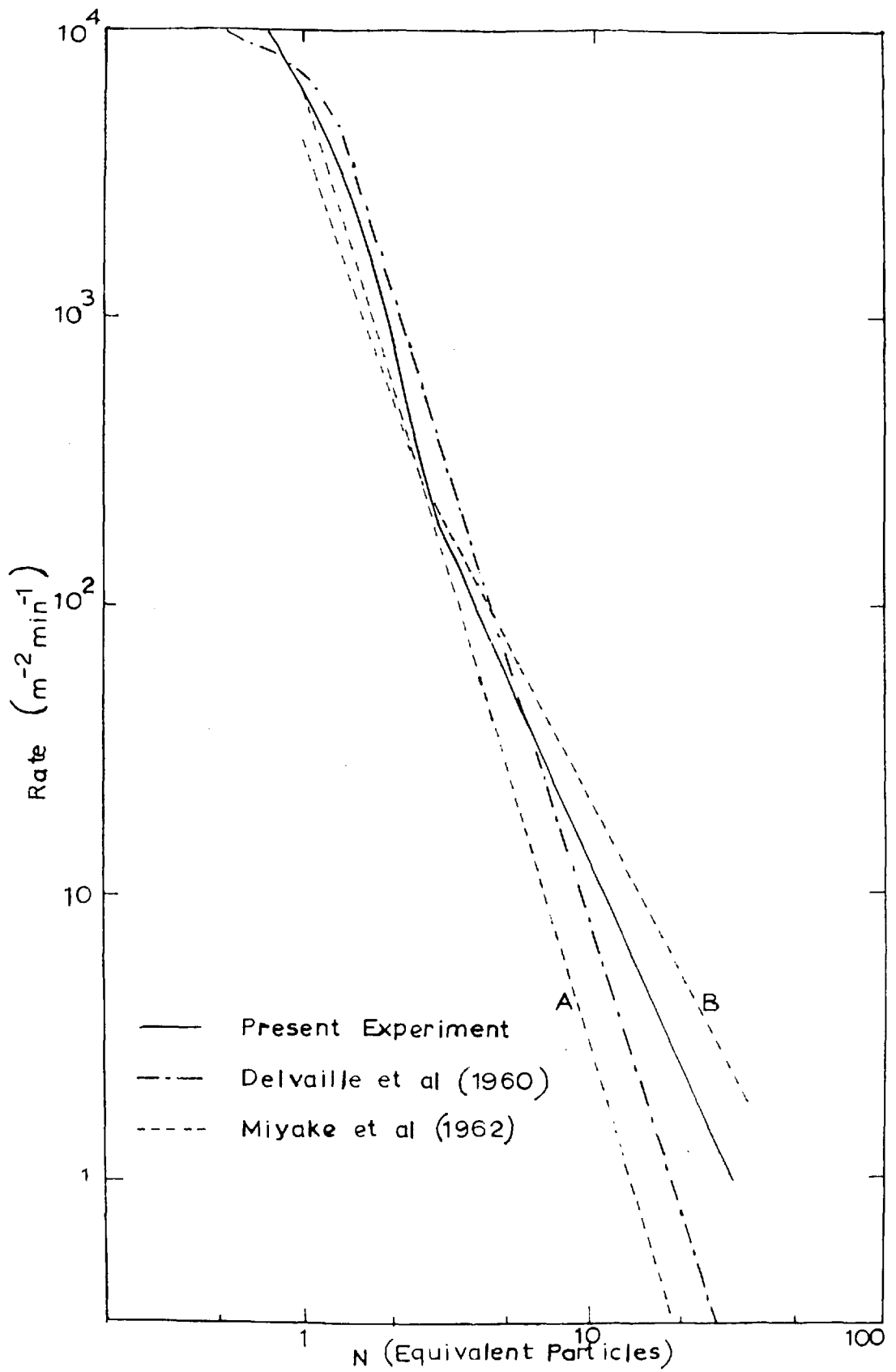


Figure 4.7

cannot be explained if their cascades are secondary to muon processes. It is; however, the predicted increase assuming nuclear-active sources.

4.7.8 Discussion

Although no definite conclusions may be drawn, there is some evidence to suggest that these narrow, local showers are results of cascades generated largely by neutral pions from comparatively low energy nuclear-active cascades at sea level. This conclusion has been shown to be compatible with an extreme fluctuation model of cascade development extended down to low primary energy regions, combined with an average inelasticity of nuclear interactions of about 0.4. The primary cosmic ray energy causing these events lies mainly between 10^{11} eV and 10^{13} eV. At sea level the electron-photon cascades produced by neutral pions are probably mixed in roughly equal proportions with those produced by muons. If further work is to be done on the investigation of the nuclear-active component in these local events with apparatus similar to the above, it would be an obvious advantage to perform experiments at mountain altitudes where the cascades would be almost entirely produced by neutral pions.

It is interesting to compare these conclusions with those pertaining to single electrons and photons at sea level. Counter telescope techniques have been used to study the soft component at both high and low energies. Barker (1956) and Palmatier (1952) used cloud chambers and carbon absorbers to measure electron energies in the region 10 MeV to several hundred MeV, while Kameda and Maeda (1960) used an ionisation chamber with lead absorbers to extend the investigations up

to 20 GeV. The Japanese group measured the total flux of electrons and photons, estimated the contribution due to muons and attributed the remainder to neutral pion decay. They concluded that 70% of the single particles of energy $\gg 2$ GeV originate from muons and 30% from nuclear-active particles, and that the relative contribution from pions increases rapidly with altitude. These conclusions are similar to those at the lower energies and also to those drawn from the present experiment, although they were not equipped to examine small showers. The combined energy spectra for the single, high energy, incident electrons and photons found by Kameda and Maeda, if completely absorbed by the water tanks would account for about half the observed pulse height spectrum, and confirms that an appreciable proportion of the experimental spectrum is due to single incident particles cascading in the water.

4.8 Small Young EAS

The portions of the integral pulse height spectra not yet considered are those occurring at densities above the change in slope (see figure 4.3). In this region the curves for the smaller detectors become parallel to that of the larger detector but displaced by about 50% towards higher densities. This behaviour may be attributed to the occurrence of small young EAS and represents the intermedial stage between the narrow local showers already discussed and the large EAS. The spectra obtained with the two smaller detectors (area: 2.25 m^2 and 9.0 m^2) almost merge at an equivalent density of $100 \text{ particles m}^{-2}$, which indicates that the showers responsible are no longer effectively

contained by a single tank, but are beginning to spread laterally. The energy carried by the shower particles near this density must be distributed fairly uniformly out to a distance of at least 2m from the shower core; otherwise the single tank would record a systematically higher equivalent density than the addition of four tanks. What the large 15-tank detector sees are mainly these small young showers averaged over its total area; this can be seen in figure 4.8 where the results for the two larger detectors (4 and 15 tanks) are replotted to show the rate per unit area of showers greater than a given size. The fact that the points are now co-linear proves that practically the whole of the shower is confined to the area of the 4-tank detector, i.e. 9.0 m^2 .

The gap between the pulse height spectrum and the density spectrum determined by Geiger counters and scintillators at this altitude, corresponds to an average electron track length in the detectors of about 1.7 detector depths per incident particle. This represents an energy loss of about 400 MeV/particle. The results of the 6m array (figure 3.7) show that for showers of size $N \sim 10^5$ particles this is the average energy loss per electron within about 2m from the shower axis, and supports the evidence that these events are in fact the cores of small EAS.

By comparing the rate of arrival of these showers at sea level with that of the incident cosmic ray flux, the energies of the primary particles responsible were found. These lie between 10^{13} eV

FIGURE 4.8 Integral rate per unit area as a function of the 'equivalent' number of recorded particles, N.

FIGURE 4.9 Density spectra obtained by Miyake et al. (1962) from a shielded scintillator for different numbers of particles in an unshielded scintillator laterally displaced by 2m.

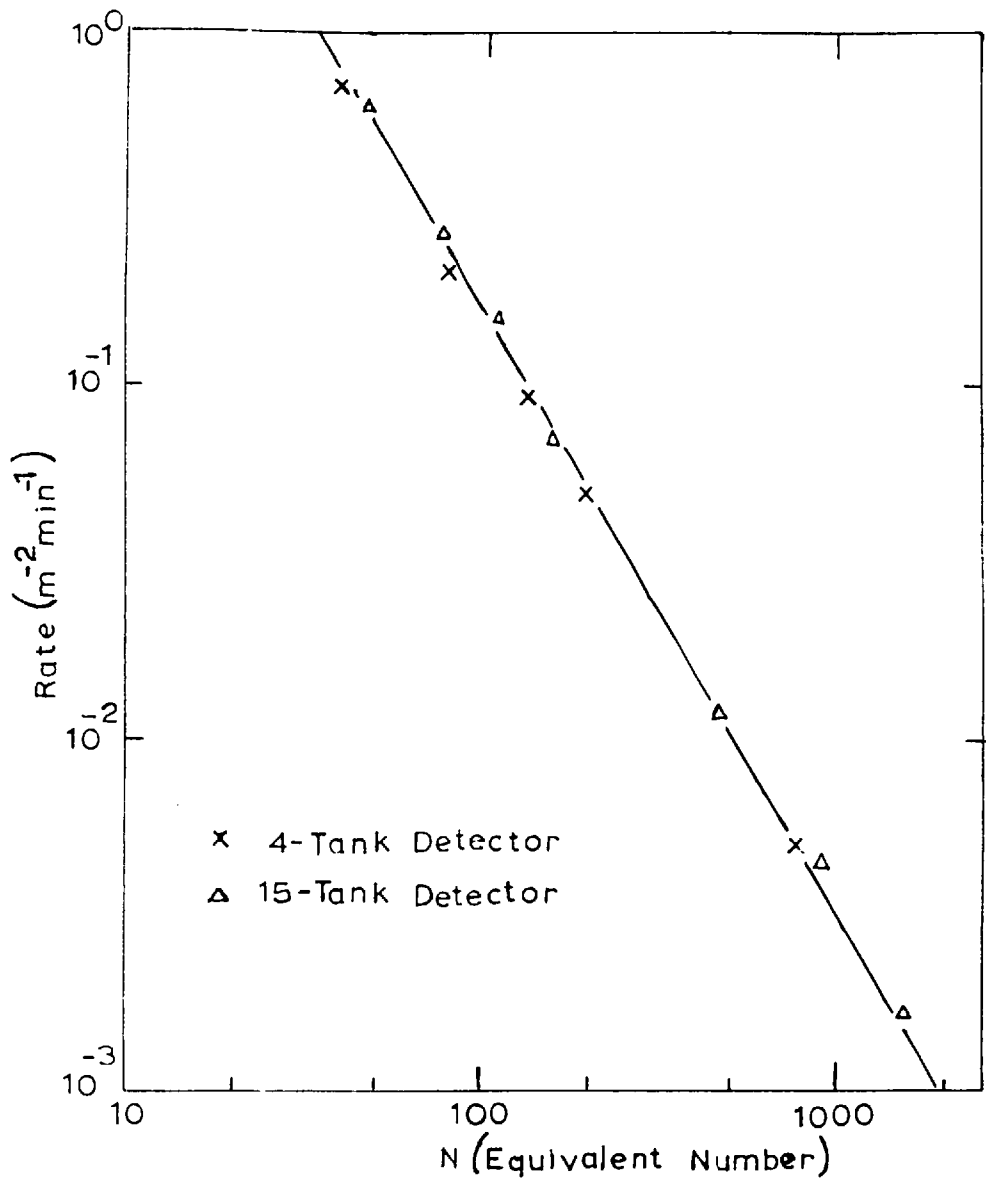


Figure 4.8

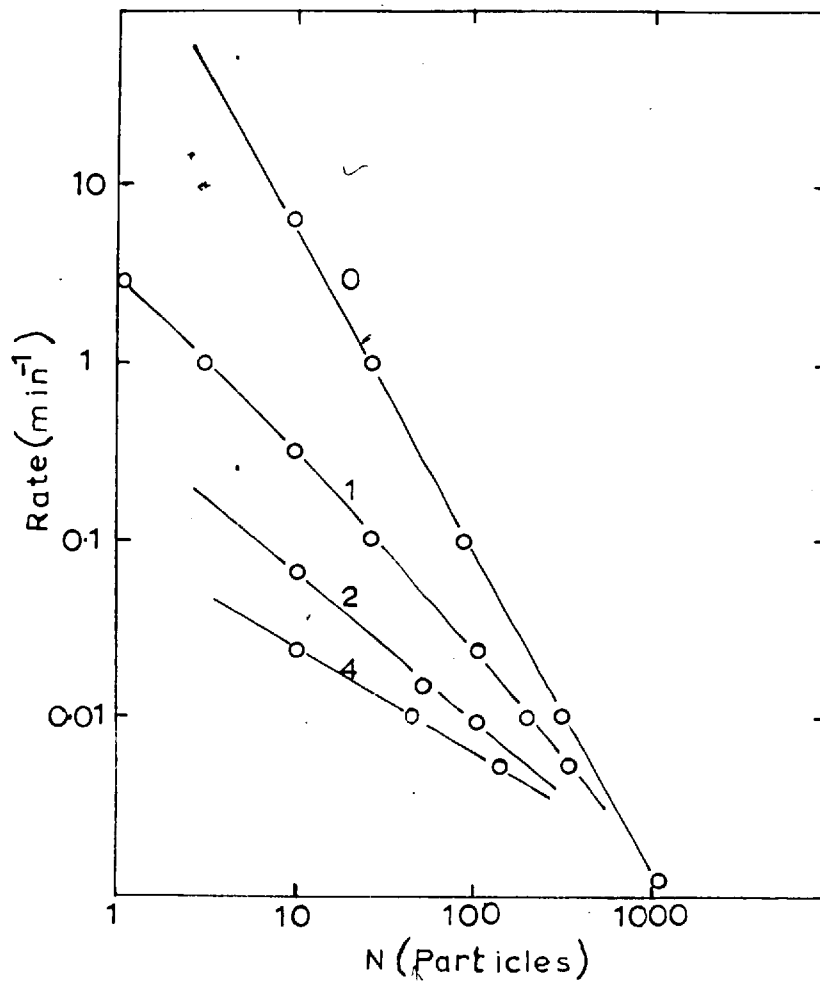


Figure 4.9

at low densities and 10^{15} eV near 100 particles m^{-2} . The fact that these showers have not spread laterally beyond a few metres suggests a point of origin in the lower regions of the atmosphere.

Similar conclusions may be drawn from the results of Miyake et al. (1962) who used an energy flow detector, consisting of a scintillator beneath 2.5 cm of lead, in coincidence with a second unshielded scintillator laterally displaced from the first by 2m. A number of density spectra were obtained from the shielded scintillator for different numbers of particles in the unshielded detector. The results are given in figure 4.9 which shows that the rate of occurrence of the high energy density showers decreases rapidly with increasing lateral spread. These authors further concluded that the events near the meeting point (1000 particles in the shielded scintillator) correspond to shower cores of various sizes, and that the character of the cores fluctuate largely below a shower size of 10^5 particles. Both these conclusions are consistent with a cascade origin one or two radiation lengths above the detector.

4.9 Conclusions

It has been shown in this chapter how the transition in the density spectrum from single particles to large EAS takes place. The many effects observed with single, energy-sensitive Cerenkov detectors can be explained on a model such as that proposed by Cranshaw and Hillas, which attributes the important sea level contributions in a cosmic ray

induced cascade to the last one or two nuclear interactions. Under this model, the narrow, local showers observed at low density arise from the primary radiation of energies between 10^{11} eV and 10^{13} eV, together with bursts generated by electrons from muon decay and knock-on processes. The primary energy interval 10^{13} eV to 10^{15} eV gives rise to small young EAS which have spread to the order of 2 or 3 metres.

CHAPTER 5

THE 500-METRE ARRAY - PART 1

5.1 Introduction

The work described in the previous chapters was carried out concurrently with the building of a large EAS array. The larger array was built in the same shape as the 6m array but with an array spacing of 500m and a detector area of 34 m^2 per station. In common with the smaller array the large one was designed to extend the results of the experiment at Silwood Park in which the shower size spectrum was investigated for values of N between 2.10^5 particles and 5.10^6 particles. In addition to the size spectrum, improved recording techniques allowed more detailed information to be obtained on the arrival directions and shapes of shower fronts. The data obtained so far, and reported in the following chapters, are essentially preliminary results in that many more events will have to be recorded before definite conclusions can be drawn about possible structural changes in the size spectrum or anisotropy in arrival directions.

5.2 Apparatus

The single tank detector unit has been described fully in an earlier chapter (section 2.2). Fifteen such units are grouped together in two parallel rows inside a wooden hut to form a detector station of area 34 m^2 ; a sixteenth unit is included to extend the range of density measurements by running at a much lower gain (about 1/50 of the standard level). A map of the site at Haverah Park with the detector stations

marked is drawn in figure 5.1; there is about a 30m variation in altitude across the array, the central station being at a height of 220m above sea level. The sixteen photomultipliers in each hut are supplied by single commercial power packs by way of individual potentiometer networks, - a system which permits an independent adjustment of the E.H.T. supplied to single photomultipliers.

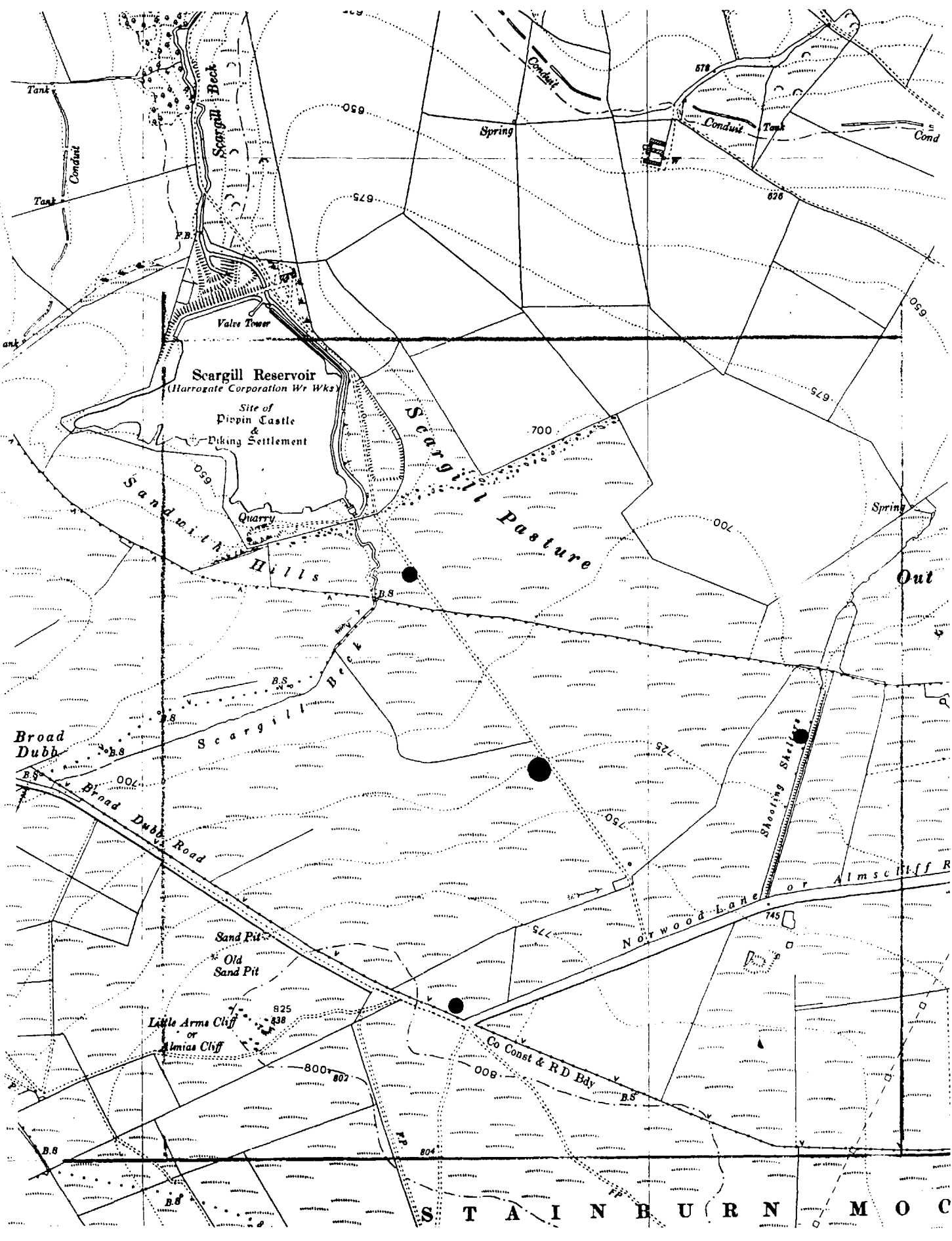
The method of recording is illustrated by the block diagram in figure 5.2. The added outputs from the 15 tanks in each outer hut is passed through 500m of high band-width Aerialite cable (No. 363), which is laid underground, and into the central hut which houses the recording equipment. Here the pulse is shaped into the waveform depicted in figure 5.3 and displayed on a recording oscilloscope (Solartron CD 1012). Four such oscilloscopes are used to record the information from each station; and a simple system of mirrors allows all four displays to be photographed on the same 35 mm film. In order to compensate for the extra time lag imposed by the 500m of transmission cable on the signals from the outer stations, a further 2.33 microseconds of Hackathal (HH 1500a) delay cable is included in the recording channel of the central hut.

In the 6m array EAS were culled from the incident radiation by demanding that densities greater than a fixed value fell in coincidence on the central and one outer detector. If the same triggering criterion is applied in the present experiment, and a resolving time of about

FIGURE 5.1 Map of the Haverah Park field station with the detector stations marked.

FIGURE 5.2 Block diagram of the recording system.

FIGURE 5.3 Pulse heights recorded when a shower axis fell within the triangular collecting area. The 'step' nature of the pulses and the time marks on the traces are clearly seen. The top of the pulse from the central detector is not visible and the first step was used for measurement.



Scargill Reservoir
(Harrogate Corporation Wr Wks)

Site of
Pippin Castle
& Piking Settlement

Scargill Pasture

Sandwith Hills

Broad Dubb Road

Norwood Lane
or Almscliff R

Little Arms Cliff
or Almas Cliff

STAINBURN MO

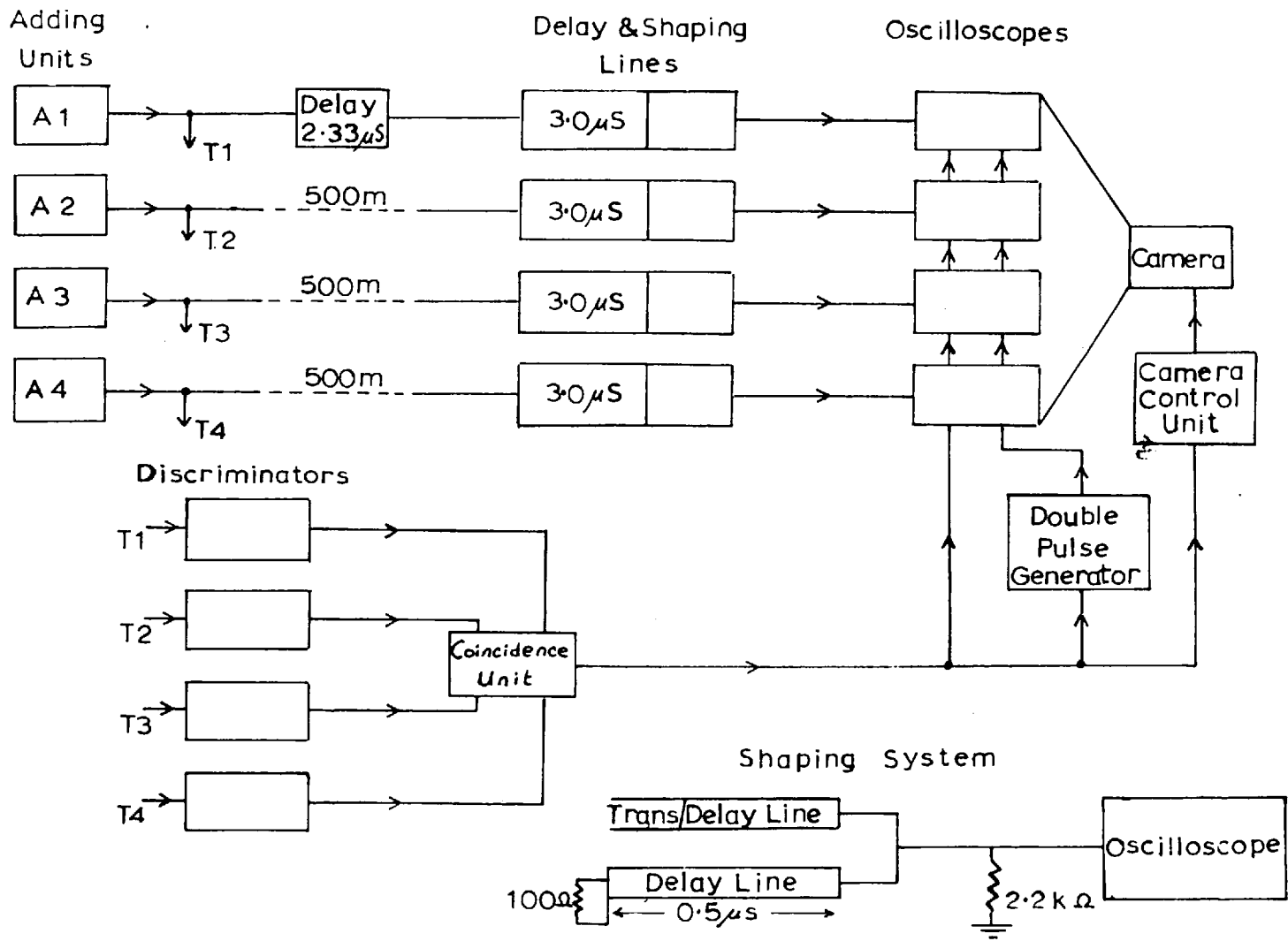
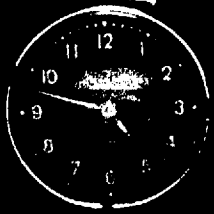


Figure 5.2



4 microseconds is allowed, then the chance coincidence rate becomes comparable with that expected for EAS. For this reason the criterion is extended such that showers are only recorded when densities greater than 10 particles per station are received in coincidence from the central and any two outer stations. To achieve this, a 2-volt trigger pulse is generated at each station and fed into a central coincidence unit whenever a density of greater than the required level is recorded. As a result of the large separation between the detectors, an EAS arriving from a direction near the horizontal may produce trigger pulses which arrive at the central detector separated in time up to a maximum of 3.8 microseconds. The resolution of the coincidence unit is therefore made equal to 4 microseconds. Finally, to allow for the possible delay in the master coincidence pulse, the shower information is further delayed by 3 microseconds with Hackethal cable, which brings the total delay in each signal channel to 5.3 microseconds.

5.3 Amplitude Display and Timing Systems

Each detector station has a linear response from 6m V to 18 V, provided that the maximum output is divided fairly uniformly between the individual tanks. This corresponds to the simultaneous arrival of between 1 and 3000 equivalent particles. At present the upper response limit is imposed by the second stage of the adding unit which has to handle the full voltage range.

The pulse profile to be displayed has a fast leading edge

followed by a slow exponential decay (time constant between 6 and 8 microseconds). The band-width of the transmission circuits is such that, except for rise times \leq 0.1 microseconds, the rise time of the leading edge is determined by the width of the shower front arriving at the detector. For distances of the order of 1 km from the shower axis, this may be as much as a microsecond (Linsley and Scarf 1962). The amplitude display must therefore allow a resolving time for the collection of shower particles of at least 1 microsecond, and also be able to present on a single cathode ray tube an amplitude range of 3000 : 1.

Two systems have so far been developed. The one used to obtain the present results was designed by Mr. G. Cescotti and consists simply of a 0.5 microsecond length of Hackathal cable, mismatched at one end such that 0.8 of an incident signal is reflected down its length (figure 5.2). Successive reflections produce a series of steps as in figure 5.3 and gives a range of about 1000 : 1. To compensate for the effect due to the exponential decay of the pulses, which causes the third or fourth step to sag below the base-line with large signals, a small padding resistance (100 ohms) is used to terminate the shaping line and slightly attenuate the reflected signal. Unfortunately, with these relatively wide steps, the ratios are very sensitive to the actual decay time of individual pulses and although the ratios have been accurately measured with a constant exponential decay, the experimental values have rather large errors; in the present experiment these are 5.1 ± 0.3 , 3.8 ± 0.5 and 4.0 ± 1.0 for the first four successive steps.

A second system which has been used for short periods with the central station makes use of a series of 20 db attenuation and delay cables to present the original pulse as a series of superimposed pulses, attenuated by different powers of ten, and delayed with respect to each other by 1.0 microsecond intervals. This system has the advantage of not being sensitive to the variable signal decay times, but does introduce a further amplification stage.

The relative arrival times of the EAS at the four detector stations are measured directly from the oscilloscope traces which are operated at sweep velocities of about 1 microsecond cm^{-1} . Each time an event is recorded two narrow, (0.2 microsecond width) 20 volt pulses, separated by 6 microseconds are applied simultaneously to the brilliance control amplifiers of the four recording oscilloscopes. These modulate the trace intensities at two points, the first of which affords a common mark from which to measure the arrival times, while the second enables a continual check on the sweep velocities to be maintained.

5.4 Calibration

The single particle calibration was described in section 2.5 in connection with the 6 m array. It was shown that the mean value obtained when all three scintillator units were positioned above the tank was identical to that obtained with the high resolution configuration when one unit was placed beneath. Accordingly the remaining tanks were not raised on girders, and the former telescope configuration was

used for the present array. Two or three independent calibrations were performed at each station at the start of the run in December 1962, and at periodic intervals since, to guard against possible drifts.

Between the successive calibrations the constancy of the tank gains was maintained by comparing their integral count rates above a discrimination level of 2 equivalent particles (about 12 mV). The procedure and subsidiary apparatus used was the same as that described in section 4.3, and for the reasons given there it was possible to maintain a uniform average response across the area of the station to within 2%. The photomultipliers and the associated electronics, housed in the head units, proved to be extremely stable provided that the temperature was kept relatively constant and, except for the occasional component failure, very little adjustment was required. Throughout the duration of this run the 60 tanks were checked manually two or three times a week; however, it is proposed to install into each adding-unit an automatic switch, regulated by the standard clock, so that the tank outputs may be sampled in turn at quarter hour intervals. Such a system has already been shown to be satisfactory by monitoring the tank rates of the central station.

A pulse generator which simulates the output from the photomultiplier head unit was used to determine the overall gain of the recording channels. Pulses from this generator were simultaneously fed to the adding units of each detector station through equal lengths of transmission cable

(Uniradio 39) at a level which corresponded to about 100 equivalent particles. The artificial, flat, vertical shower which was thus generated was photographed in the normal way and yielded directly a multiplying factor for each channel by which the projected pulse heights were converted to the equivalent number of incident particles. These calibration pulses were recorded on the beginning and end of each film and at intermediate stages when the film was not renewed daily. Although the detectors were stable over long periods, the gains of the recording channels occasionally drifted by about 5% overnight, due to drifts in the oscilloscope Y-amplifiers.

The 6 microsecond gap between the time marks on the oscilloscope traces was frequently checked against the delay produced by reflecting a signal down a measured 3 microsecond length of delay cable.

5.5 Analysis

The analysis began with a determination of the azimuth and zenith angles of the shower axes (ϕ and θ respectively). If the shower particles are assumed to be concentrated in a narrow, plane front, perpendicular to the axis, then three independent time measurements are sufficient to define the direction of the shower. Whenever possible the three outer detectors were used for this purpose and the central detector only utilized if the leading edge of one of the outer signals was not sufficiently well defined to allow an accurate measurement. A description of the relevant calculations is given in Appendix 3.

For the initial analysis the showers were separated into two groups depending on whether their zenith angles were greater or less than 30° . The near-vertical showers in the latter group had developed over distances which varied between 1.0 and 1.15 atmospheric depths; while the former group included showers which had developed over a much wider range of distance.

The subsequent shower analysis was basically the same as that for the 6m array. The variation of the equivalent density, δ , with distance from the shower axis may be described by the equation,

$$\delta = k N j_\theta (r)$$

Here, $j_\theta(r)$ is the lateral structure function appropriate to a detector of depth 3.4 radiation lengths, and a shower of zenith angle θ , and k is a constant which depends for its value on the unit of $j_\theta(r)$. For showers near the vertical the particle density structure function given by Greisen (1960), that is applicable to EAS out to distances of 1.5 km, was used as a starting trial function. A number of power law distributions were also chosen and each tested by the trial and error method outlined in section 2.6.1. The value of the resulting exponent which best fitted the data was found to be -3.1 ± 0.1 ; which, within the limits of error, is identical with the Greisen function over the range of distances in which the majority of the shower particles were detected ($200\text{m} < r < 800\text{m}$).

The effective shape of the array for an incident shower depended on

its direction of arrival. In general, the area diminished as $\cos \theta$ and for zenith angles less than 30° the net effect was small. With the more inclined showers, however, the distances contracted rapidly with increasing zenith angle; and for these events, the relative positions of the detectors in a plane normal to the shower axis were calculated and a scale drawing of the projected array constructed. A graphical representation of these relative positions for different zenith and azimuth angles has previously been given by Bryant (1958) and is reproduced in figure 5.4. For each trial function, sets of loci for different density ratios were drawn and scaled for a number of detector spacings between 250m and 500m (taken in 50m intervals). Figure 5.5 shows the location by loci intersection of a typical inclined shower on a plan of the projected array. Various trial functions were tested as before and the best value for the exponent of a power law structure function for showers of $\theta < 30^\circ$ was found to be 2.7 ± 0.1 .

The statistics at this stage did not allow a further resolution of the variation of the structure function exponent with zenith angle; but it is clear from table 5.1, where the goodness of fit of various structure functions is given for increasing zenith angles, that between 0° and 60° the exponent gradually increases from -3.1 to -2.5.

FIGURE 5.4 The relative positions of the detectors
for different azimuth and zenith angles.

FIGURE 5.5 The location of a typical inclined
shower.

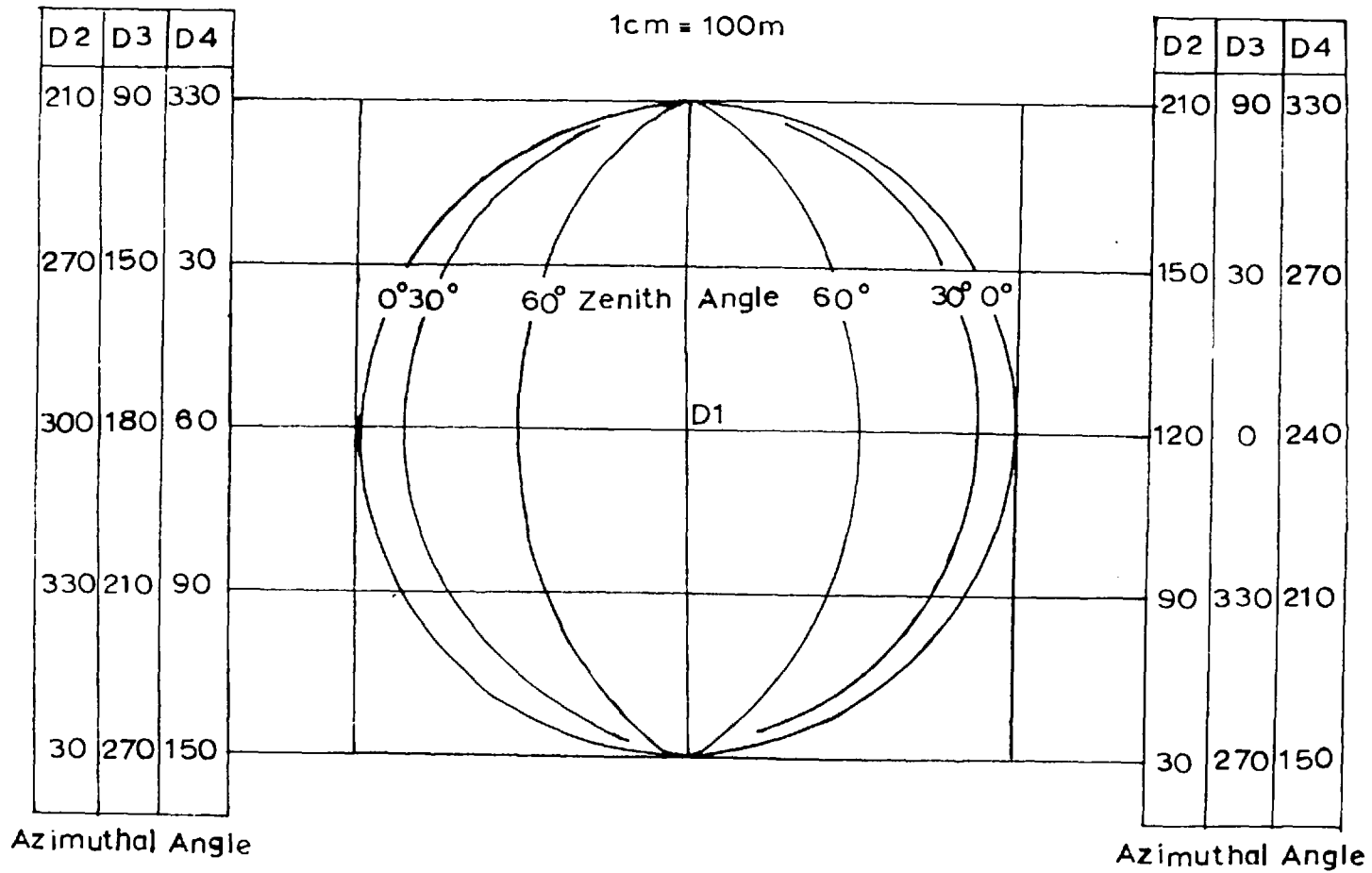


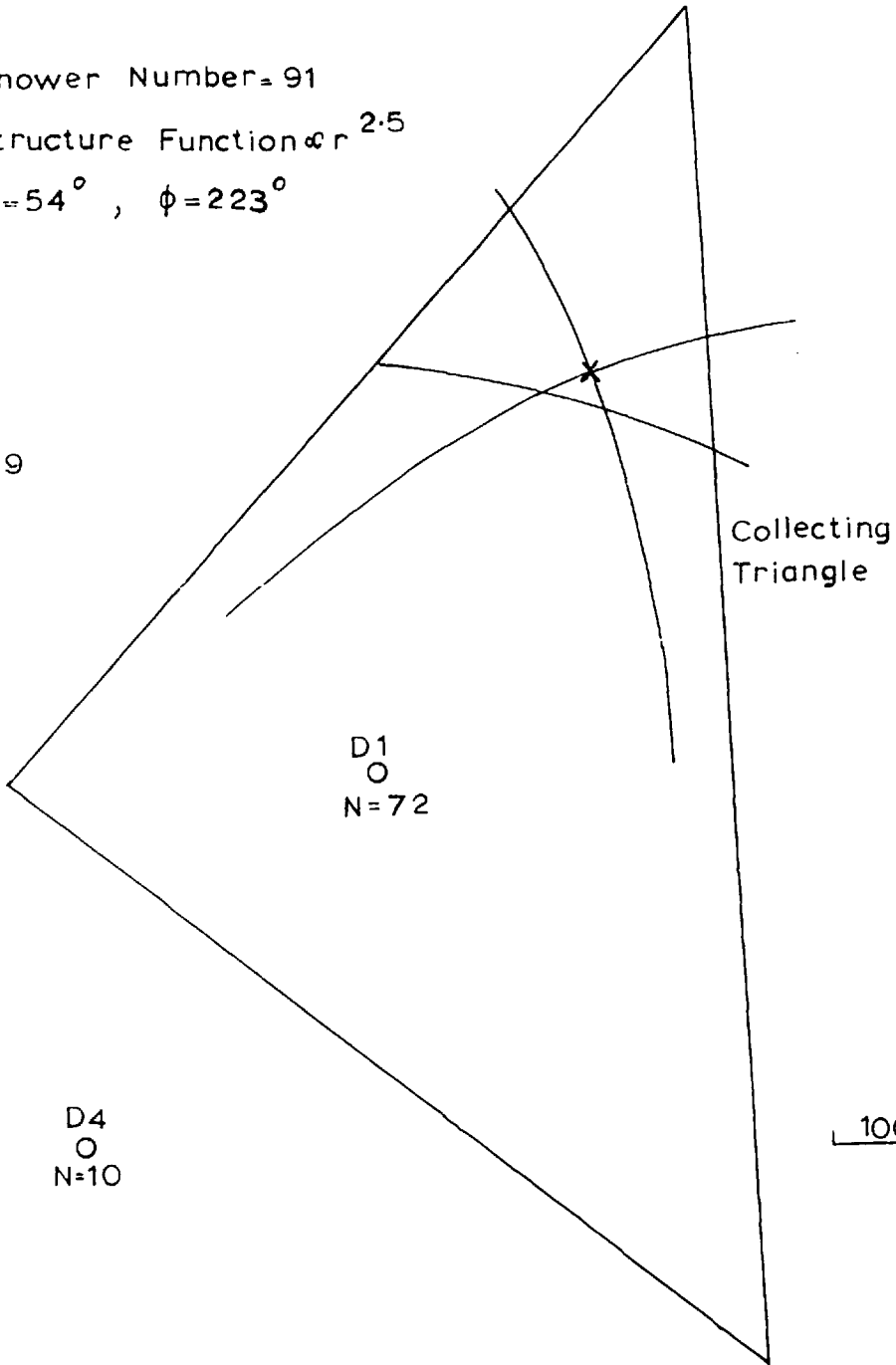
Figure 5,4

Shower Number = 91

Structure Function $\propto r^{2.5}$

$\theta = 54^\circ$, $\phi = 223^\circ$

D3
○
N=29



D1
○
N=72

D2
○
N=29

D4
○
N=10

100m

Figure 5.5

TABLE 5.1: Variation of structure function
with zenith angle

θ°	$r^{-3.1}$			$r^{-2.5}$		
	S	F	X	S	F	X
0 - 10°	9	6	5	28	6	6
10° - 20°	20	17	16	67	10	13
20° - 30°	22	33	13	71	16	25
30° - 40°	26	35	9	59	29	15
40° - 50°	7	22	6	20	21	9
50° - 60°	1	7	1	4	7	1
> 60°	0	2	1	1	1	1

S refers to the number of showers which required a steeper structure function, and F to the number which required a flatter one. The numbers beneath X are the showers which fitted the trial function.

In the table, more showers appear under $r^{-2.5}$ than $r^{-3.1}$. This is because the critical size for analysis is smaller for showers with a flatter distribution of particles.

The selection criteria imposed on the showers used in the 6m array were applied without modification in this experiment. The shape of the triangular collecting area for the inclined showers was no

longer equilateral and varied from shower to shower. Consequently the critical size also had to be determined separately for each event. Because a far greater proportion of the showers which triggered the 500m array fell inside the collecting triangles than was the case with the 6m array (45% as compared with 20%), a greater percentage of the recorded showers were used in the determination of the structure function. A total of 3600 showers were recorded in this initial phase, of which 309 satisfied the selection criteria; 141 of these showers had zenith angles less than 30° .

5.6 Comparison with Previous Work

It is interesting to compare these results with the structure function variation found by Linsley et al. (1962) at Volcano Ranch at an altitude of 1800m. These authors selected showers at different zenith angles and in this way examined the variation of structure function with atmospheric depth. They found that for radial distances which were large compared to the scattering length, r_0 , (79 metres at sea level) the structure function approached a power law of the form r^{-n} . For showers of size $N \sim 2 \times 10^7$ particles, the value of n varied between 3.3 and 3.1 for atmospheric depths which corresponded to sea level zenith angles between 0° and 30° , and fell to a value of 2.0 at $\theta = 60^\circ$. The depth at which n was 2.7 was equivalent to a sea level zenith angle of 45° . These results agree almost exactly with those found in the present experiment using much deeper detectors. The slopes in the latter experiment are however slightly flatter which would be expected if it is considered that

the deep detectors are more than twice as sensitive to the flatter muon distribution than to that of the electron-photon component (see section 3.1).

Linsley et al. also found that 5 showers which had travelled 2000 g cm^{-2} (equivalent to a sea level zenith angle of 60°) consisted almost entirely of muons and had a structure function proportional to r^{-2} . This figure may therefore be taken to represent the muon structure function for a zenith angle of 60° and for radial distances $r \gg 79$ metres. For showers which in the present experiment corresponded to a vertical incidence, the proportion of muons increased as $r^{0.74}$ over the range $100\text{m} < r < 1 \text{ km}$. It follows that the muon structure may here be represented as

$$r^{-3.1 + 0.74} \approx r^{-2.4}$$

Consequently, it would appear that the exponent of the muon structure function flattens from about -2.4 to -2.0 as the zenith angle increases from 0° to 60° .

Various authors (see section 1.2) have reported that at distances out to about 200m from the shower core, the structure function is independent of zenith angle. At such distances the proportion of muons is only a few percent, and the structure is effectively that of the electron-photon cascade. If these conclusions can be extended out to greater distances, the flattening of the particle distribution may be attributed simply to the increasing relative contribution of the muon component.

5.7 Normalisation of Structure Function

The procedure so far gave only the approximate shape of the structure functions. Provided that the inclined and vertical shower structure functions are normalised in the same way, the quantity kN can be regarded as an internally consistent shower size parameter. However, to relate these measurements to those obtained by other workers who have used density sensitive detectors, the Cerenkov detector structure functions must be normalised to the particle density distribution. If the value of the Cerenkov functions are made equal to that of the density function at the distances at which the equivalent density equals the true density, then the constant, k , has a value of unity. The relation between these functions near the shower axis was determined, in the 6m array, by using Geiger counters to find the mean pulse height per shower particle. In the present experiment the corresponding recorded densities were smaller by more than an order of magnitude and the Geiger counter calibration was inadequate. A scintillation detector of total area $4m^2$ is being developed and may eventually be used for this purpose. Even so the calibration will still be very slow (\sim months) because of the large statistical fluctuations on the small number of particles sampled.

It is possible to estimate the average response of the detectors to the incident flux from a knowledge of the principal processes prevalent at large distances from the shower axis. For vertical showers it has been shown that, over the range $200m < r < 800m$, the Cerenkov detector structure function is parallel to the particle density structure function

given by Greisen. Thus the track length per incident particle, and hence the associated energy absorbed by the detector, remains fairly constant in this interval.

In section 3.1 it was shown that at large distances from the shower core ($> 100\text{m}$) the electron-photon component is propagated almost wholly by low energy photons, which results in a track length per particle of

$$\lambda_a (1 - e^{-t/\lambda_a})$$

As the radial distance is increased, the individual photon energies approach that corresponding to a minimum absorption, which leads to a limiting value for the production of track length of 0.42 detector depths per particle.

In section 1.6 it was shown that the proportion of penetrating muons in an EAS has been found to increase from 10% at 200m to about 35% at 800m from the shower axis. These particles contribute a track length equal to the thickness traversed.

The combined estimate for both the above components indicate that the Cerenkov response function, $n(r)$, should increase from 0.48 at 200m to 0.62 at 800m. A reasonable average for $n(r)$ would appear to be 0.55 ± 0.1 .

The proportion of muons in inclined showers is not well known. Linsley et al. (1962) found that for an atmospheric depth, $X > 1100 \text{ g cm}^{-2}$, the proportion of penetrating particles at a given radial distance fluctuates from shower to shower, the magnitude increasing with increasing atmospheric depth. It has, however, been suggested, in the previous section, that the flattening of the structure function may simply be due to the increased contribution from a flat muon distribution. With this assumption the two power law functions which represent the structure of the electron - photon and muon components (exponents of -3.1 and -2.2 respectively) were combined empirically to produce a mean exponent of -2.7 over the range $200\text{m} \leq r \leq 800\text{m}$. The resulting structure function, normalised to the Greisen function is given in figure 5.6 together with that for the vertical showers.

It can be seen in figure 5.6 that the two Cerenkov detector structure functions merge at a distance between 100m and 200m from the shower axis. This is to be expected when it is considered that at these distances the muon component contributes less than 10% to the particle density. Also, as more than half the shower particles fall inside 70m, any variation of the structure function outside 200m should have little effect on the normalisation near the shower axis. Because of this, the observed variation with zenith angle of the present structure function is not in conflict with the apparent invariance found at closer distances (see section 1.2)

FIGURE 5.6 A - particle density structure function, $f(r)$,
(Greisen 1960).

B - Cerenkov detector lateral structure function
for zenith angles greater than 30° .

C - Cerenkov detector lateral structure function
for zenith angles less than 30° .

FIGURE 5.7 The Cerenkov detector lateral structure
functions obtained from the 6m and 500m
arrays compared with the particle density
structure function (Greisen 1960).

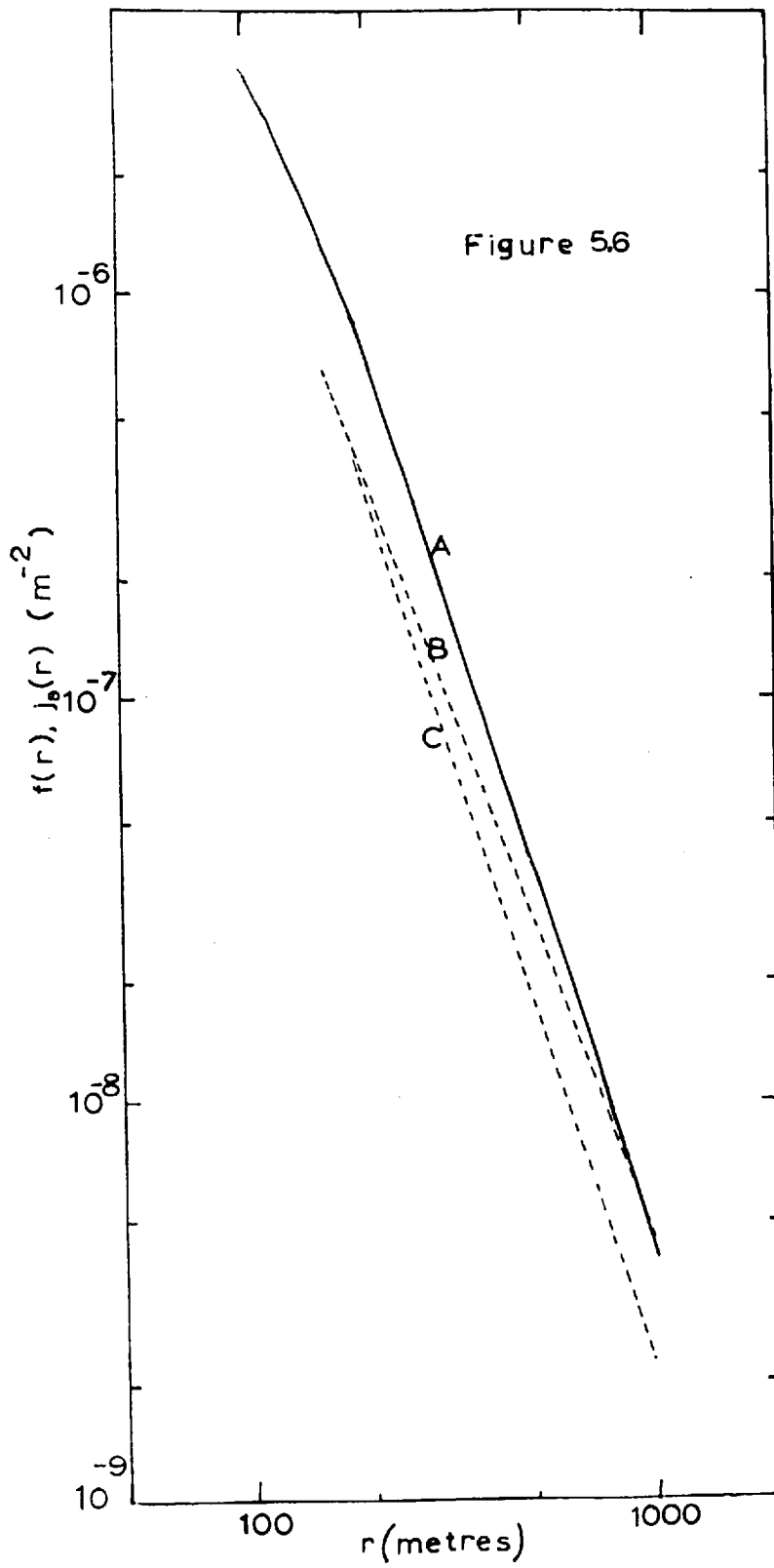
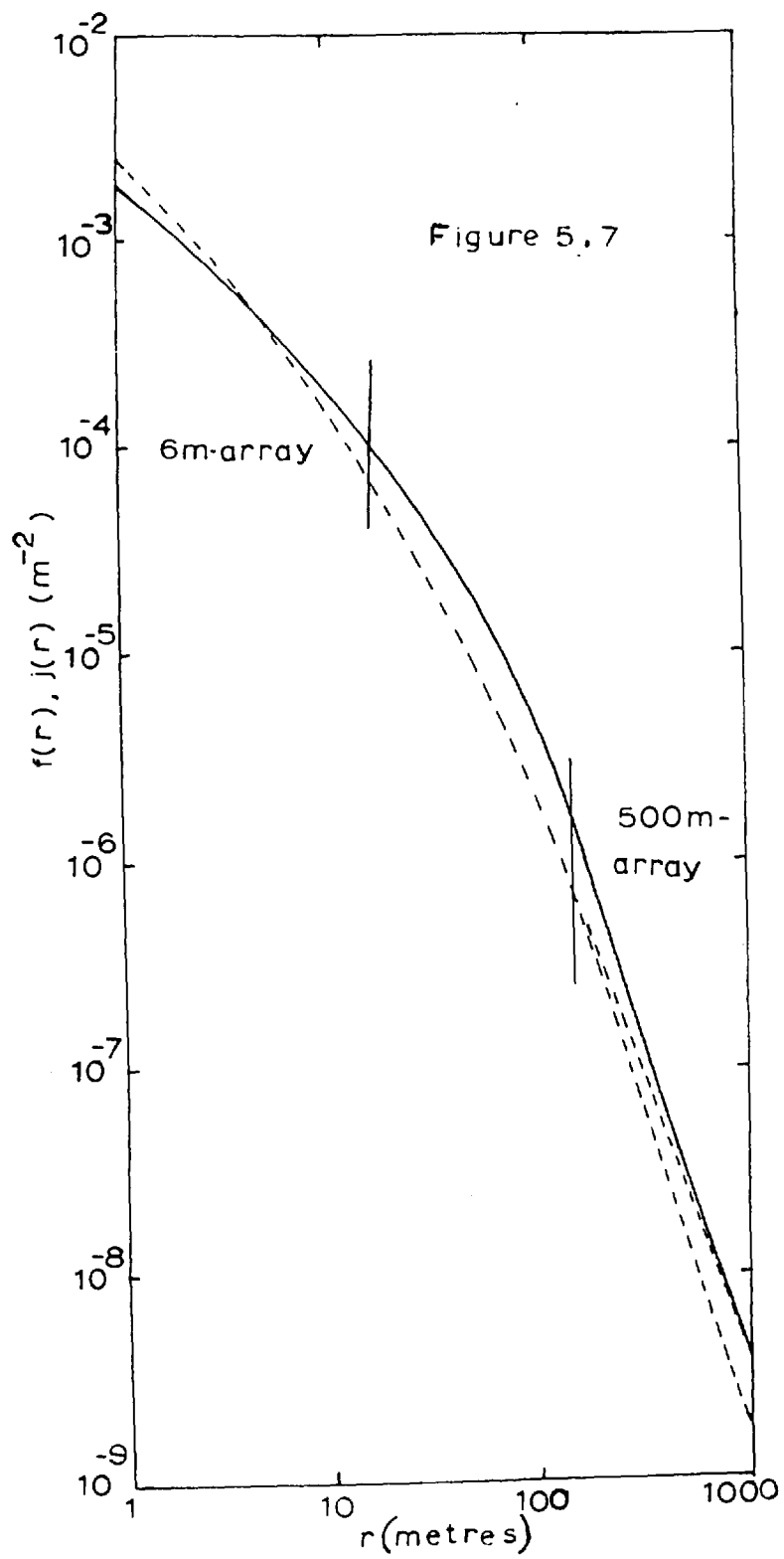


Figure 5.6



The function, $f(r)$ is normalised according to the equation

$$\int_{r=0}^{r=\infty} 2\pi r f(r) dr = 1$$

If the average track length in the detector per particle for all particles in the shower is L , then a similar normalisation gives

$$\int_{r=a}^{r=\infty} 2\pi r j(r) dr = L$$

In figure 5.7 the structure function obtained out to 15m by the 6m array is joined on to those obtained above by a broken line drawn parallel to the Greisen function. The combined curves were integrated to find L . The values for both functions were indistinguishable, being about 0.6 detector depths per particle, and illustrates the insensitivity of the structure function normalisation to small variations outside 200m.

In order to check the relative normalisation between the two Cerenkov detector structure functions for showers with zenith angles greater, or less than 30° ; 56 showers which fell in the interval $25^\circ < \theta < 35^\circ$ were analysed using both functions and the results compared. It was found that the shower sizes calculated using the flatter distribution (for $\theta > 30^\circ$) were on average 12% smaller; - a satisfactory agreement in view of the

crudeness of the check and the magnitude of the random errors in shower size (section 6.1).

CHAPTER 6

THE 500-METRE ARRAY - PART 2

6.1 Introduction

The Cerenkov detector lateral structure functions obtained in the previous chapter enabled the recorded EAS to be located by the method of intersecting loci with an accuracy of 50m. This error resulted in an uncertainty in the corresponding equivalent size, kN , of about 30% for both the inclined and vertical showers. Further, systematic errors may have been introduced in the normalisation of the structure functions due to uncertainties in the values of the response functions $n_{\theta}(r)$ (section 5.7), but these are estimated to be not more than 20%. The preliminary results which follow, although not sufficient for high accuracies, do establish the broad characteristics of large, sea-level EAS and indicate the nature of the results to be expected from further study.

6.2 Absorption Length of Showers

A convenient method of determining the absorption coefficient of large showers is from the zenith angle distribution of the incident flux. With the selection criteria imposed in this experiment, the effective area of the collecting triangle did not vary as the cosine of the zenith angle; the contribution to the flux from the inclined showers had therefore to be treated separately. For each of these showers the collecting triangles were first constructed in a plane normal to the shower axis and then projected on to the horizontal.

The angular distribution of shower intensity is plotted in figure 6.1 in intervals of θ corresponding to increasing solid angle increments of $\pi/16$ steradians, and includes showers of all sizes exceeding 3×10^7 particles. The latter is the critical size for vertical showers, calculated assuming a structure function of the form $r^{-3.1}$, and is in general considerably greater than those calculated for the inclined showers. The errors indicated on the flux values are purely statistical and, as only 190 events of sufficient size were recorded, quite large. Plotted also on this graph is the distribution expected assuming a cosine power law of the form

$$I(\theta) = I(0) \cos^n \theta.$$

where $I(\theta)$ is the intensity from a direction θ . A least squares fit of these curves to the experimental points gives $n = 7.5$ as the best value. The poor statistics, however, allow a considerable deviation from this and $n = 7.5 \pm 1$ is a reasonable estimate. The slight deficiency in the measured flux at small zenith angles may be attributed to the non-cancelling effect of random errors in this region. The actual error varies from $\pm 5^\circ$ for directions near the zenith to $\pm 10^\circ$ for zenith angles greater than 60° .

In section 1.3 it was shown that the shower absorption length, Λ , is approximately related to the value, n , by the expression

$$n \approx \frac{t}{\Lambda} \sec \theta_{av}$$

FIGURE 6.1 The angular distribution of shower intensity for all showers of sizes exceeding $3 \cdot 10^7$ particles. The solid curves are distributions of the form $\cos^n \theta$, where n is the number attached to each curve.

FIGURE 6.2 The equivalent vertical intensity per unit solid angle for showers of sizes exceeding $3 \cdot 10^7$ particles, as a function of atmospheric depth.

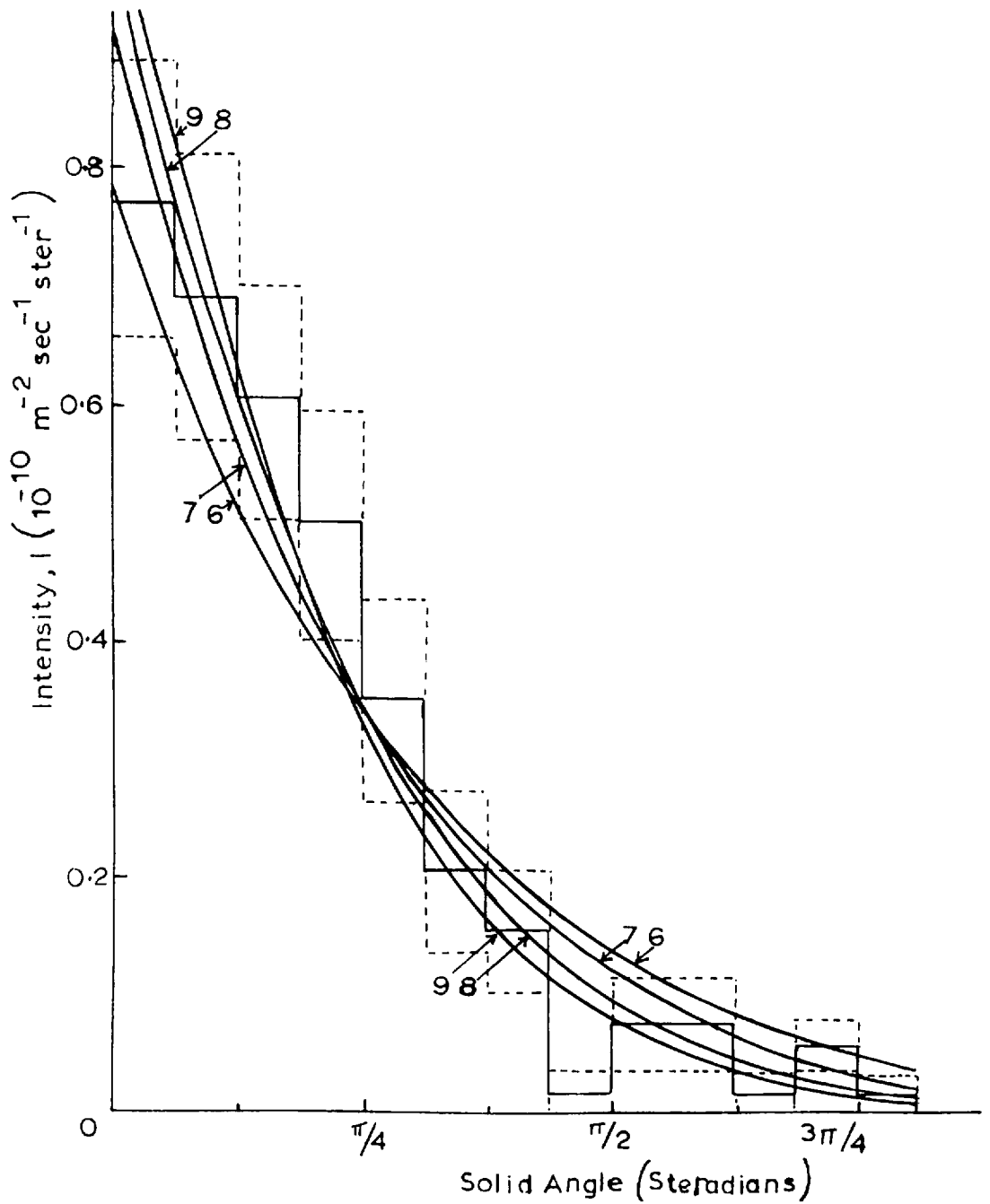


Figure 6.1

Intensity, $I \left(10^{-10} \text{ m}^{-2} \text{ sec}^{-1} \text{ ster}^{-1} \right) \times \text{sec } \theta$ Number of Events

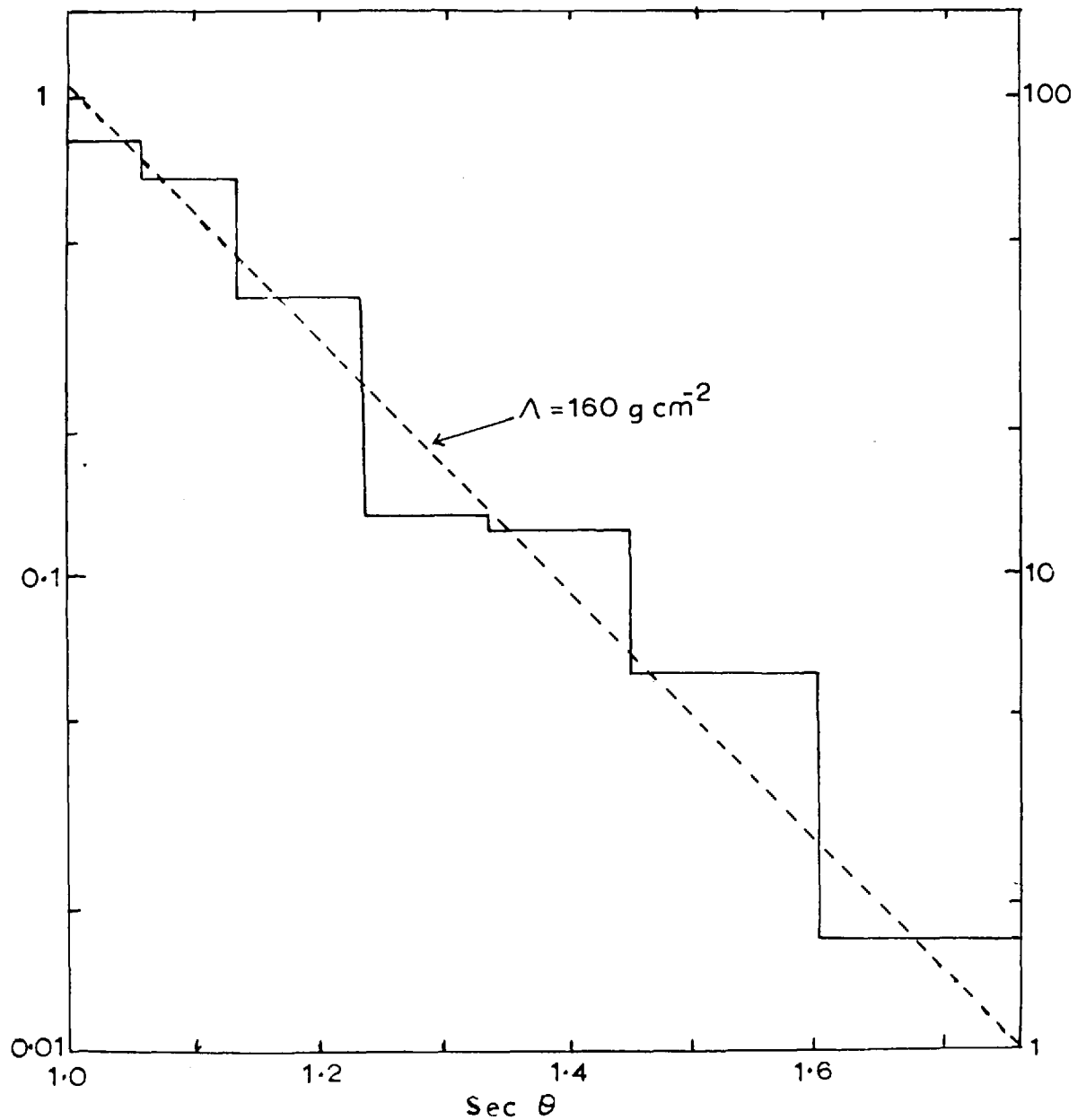


Figure 6.2

where t is the atmospheric depth at the level of observation (1010 g cm^{-2}) and θ_{av} is the average zenith angle (24°). Thus, for $n = 7.5 \pm 1.0$

$$\Lambda \approx 145 \pm 20 \text{ g cm}^{-2}$$

A more direct method of finding the absorption length is to plot the equivalent vertical intensity per unit solid angle ($I(\theta) \sec \theta$) as a function of atmospheric depth (see section 1.3). This has been done in figure 6.2 for depths between 1010 g cm^{-2} and 1800 g cm^{-2} . The straight line corresponds to an exponential absorption with $\Lambda = 160 \pm 25 \text{ g cm}^{-2}$.

It may be concluded that for the average size of shower used in this determination ($6 \cdot 10^7$ particles) the absorption length is about 150 g cm^{-2} . This value is considerably greater than that obtained for smaller showers (about 120 g cm^{-2} for size, $N \sim 10^5$ particles) but agrees with that obtained by the Cornell group (Bennett et al. 1962) for showers of similar size; and is further evidence in support of the suggestion in section 3.1 that the electron-photon component is approaching maximum development at these sizes, so that the absorption is no longer determined by the nuclear-active particles.

6.3 Size Spectrum

Integral shower size spectra for the vertical ($\theta < 30^\circ$) and inclined ($\theta > 30^\circ$) events are plotted separately in figure 6.3. There is no evidence for a change in the exponent with increasing zenith angle and

a value of -2.0 ± 0.3 fits both sets of data. In figure 6.4 the data are combined and compared with the results of other workers. The vertical intensity of showers in this range was calculated from the recorded running time of the array, the collecting area dimensions, and the measured zenith angle distribution ($n = 7.5 \pm 1.0$). The spectrum for the range $2.10^7 < N < 2.10^8$ may be expressed as

$$K (> N) = (2.5 \pm 0.5) \times 10^{-10} \left(\frac{N}{2.10^7} \right)^{-\gamma}$$

where γ is 2.0 ± 0.2

This is seen to be in satisfactory agreement with the summary of EAS data given by Greisen (1960) and with the more recent results of Miura et al. (1962), Delvaille et al. (1962) and Clark et al. (1961).

Both the shower absorption and size spectrum results are in accord with the conclusions of other workers who have used particle counting devices as detector units in large EAS arrays, and thus confirm experimentally the validity of the procedure adopted in the previous chapter to normalise the Cerenkov detector structure functions. Before any examination can be made of possible variation of these parameters with the zenith angle or shower size, much stronger statistical reliability will have to be obtained.

FIGURE 6.3 Integral shower size spectra for vertical ($\theta < 30^\circ$) and inclined ($\theta > 30^\circ$) showers.

FIGURE 6.4 Integral size spectrum of extensive air showers, as observed in the present experiment and by other authors.

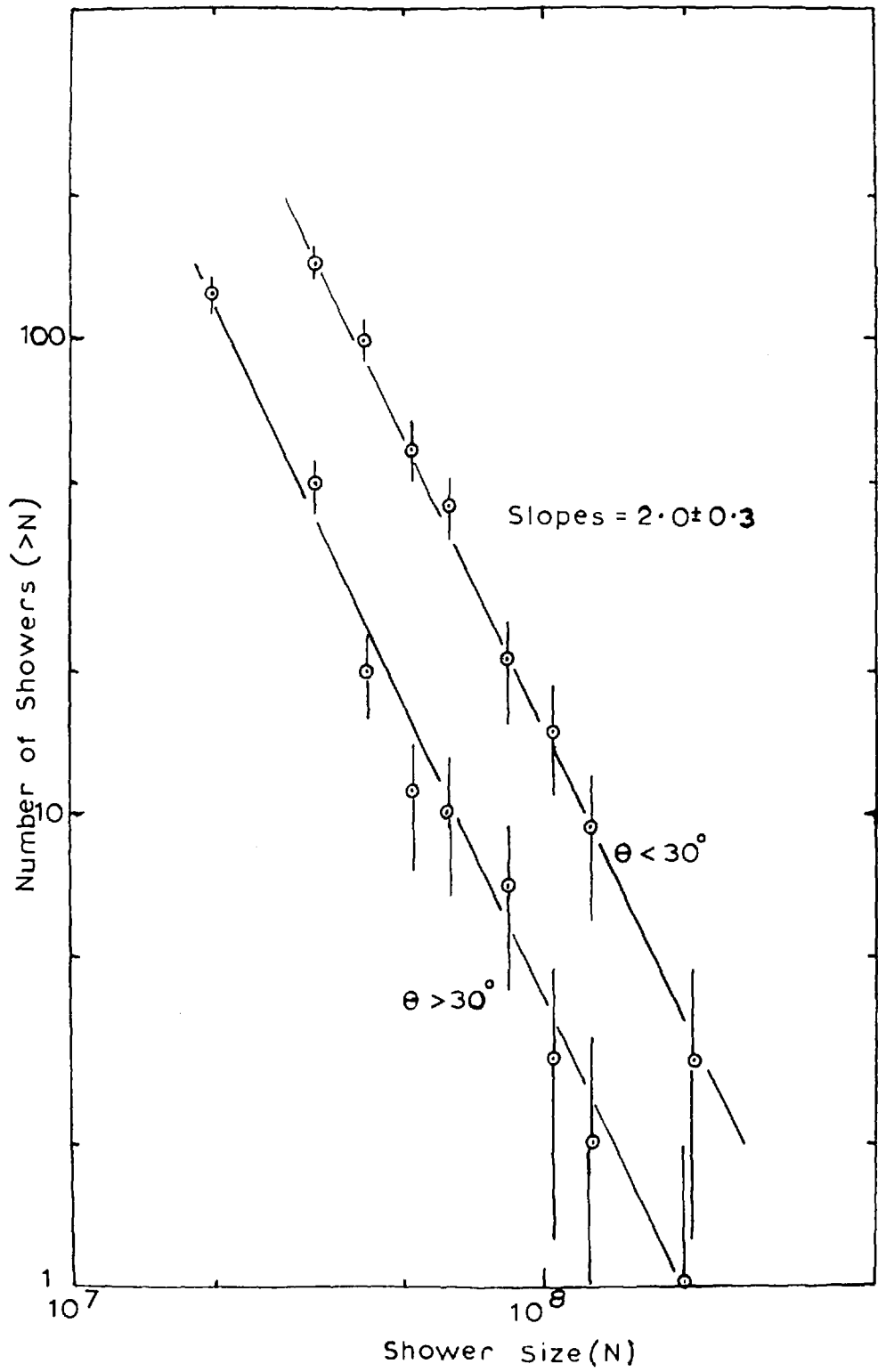


Figure 6.3

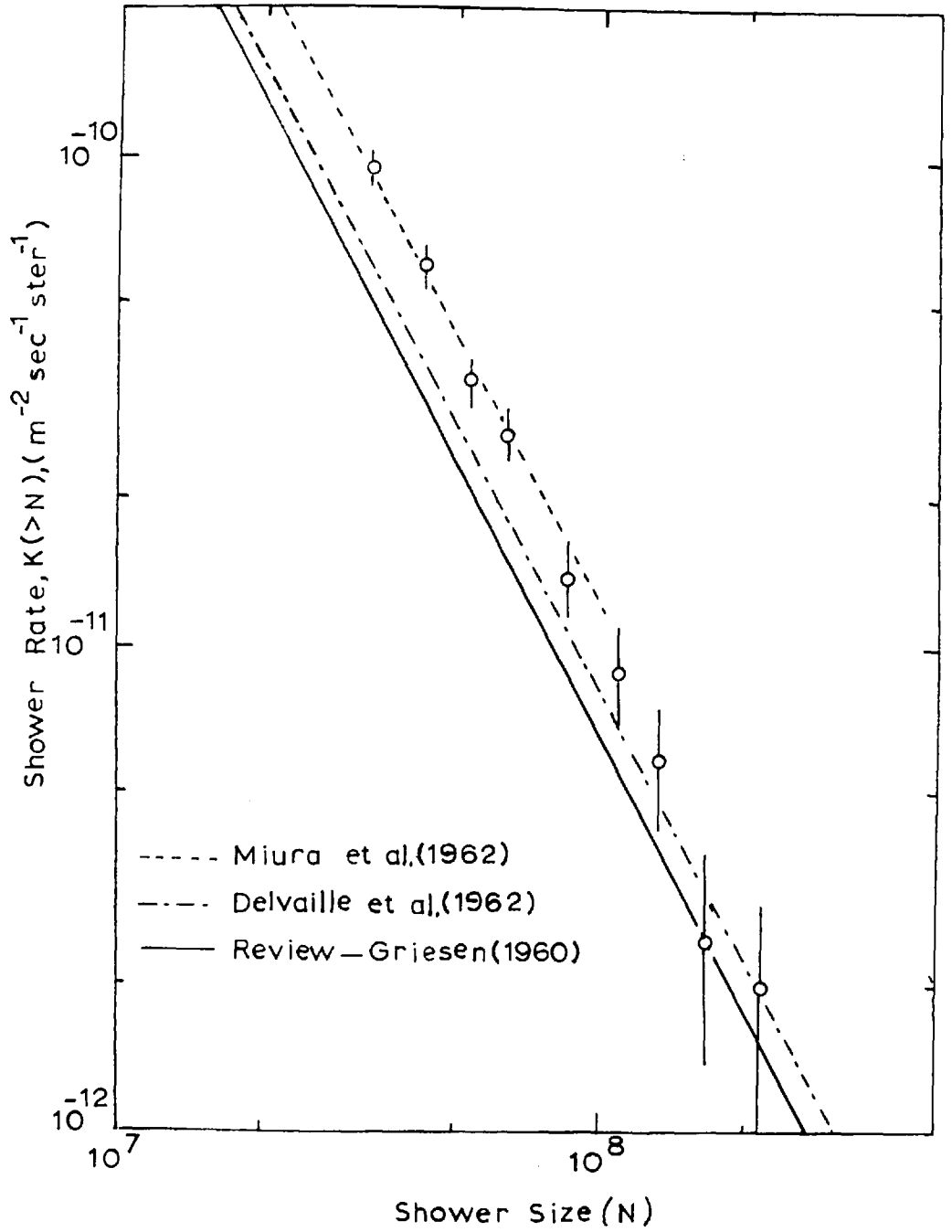


Figure 6.4

6.4 Curvature of the Shower Front

The particles which are detected in an EAS array have travelled out to large radial distances from an origin in the core region of the shower. The electron-photon component is in general the product of cascades which have been laterally dispersed by Coulomb scattering, while a significant portion of the lateral spread of the muons is due to the transverse momentum imparted to them at production. These two components are generated along the entire length of the core and combine to form the shower front. With such an extended source the structure of the front might be expected to be quite complex. If, however, it is assumed that different contributory processes dominate over different regions of the core, then the curvature of the shower front will reflect the approximate height of initiation of these separate processes.

In the present experiment the showers were sampled at the four array stations and the arrival times measured to the first detectable deflection on the time bases of the recording oscilloscopes, - a level which corresponded to the first two or three particles to arrive at the detector. The apparent radius of curvature of each front was calculated using the following relation, which is derived in Appendix 4.

$$\frac{1}{R} = \frac{20 \sum t_i}{25 - 3 \sum t_i^2} \quad (6.1)$$

where R is measured in km and t_i is the relative time of arrival of the shower front at detector i compared with the central detector, measured

in microseconds. The relative times in the above equation were measured accurately to 0.1 microsecond and led to a standard deviation on the individual curvature values of 0.15 km^{-1} .

Histograms of the distributions of the values of the curvature for all showers which fell within the triangular collecting area were first plotted for the three zenith angle intervals, $0^\circ < \theta < 30^\circ$, $30^\circ < \theta < 40^\circ$ and $\theta > 40^\circ$. The difference in the mean values and widths of the distributions for the first two intervals was found to be not significant and in figure 6.5 the data for $\theta < 40^\circ$ is combined into a single distribution. The data for $\theta > 40^\circ$ is shown in figure 6.6. In both figures the efficient showers have been plotted separately as these are free from any bias that might be introduced by selecting showers with a predominantly flat lateral distribution of particles. The average curvature can be seen to be independent of the selection criteria and for the intervals $\theta < 40^\circ$ and $\theta > 40^\circ$ corresponds to radii of 3.4 km and 4.0 km respectively. Plotted also on these graphs is the Gaussian error distribution which would be expected if all shower fronts possessed the mean curvature. It is obvious that this is not the case and the shape of the distributions are best explained if the radius of curvature fluctuates from shower to shower over a range between 1 km and 10 km.

In the above measurements the average distance of the shower axis from the stations for the efficient showers was 250m for the central station and between 510m and 600m for the outer three. In general the array recorded showers at preferred positions close to the central

FIGURE 6.5 Distributions of the values of the curvature of the shower fronts for showers with zenith angles less than 40° .

(a) - 'efficient' showers only

(b) - all showers which fell within the triangular collecting area.

FIGURE 6.6 Distributions of the values of the curvature of the shower fronts.

(a) - zenith angles greater than 40° , - 'efficient' showers only.

(b) - zenith angles greater than 40° , - all showers which fell within the triangular collecting area.

(c) - zenith angles greater than 60° , - all showers which fell within the triangular collecting area.

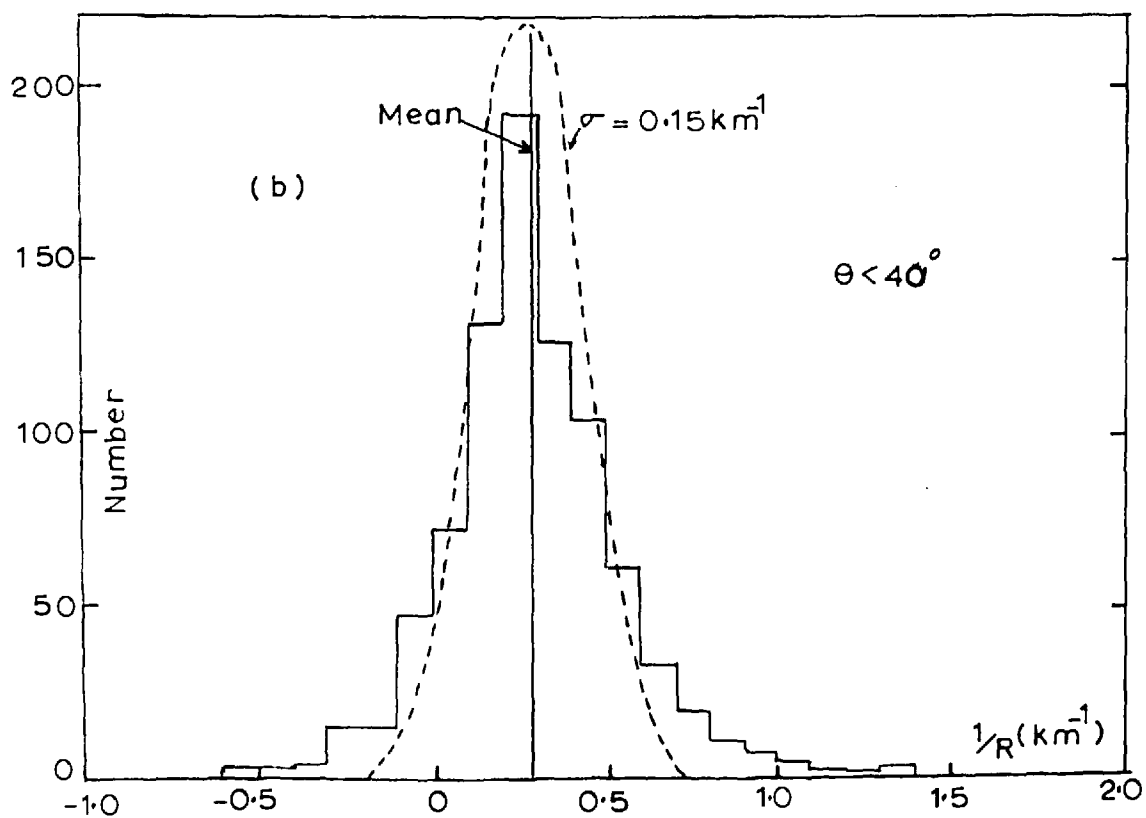
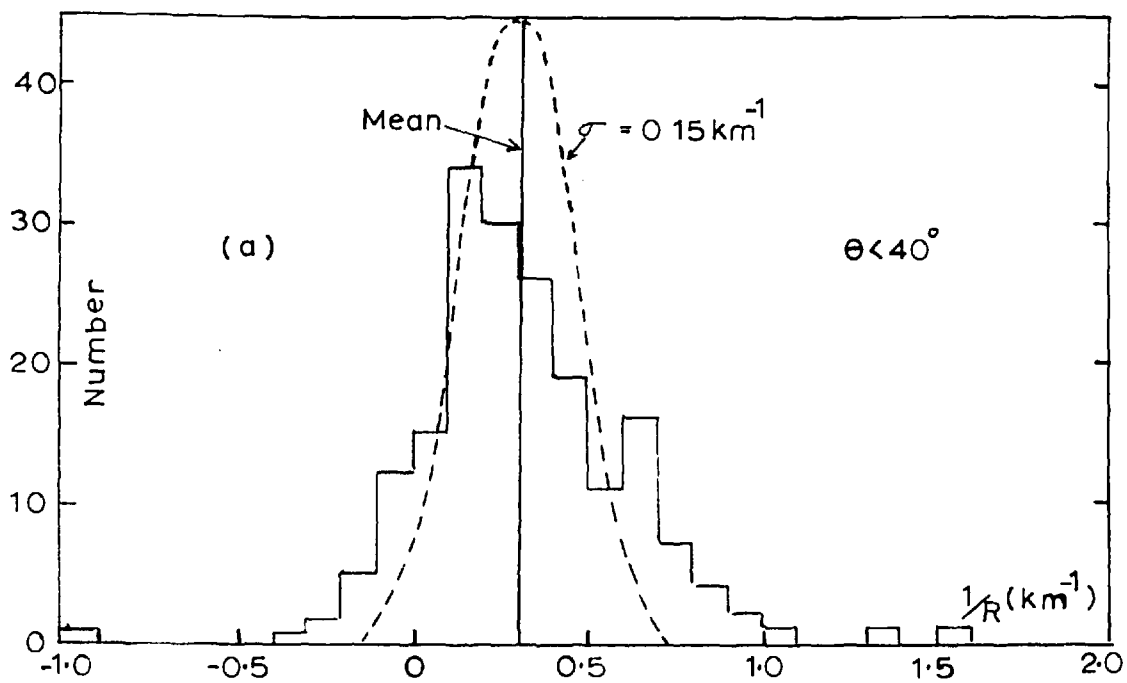


Figure 6.5

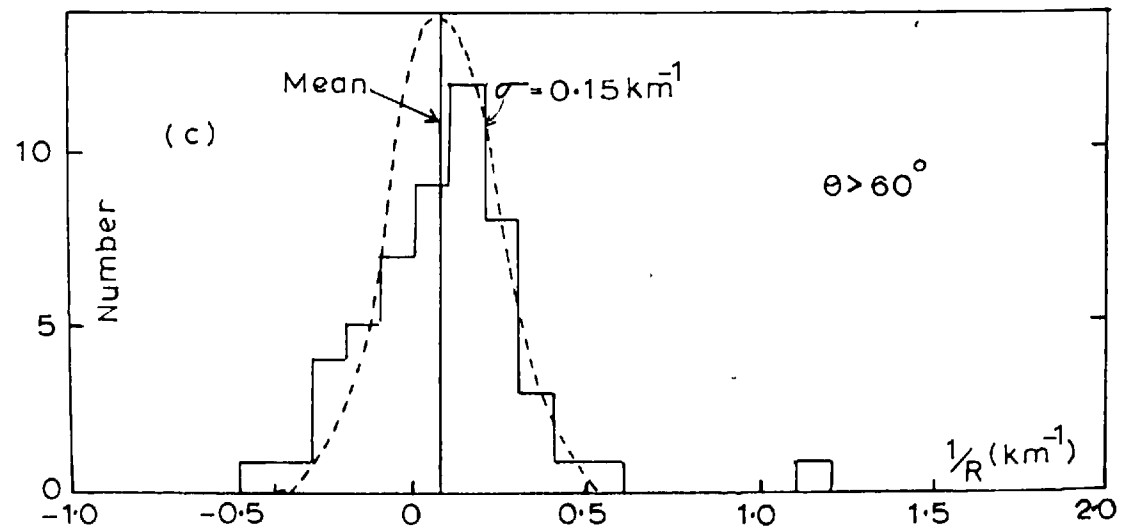
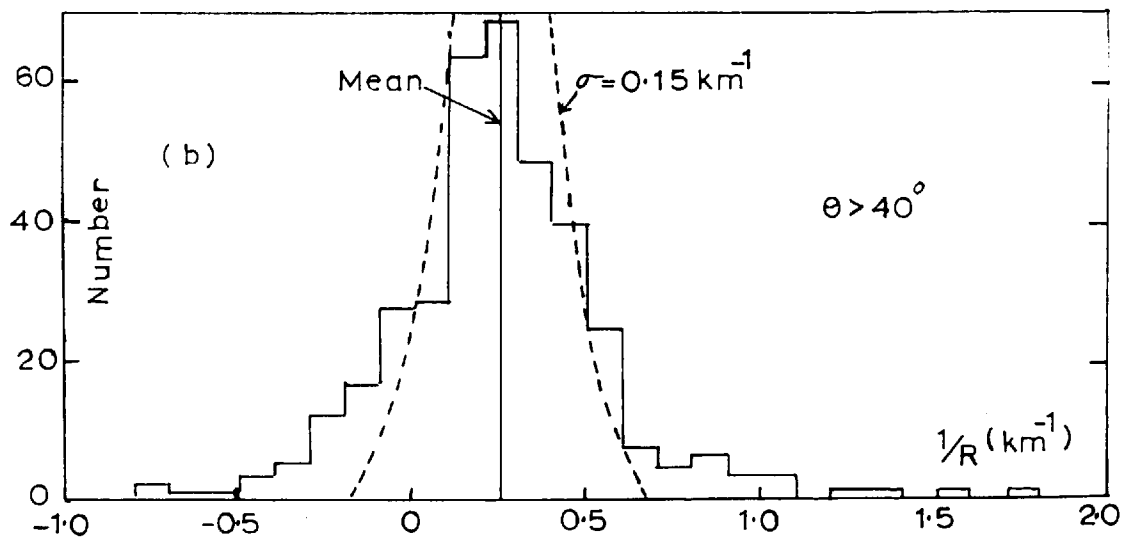
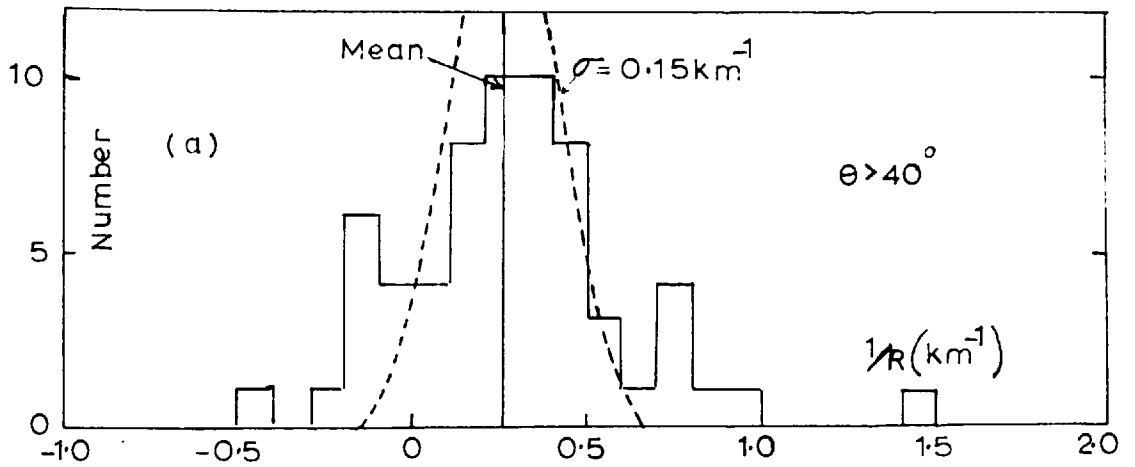


Figure 6.6

station which probably accounts for the slightly narrower distribution obtained for the plot which includes all showers which fell within the triangular collecting area.

During this initial phase of the experiment 53 showers were recorded whose axes were inclined at angles greater than 60° from the zenith (equivalent to a depth of 2 atmospheres) and which also fell within the collecting triangle, although only three of these events were sufficiently large to satisfy the selection criteria for efficient showers. The distribution in curvature of the leading surfaces of all these showers is plotted in figure 6.6(c). It can be seen that the width of the distribution is much less than that for the less inclined showers and corresponds to that expected for a unique radius of curvature of about 11 km.

The shower parameter which has been determined in these measurements has been termed by the M.I.T. group (Linsley and Scarsi 1962b) as the 'extreme front' and is defined by the first detectable particles in the shower. They point out that the ability to measure this quantity will depend on the probability of detecting the leading particles and the results obtained will thus depend on the area of the detectors and the sizes of showers investigated. For showers of sizes exceeding 10^9 particles they found that the radius of curvature of the measured extreme front fluctuated considerably but concluded that its average centre must be located above a depth of 320 g cm^{-2} (a height of about 9 km above sea level), as this is the median source for the muons.

The Cornell group (Bennett et al. 1962) have used an EAS array of similar dimensions and at nearly the same altitude as Haverah Park and have found that the average curvature at large distances from the axis is equivalent to a radius of 2.8 km, in fair agreement with the above figure of 3.4 km for the same quantity. The slight difference may be attributed to the fact that their total detector area was very much less than in the present array (13m^2 as opposed to 135m^2).

It may be concluded that although there is strong evidence to suggest that the first interaction occurs near the top of the atmosphere (above 320 g cm^{-2}) the bulk of the shower particles observed at sea level are initiated at heights below 3 km above the level of observation.

The steeply inclined showers plotted in figure 6.6(c) are probably almost entirely muonic in composition (see section 5.6). If so, the results are consistent with a well defined source at a height of about $11 \cos 60$ km, but the errors here are extremely large.

In addition to measuring the curvature of the extreme surface, the timing data can be used to give information about the structure of the shower front. As the majority of particles which fall within 600m of the shower axis are electrons, the shape of the display pulses would be expected to reflect the character of this component. For showers which fell near the central station ($\sim 200\text{m}$) the pulse rise times were 0.1 microseconds (corresponding to a 30m wide distribution), while

the value at the outer stations fluctuated about an average near 0.3 microsecond (90m wide distribution). Thus, if the median delay of the electrons with respect to the measured extreme front is taken to be half the pulse rise time; the quantity $\sum t_i$ in the expression for the curvature of the shower front (equation 6.1) increases by ~ 0.3 microseconds. This results in an average curvature for the median surface of shower electrons between $(1 \text{ km})^{-1}$ and $(2\text{km})^{-1}$. More work has yet to be done in correlating the rise times of pulses with distance from the shower axis before more detailed conclusions can be drawn. At an altitude of 1800m, the M.I.T. group (Linsley and Scarsi 1962b) have found that the radius of curvature for the electrons varies from about 1 km at 400m from the shower axis to 3km at 1200m.

6.5 Future Programme

The principal task in the coming months is to accumulate shower data in order to reduce the limits of error on the foregoing results and also to study the variation of the shower parameters with increasing shower size and atmospheric depth. An investigation of the variation with depth is very valuable in understanding the development of large showers and permits the testing of models of shower production.

Two quantities which are being measured, but on which are not yet sufficient data to present even preliminary results, are the barometer coefficient and the spatial distribution of arrival directions. Both these measurements began with the installation of the standard clock which

registers the time of arrival, in G.M.T., of each shower recorded.

In section 1.3 it has been shown that the barometer coefficient, B, is approximately related to the absorption length, Λ , by the equation

$$\Lambda \approx \frac{13.6 \text{ sec } \theta_{av}}{B}$$

where B is the fractional change in shower rate with pressure (cm Hg), and θ_{av} is the average zenith angle. Thus with a measured value of $\Lambda \approx 150 \text{ g cm}^{-2}$, the barometer coefficient is expected to be of the order of $10\% (\text{cm Hg})^{-1}$.

Since the installation of the standard clock, 1000 showers have been recorded which fell inside the collecting triangle; of these, about 100 have been larger than 3×10^7 particles. Both groups have been analysed for the distribution in right ascension of their arrival directions, and the results corrected for the 'on-time' of the array. The evidence so far is consistent with an isotropic distribution of primary particles. A full report on the possible anisotropy in the arrival directions of large EAS will be presented by Mr. B.R.Dennis in a succeeding thesis when a much better statistical sample is recorded.

It has been shown in the preceding work (see section 6.4) that, owing to the sensitivity of the detectors to the more energetic muon component, the array is biased towards the detection of relatively small,

muon-rich showers arriving at large zenith angles. This property allows a broader band of declination than is normally available to be observed; and enables the present array to see a comparatively large region of the sky. It may also be utilized in the investigation of the character of large zenith angle showers such as the shape of the shower front which has been described in the previous section. Further work of interest on these steeply inclined showers includes the determination of their structure function, absorption properties and thickness of shower front (obtained from the pulse profile).

It is proposed in the near future to extend considerably the investigations on the muon component of large EAS. It has been noted by Fukui et al. (1960) that, in respect of the primary energy spectrum, the total number of muons, N_{μ} , may be a better parameter to measure than the total number of shower particles, N . This is because after a certain depth the value of N_{μ} remains fairly constant, due to the long attenuation length of the muons, while N decreases fairly rapidly after the level of maximum development. Large fluctuations in the proportion of muons in EAS have been observed by the Tokyo group (Fukui et al. 1960, Hasegawa et al. 1962) which indicate that the size of the shower is strongly influenced by factors other than the primary energy. A large muon detector of area about 10 m^2 is being designed to study this component of EAS and will be situated near the central hut. At present two possibilities are being investigated: a separate, lead shielded, particle counter (Geiger counters or scintillators), or a shielded section of the main array Cerenkov detector.

If the latter possibility is adopted and extended to the outer huts, it would be quite a simple matter to measure the quantities N_{μ} and N simultaneously. Conversely, a large area particle counter, when unshielded, would provide a convenient means of calibrating the detector station (see section 5.7).

In addition to measuring the lateral structure function and proportion of muons in EAS; it is also proposed to measure their energy spectra as a function of distance from the shower axis, and the ratio of positive to negative particles. For this purpose a magnetic spectrograph is to be installed by the Durham group close to the central hut.

It is planned to accomplish the work outlined above while the array is in its present form. This stage will allow a thorough investigation of the shower properties between the sizes of $3 \cdot 10^7$ particles and $3 \cdot 10^8$ particles. If, in subsequent stages, it is intended to investigate thoroughly the shower size spectrum from $N = 3 \cdot 10^7$ particles up to the high energy cut-off; then, to achieve a measure of overlap in shower size, the next stage should be designed to study showers whose sizes exceed 10^8 particles. The design calculations may be performed using the structure function and shower size spectrum obtained earlier (section 5.7 and 6.3). At present, showers of size greater than $3 \cdot 10^7$ particles are recorded at the rate of 2 day^{-1} using a collecting area of 0.32 km^2 . In order to raise this lower size limit to 10^8 particles and still maintain the same recording rate an increase in the collecting area of $(3.3)^4$

is required. If, also, the same array spacing is preserved (500m); then, for the same statistical accuracy, the area of each detector may be reduced by the factor, 3.3. Thus, ideally an array is required which has 5 tanks per station and encloses a collecting area of 3.5 km^2 . A close approximation to this is found in the 'cell' configuration in figure 6.7 which has 12 stations (a total of 60 tanks) and covers an area of 1.9 km^2 (6 triangular cells). This scheme would enable showers of sizes exceeding 10^8 particles to be recorded at the rate of 1 day^{-1} .

Another approach is to maintain the original configuration but increase the array spacing and employ larger detector units. Before this could be done a pilot stage would be necessary to test the structure function (assumed in the following calculations to be of the form r^{-3}) out to distances beyond 1km. A fifth station run in coincidence with the present array at a distance of about 1.5 km from its centre would give the required information. For array spacings of 750 m, 1 km and 1.5 km, the corresponding detector areas become equivalent to the addition of 15 tanks, 36 tanks and 120 tanks respectively, and the collecting triangles become equal to 0.73 km^2 , 1.3 km^2 and 2.9 km^2 .

Now that the initial stage has been shown to operate satisfactorily, the intermediate stage may well be omitted and instead an array constructed to accept showers an order of magnitude larger than at present, and which would be able to extend the observations up to a size of 10^{10} particles. The 12 stations in figure 6.7 are a convenient limit for this type of

FIGURE 6.7 Proposed 'cell' configuration of
detectors.

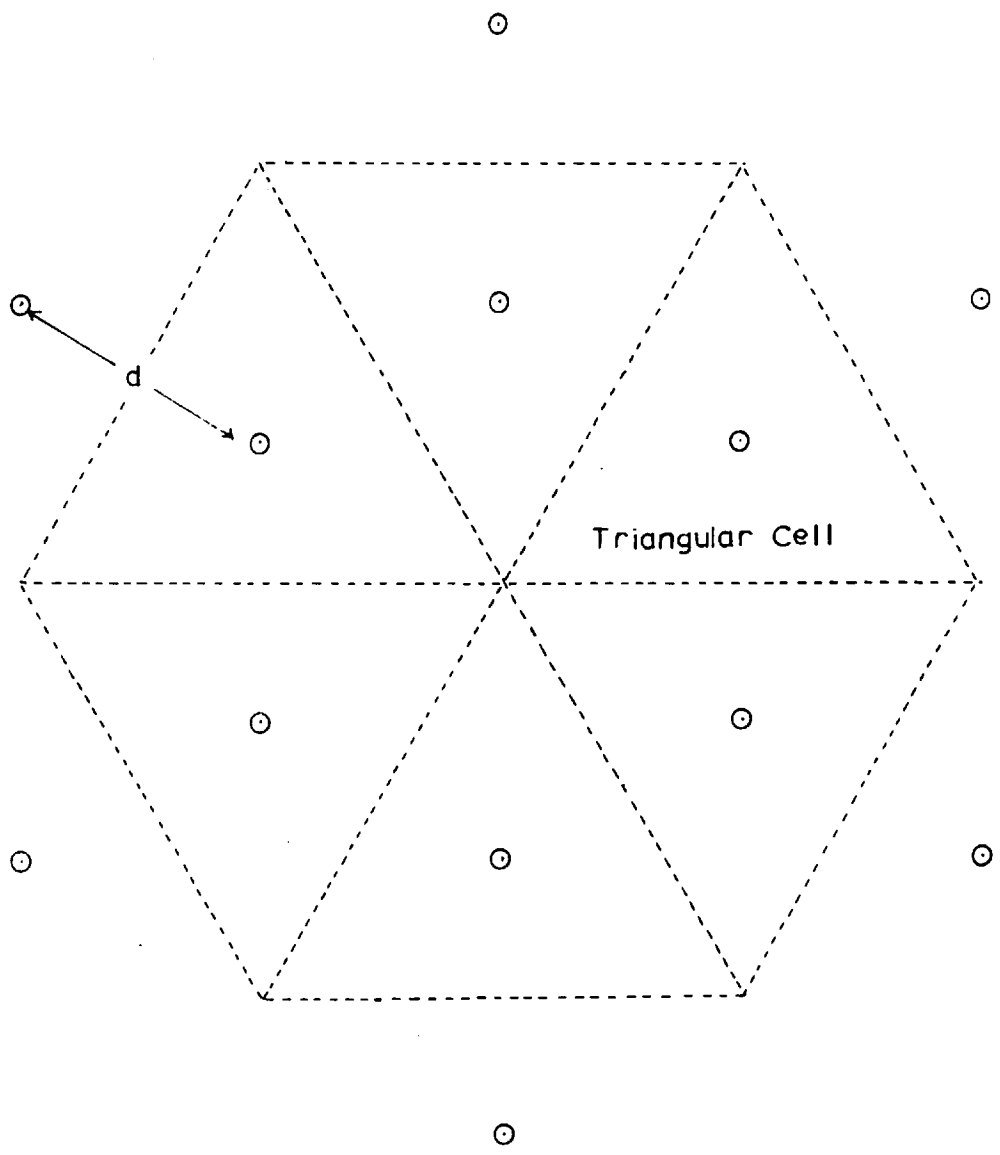


Figure 6.7

cell configuration (the next would require 36 stations forming 24 cells). With this arrangement, array spacings of 1 km, 1.5 km and 2 km correspond to collecting areas of 7.8 km^2 , 17.5 km^2 and 31 km^2 . These would intercept, at the rate of 1 day^{-1} , EAS of size greater than $2 \cdot 10^8$, $3 \cdot 10^8$ and $4 \cdot 10^8$ and would require stations of area equivalent to 10, 45 and 80 tanks respectively. The 31 km^2 array would record EAS of size, $N > 10^{10}$ particles, at about 1 yr^{-1} .

6.6 Conclusion

The present work has shown the feasibility of detecting large EAS with an array of just four water Cerenkov detectors, - the minimum number required to be able to locate the shower axis and determine the shower size. Already several shower characteristics have emerged from the preliminary results, and the array has now been developed to a stage that allows continuous operation, and the gathering of the large amount of statistical data that is required to observe the quantities of astro-physical interest: the shower size spectrum and the celestial distribution of arrival directions.

APPENDIX 1

DETECTOR RESPONSE TO MUON FLUX

Let the vertical intensity of muons through a horizontal area be $I \text{ m}^{-2} \text{ min}^{-1} \text{ ster}^{-1}$ and the zenith angle distribution be of the form $\cos^n \theta$.

(a) Spherical Detector

The single tank detector is represented by a sphere of the same volume. If the sphere has a radius, R , then the total muon count rate, N , is

$$\begin{aligned} N &= \int \pi R^2 I \cos^n \theta \sec \theta d\theta \\ &= \pi R^2 I \int_0^{2\pi} d\phi \int_0^{\pi/2} \cos^{n-1} \theta \sin \theta d\theta \\ &= \frac{2 \pi^2 R^2 I}{n} \end{aligned}$$

The track length, $z(r)$, produced by a muon of sufficient energy to completely traverse the detector is

$$z(r) = 2 \sqrt{R^2 - r^2}$$

where r is the perpendicular distance of the muon trajectory to a

parallel diameter (figure A.1)

$$\begin{aligned} \therefore \text{Rate of tracks } (> z(r)) &= \frac{\pi r^2}{\pi R^2} N \\ &= \frac{2 \pi^2 r^2 I \text{ min}^{-1}}{n} \end{aligned} \quad (\text{A.1.1})$$

(b) Large Flat Detector

The 15-tank detector is represented by an infinite area flat detector of finite thickness. Consider a section of area, A; the rate of muons incident at angles greater than θ° is

$$\begin{aligned} N(>\theta) &= \int_0^{2\pi} d\phi \int_\theta^{2\pi} I A \cos^n \theta \sin \theta d\theta \\ &= 2\pi I A \frac{\cos^{n+1} \theta}{n+1} \end{aligned}$$

The track length produced in the detector by a muon arriving at an angle θ is $t \sec \theta$, where t is the depth of the detector.

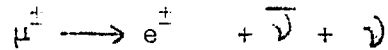
$$\therefore \text{Rate of tracks } (> t \sec \theta) = \frac{2 \pi I A \cos^{n+1} \theta \text{ min}^{-1}}{n+1} \quad (\text{A.1.2})$$

Equations A.1.1. and A.1.2., for $n = 2$, are plotted in figure 4.4 as curve A and curve B respectively.

APPENDIX 2

MUON DECAY

Consider the three-body muon decay



Let m be the mass of the muon and m_e that of the secondary electron. Also let u_e^* and p_e^* be the average total energy and the momentum of the electron in the frame of reference in which the muon is at rest. In the same frame of reference, let θ^* be the angle of emission of the electron measured from the trajectory of the primary muon. In the laboratory system, let u , p and β be the total energy, momentum and velocity of the primary muon; let u_e and p_e be the average total energy and the momentum of the secondary electron. The Lorentz transformation yields

$$u_e = \frac{u_e^* + \beta c p_e^* \cos \theta^*}{\sqrt{1 - \beta^2}}$$

$$= \frac{u}{mc^2} u_e^* + \frac{p}{m} p_e^* \cos \theta^*$$

In the frame of reference of the primary muon, the probability of emission of the secondary electron is the same in all directions. Therefore the average value of $\cos \theta^*$ is zero. Thus

$$u_e = \frac{u_e^*}{mc^2} u_e$$

A number of experimenters have measured the energy spectrum of electrons arising from decay muons (Leighton et al. 1949, Sagane et al. 1951, Bramson and Havens, 1951) and have found that their average energy in the frame of reference of the muon is close to a third of the rest energy of the muon.

$$\text{Thus } u_e = \frac{u}{mc^2} \left(\frac{mc^2}{3} + m_e c^2 \right)$$

If E is the Kinetic energy of the muon in the laboratory system and E_e that of the electron

$$E_e + m_e c^2 = \frac{E + mc^2}{3} \quad (35 + 0.51)$$

Also, if $E \gg mc^2$ (i.e. $E \gg 1 \text{ GeV}$)

$$E_e + 0.51 \approx \frac{E}{3} \quad (35 + 0.51)$$

$$\therefore E_e \approx \frac{E}{3} \quad (\text{A.2.1})$$

Thus, the average kinetic energy of the decay electron is a third of the kinetic energy of the decay muon provided that the latter is considerably greater than the muon rest energy.

APPENDIX 3

Shower Arrival Directions

The information which is obtained directly from the film records is the relative times of arrival, in microseconds, of the shower front at each detector station. When measured with respect to the central station these relative times are denoted by t_2 , t_3 and t_4 , and when with respect to station 2, by T_1 , T_3 and T_4 .

$$\text{Thus } T_3 = t_3 - t_2$$

$$T_4 = t_4 - t_2$$

Consider a shower incident from a direction defined by a zenith angle, θ , and an azimuth angle, ϕ , measured with respect to a line joining stations 1 and 2. If it assumed that the leading particles in the shower lie on a plane front, then, from figure A.2 (a),

$$s_3 = d \sin (\phi + 60)$$

$$s_4 = d \sin (60 - \phi)$$

and from figure A.2 (b),

$$\frac{s_3}{s_4} = \frac{cT_3}{cT_4} = \frac{\sin (\phi + 60)}{\sin (60 - \phi)}$$

$$\therefore \frac{T_3}{T_4} = \frac{\tan \phi + \sqrt{3}}{\sqrt{3} - \tan \phi}$$

$$\therefore \phi = \tan^{-1} \frac{\sqrt{3} (T_3 - T_4)}{(T_3 + T_4)} \quad (\text{A.3.1})$$

From figure A.2 (b)

$$\sin \theta = \frac{cT_3}{\sqrt{3}} = \frac{cT_3}{d \sin (\theta+60)}$$

Substituting in the value for θ , this expression reduces to

$$\sin \theta = \frac{2c}{d\sqrt{3}} (T_3^2 + T_4^2 - T_3 T_4)^{\frac{1}{2}}$$

Now $d = 500 \sqrt{3}m$, thus if the time is measured in microseconds and the velocity in $m \text{ microseconds}^{-1}$

$$\theta = \sin^{-1} \frac{2c}{500.3} (T_3^2 + T_4^2 - T_3 T_4)^{\frac{1}{2}} \quad (\text{A.2.2})$$

FIGURE A.1 Construction for Appendix 1.

FIGURE A.2 Construction for Appendix 3.

FIGURE A.3 Construction for Appendix 4.

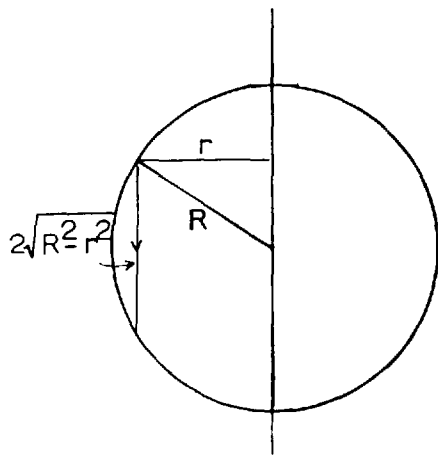


Figure A.1

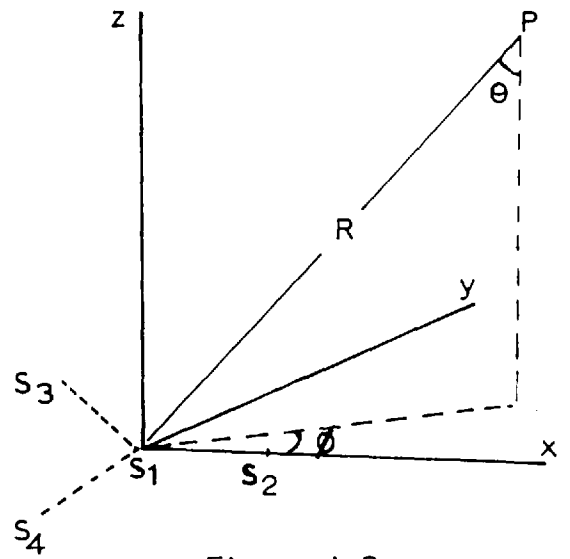


Figure A.3

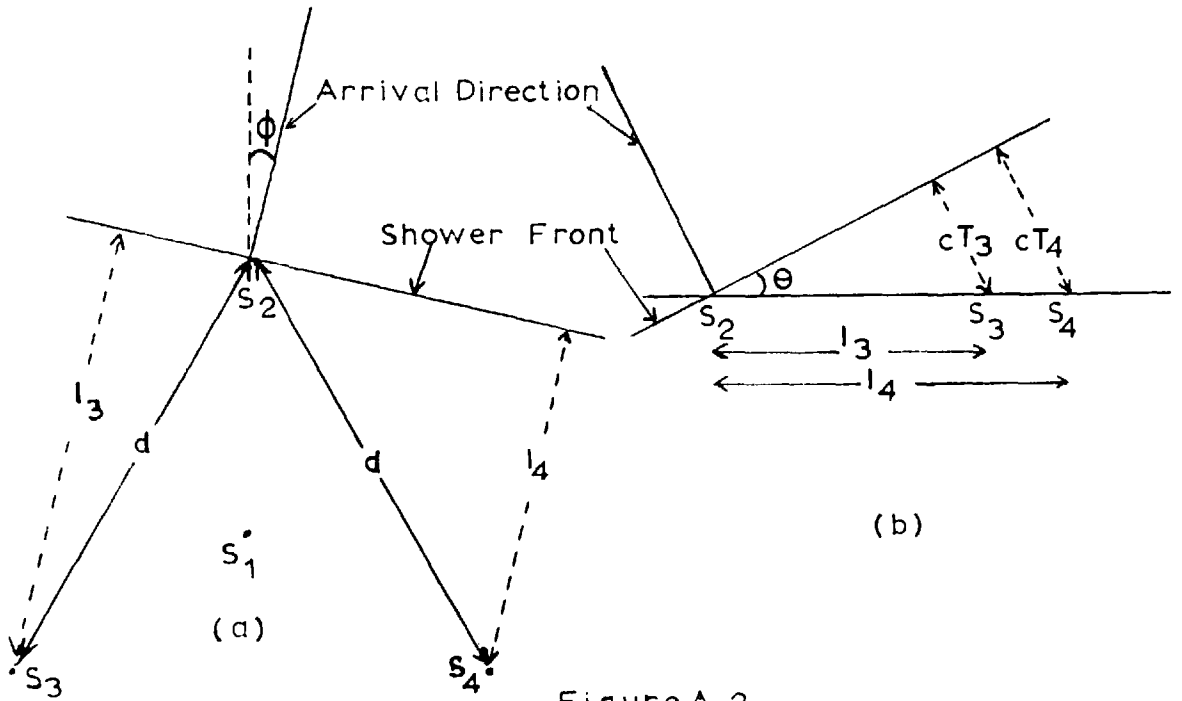


Figure A.2

APPENDIX 4

Curvature of the Shower Front

The radius of curvature of the shower front (assumed to be spherical) is calculated from the measurements of its time of arrival at the four stations of the 500m array. Consider the instant at which the shower front reaches the central detector (figure A.3). If P is the point of origin of the shower particles, then the radius of curvature of the shower surface is simply PS_1 .

Co-ordinates of the stations, and P (in units of 500m)

$$S_1, (0, 0, 0)$$

$$S_2, (1, 0, 0)$$

$$S_3, \left(-\frac{1}{2}, \frac{\sqrt{3}}{2}, 0\right)$$

$$S_4, \left(-\frac{1}{2}, -\frac{\sqrt{3}}{2}, 0\right)$$

$$P, (R \sin \theta \cos \phi, R \sin \theta \sin \phi, R \cos \theta)$$

From which

$$PS_1 = R$$

$$PS_2 = \left[(R \sin \theta \cos \phi - 1)^2 + (R \sin \theta \sin \phi)^2 + (R \cos \theta)^2 \right]^{\frac{1}{2}}$$

$$PS_3 = \left[(R \sin \theta \cos \phi + \frac{1}{2})^2 + (R \sin \theta \sin \phi - \frac{\sqrt{3}}{2})^2 + (R \cos \theta)^2 \right]^{\frac{1}{2}}$$

$$PS_4 = \left[(R \sin \theta \cos \phi + \frac{1}{2})^2 + (R \sin \theta \sin \phi + \frac{\sqrt{3}}{2})^2 + (R \cos \theta)^2 \right]^{\frac{1}{2}}$$

Let $L_i = PS_i - R$

$$\therefore L_i^2 = PS_i^2 - 2RL_i - R^2$$

$$\therefore PS_i^2 = L_i^2 + 2RL_i + R^2$$

Equating the values of PS_i

$$L_2^2 = 1 - 2R (\sin \theta \cos \phi + L_2)$$

$$L_3^2 = 1 + R (\sin \theta \cos \phi - \sqrt{3} \sin \theta \sin \phi - 2L_3)$$

$$L_4^2 = 1 + R (\sin \theta \cos \phi + \sqrt{3} R \sin \theta \sin \phi - 2L_4)$$

$$\begin{aligned} \therefore L_3^2 + L_4^2 &= 2 + 2R (\sin \theta \cos \phi - L_3 - L_4) \\ &= 2 + 1 - L_2^2 - 2R (L_2 + L_3 + L_4) \end{aligned}$$

$$\therefore R = \frac{3 - \sum L_i^2}{2 \sum L_i}$$

$$\text{Now } L_i = ct_i$$

$$\therefore R = \frac{3 - c^2 \sum t_i^2}{2c \sum t_i}$$

where R is measured in 500m units. If R is in km and $C = 3.10^8 \text{ m sec}^{-1}$

$$R = \frac{25 - 3 \sum t_i^2}{20 \sum t_i} \quad (\text{A.4.1})$$

ACKNOWLEDGMENTS

I am indebted to Professor P.M.S.Blackett for the privilege of working in his laboratories, and to Professor H.Elliot for his guidance and unfailing interest in the present work.

I am most grateful to Dr. H.R.Allan for his continued encouragement and advice and for many valuable discussions.

The major part of the experimental work reported was carried out at the Joint Universities Air Shower Project at Haverah Park, Yorkshire; and I am grateful to Professor E.C.Stoner and Professor J.G.Wilson for the facilities generously made available in the Physics Department at Leeds University. I also wish to express my thanks to all the members of the Haverah Park group for their co-operation in the running of the equipment and the analysis of the results.

I am grateful to Dr. R.D.Wills for his assistance in the analysis of the 6-metre array results, and to Mr. G.M.Cescotti for the design of much of the electronic equipment.

Finally my thanks are due to the Department of Scientific and Industrial Research for the provision of a maintenance grant during the course of the experiment.

REFERENCES

- ABROSIMOV, A.T., BASILEVSKAYA, G.A., SOLOVIEVA, V.I., and KRISTIANSEN, G.B., 1960, Zh.Eksp.Teor.Fiz., 38, 100 (Soviet Phys., JETP, 11, 74).
- ALICHINIAN, A., ASATIANI, T., and MUSKHELISHVILLI, G., 1947, Journ.Phys. USSR, 11, 16.
- ALLAN, H.R., BEAMISH, R.F., BRYANT, D.A., KASHA, H., and WILLS, R.D., 1960, Proc.Phys.Soc., 76, 1.
- ALLAN, H.R., BEAMISH, R.F., GLENCROSS, W.M., THOMSON, D.M., and WILLS, R.D., 1962, Proc.Phys.Soc., 79, 1170.
- AUGER, P., MAZE, R., and GRIVET-MAYER, T., 1938, C.R.Acad.Sci., Paris, 206, 1721.
- AZIMOV, S.A., ABDULLAEV, A.M., MJALKOVSKI, V.M., and JULDASBAEV, T.S., 1962, J.Phys.Soc. Japan, 17, Suppl. A3, 394.
- BARADZEI, L.T., RUBSTOV, V.I., SMORODIN, Y.A., SOLOVYOV, M.V., and TOLKACHEV, B.V., 1962, J.Phys.Soc. Japan, 17 Suppl.A3, 433.
- BARKER, P., 1955, Phys.Rev., 100, 867.
- BASSI, P., CLARK, G., and ROSSI, B.B., 1953, Phys. Rev., 92, 441.
- BEAMISH, R.F.W., 1959, Ph.D. Thesis, University of London.
- BENNETT, S., DELVILLE, J., GREISEN K., and KENDZIORSKI, F., 1962, J.Phys.Soc. Japan, A3, 17, 196.
- BHABHA, H.J., 1938, Proc.Roy.Soc., A 164, 257.
- BRAMSON, H., and HAVENS, W.W., 1951, Phys.Rev., 83, 861.
- BRENNAN, M.H., MILLAR, D.D., and WALLACE, C.S., 1958, Nature, 182, 905.
- BRYANT, D.A., 1958, Ph.D. Thesis, University of London.
- BRYANT, D.A., 1958a, Haverah Park EAS Experiment Report.
- BUTCHER, J.C., and MESSEL, H., 1960, Nuclear Physics, 20, 15.
- CHATTERJEE, B.K., MURTHY, G.T., NARANAN, S., SREEKANTAN, B.V., and SRINIVASA RAO, M.V., 1960, Nuovo Cimento, 18, 1148.

- CHATTERJEE, B.K., MURTHY, G.T., NARANAN, S., RANGA SWAMY, T.N.,
SREEKANTAN, B.V., and SRINIVASA RAO, M.V., 1962,
J.Phys.Soc.Japan, 17, Suppl. A3, 247.
- CHUDAKOV, A.E., NESTEROVA, N.M., ZATSEPIN, V.I., and TUKISH, E.I., 1960,
Proc.Moscow Cosmic-Ray Conf. (IUPAP), 2, 50.
- CLARK, G.W., EARL, J., KRAUSHAAR, W.L., LINSLEY, J., ROSSI, B.B., and
SCHERB, F., 1957, Nature, 180, 353.
- CLARK, G.W., EARL, J., KRAUSHAAR, W.L., LINSLEY, J., ROSSI, B.B., and
SCHERB, F., 1958, Suppl. Nuovo Cimento, 8, 623.
- CLARK, G.W., EARL, J., KRAUSHAAR, W.L., LINSLEY, J., ROSSI, B.B.,
SCHERB, F., and SCOTT, D.W., 1961, Phys.Rev.,
122, 637.
- COCCONI, G., 1949, Rev.Mod.Phys., 21, 26.
- COCCONI, G., 1961, Handbuch der Physik, XLVI, 215.
- COCCONI, G., and TONGIORGIO, V.E., 1949, Phys.Rev., 79, 730.
- CRANSHAW, T.E., GALBRAITH, W., PORTER, N., de BEER, J., and HILLAS, A.M.,
1958, Nuovo Cimento, 8, Suppl. 2, 567.
- CRANSHAW, T.E., and HILLAS, A.M., 1960, Proc.Moscow Cosmic-Ray Conf.
(IUPAP), 2, 210.
- DEDENKO, L.G., 1961, Zh. Eksp. Teor. Fiz., 40, 630, (Soviet Phys. JETP,
13, 439).
- DELVAILLE, J., KENDZIORSKI, F., AND GREISEN, K., 1960a, Proc.Moscow Cosmic-Ray
Conf. (IUPAP), 2, 79.
- DELVAILLE, J., KENDZIORSKI, F., and GREISEN, K., 1960, Proc.Moscow Cosmic-
Ray Conf. (IUPAP), 2, 101.
- DELVAILLE, J., KENDZIORSKI, F., and GREISEN, K., 1962, J.Phys.Soc.Japan, 17,
Suppl. A3, 76.
- DMITRIEV, V.A., KULIKOV, G.V., MASSALSKII, E.I., and KHRISTIANSEN, G.B.,
1959, Zh. Eksp. Teor. Fiz., 36, 992 (Soviet Phys.,
JETP, 9, 702).
- DOBROVOLSKI, S.P., NIKOLSKIJ, S.I., TUKISH, I.I., and IAKOVLIEV, V.I., 1956,
Zh.Eksp.Teor.Fiz., 31, 939.
- EIDUS, L.K., ADAMOVICH, M.L., IVANOVSKAYA, I.A., NIKOLAEV, V.S., and
TULYANKINA, M.S., 1952, Zh. Eksp. Teor. Fiz., 22, 440.

- FUJIOKA, G., 1953, Int. Conf. Theor. Phys., Japan.
- FUKUDA, H., OGITA, N., and UEDA, A., 1959, Progr. Theor. Phys., 21, 29.
- FUKUI, S., HASEGAWA, H., MATANO, T., MIURA, I., ODA, M., SUGA, K., TANAHASHI, G., and TANAKA, Y., 1960, Suppl. Progr. Theor. Phys., 16, 1.
- GALBRAITH, W., 1958, Extensive Air Showers; Butterworths Scientific Publications, London.
- GLENCROSS, W. M., 1962, Ph.D. Thesis, University of London.
- GREEN, J. R., and BARCUS, J. R., 1959, Nuovo Cimento, 14, 1356.
- GREEN, J. R., and BARCUS, J. R., 1962, Nuovo Cimento, 23, 708.
- GREISEN, K., 1956, Progress in Cosmic Ray Physics (Ed. J. G. Wilson), 3, Chapter 1, North Holland Publishing Co., Amsterdam.
- GREISEN, K., 1960, Ann. Rev. Nucl. Sci., 10, 63.
- GREISEN, K., DELVAILLE, J., and KENDZIORSKI, F., 1960, Proc. Moscow Cosmic-Ray Conf. (IUPAP), 2, 174.
- GRIGOROV, N. L., and SHESTOPEROV, V. Y., 1958, Zh. Eksp. Teor. Fiz., 34, 1539 (Soviet Phys. JETP, 7, 1061).
- GORJUNOV, N. N., DEDEENKO, L. G., and ZATSEPIN, G. T., 1962, J. Phys. Soc. Japan, 17, Suppl. A3, 103.
- GUSEVA, V. V., DOBROTIN, N. A., ZELEVINSKAYA, N. G., KOTELNIKOV, K. A., LEBEDEV, A. M. and SLAVOTINSKY, S. A., 1962, J. Phys. Soc. Japan, 17, Suppl. A3, 375.
- HASEGAWA, H., MATANO, T., MIURA, I., ODA, M., SHIBATA, S., TANAHASHI, G., and TANAKA, Y., 1962, J. Phys. Soc. Japan, 17, Suppl. A3, 86.
- HASEGAWA, H., NARANAN, S., MATANO, T., MIURA, I., ODA, M., SHIBATA, S., TANAHASHI, G., and TANAKA, Y., 1962, J. Phys. Soc. Japan, 17, Suppl. A3, 189.
- HERSIL, J., ESCOBAR, I., SCOTT, D., CLARK, G., and OLBERT, S., 1961, Phys. Rev. Letters, 6, 22.
- HERSIL, J., ESCOBAR, I., CLARK, G., OLBERT, S., MOORE, C., and SCOTT, D., 1962, J. Phys. Soc. Japan, 17, Suppl. A3, 243.
- IVANOVSKAYA, I. A., KULIKOV, G. V., RAKOBOL'SKAYA, I. V., and SARYCHEVA, L. I., 1957, Zh. Eksp. Teor. Fiz., 33, 358 (1958, Soviet Phys. JETP, 6, 276).

- JELLEY, J.V., 1958, Cerenkov Radiation and its Applications, London: Pergamon Press.
- JELLEY, J.V., and WHITEHOUSE, W.J., 1953, Proc. Phys. Soc., A 66, 454.
- KAMATA, K., and NISHIMURA, J., 1958, Progr. Theor. Phys. Suppl. 6, 93.
- KAMEDA, T., 1960, J. Phys. Soc. Japan, 15, 1175.
- KAMEDA, T., and MAEDA, T., 1960, J. Phys. Soc. Japan, 15, 1367.
- KAMEDA, T., TOYODA, Y., and MAEDA, T., 1962, J. Phys. Soc. Japan, 17, Suppl. A3, 270.
- KAPLON, M.F., RITSON, D.M., and WOODRUFF, E.P., 1952, Phys. Rev., 85, 933.
- KHRISTIANSEN, G.B., 1958, Nuovo Cimento, Suppl., 8, 598.
- KOLHÖRSTER, W., MATTERS, I., and WEBER, E., 1938, Naturwissenschaften, 26, 576.
- KRAUSHAAR, W.L., 1957, Nuovo Cimento, Suppl., 8, 631.
- LAL, D., 1953, Proc. Ind. Acad. Sci., A 37, 93.
- LAL, S., PAL, Y., and RAGHAVAN, R., 1962, J. Phys. Soc. Japan, 17, Suppl. A3, 393.
- LEIGHTON, R.B., ANDERSON, C.D., and SERIFF, A.J., 1949, Phys. Rev., 75, 1432.
- LILLICRAP, S.C., WILLS, R.D., and TURVER, K.E., 1963, Proc. Phys. Soc., 82, 95.
- LINSLEY, J., 1962, Phys. Rev. Letters, 9, 126.
- LINSLEY, J., 1963, Phys. Rev. Letters, 10, 146.
- LINSLEY, J., and SCARSI, L., 1962a, Phys. Rev. Letters, 9, 123.
- LINSLEY, J., and SCARSI, L., 1962b, Phys. Rev., 128, 2384.
- LINSLEY, J., SCARSI, L., and ROSSI, B.B., 1962, J. Phys. Soc. Japan, 17, Suppl. A3, 91.
- LINSLEY, J., SCARSI, L., ECCLES, P.J., and ROSSI, B.B., 1962, Phys. Rev. Letters, 8, 286.
- MANDÓ, M., 1954, Nuovo Cimento, 12, 1.

- MASSEY, H. J., and CORBEN, H. C., 1939, Proc. Camb. Phil. Soc., 35, 463.
- MIURA, I., and HASEGAWA, H., 1962, J. Phys. Soc. Japan, 17, Suppl. A3, 84.
- MIYAKE, S., 1958, Progr. Theor. Phys., 20, 844.
- MIYAKE, S., HINOTANI, K., KATSUMATA, I., KANEKO, T., and ITO, N., 1962, J. Phys. Soc. Japan, 17, Suppl. A3, 240.
- NISHIMURA, J., and KAMATA, K., 1950, Progr. Theor. Phys., 5, 899.
- NISHIMURA, J., and KAMATA, K., 1951, Progr. Theor. Phys., 6, 262, 628.
- NISHIMURA, J., and KAMATA, K., 1952, Progr. Theor. Phys., 7, 185.
- PALMATIER, E. D., 1952, Phys. Rev., 88, 761.
- PERKINS, D. H., 1960, Progress in Cosmic Ray Physics (Ed. J. G. Wilson), 5, Chapter 4; North Holland Publishing Co., Amsterdam.
- PORTER, N. A., CRANSHAW, T. E., de BEER, J. F., PARHAM, A. G., and SHERWOOD, A. C., 1958, Phil. Mag., 3, 826.
- ROSSI, B. B., 1960, Proc. Moscow Cosmic-Ray Conf. (IUPAP), 2, 18.
- ROSSI, B. B., 1952, High Energy Particles, Prentice Hall Inc., New York.
- ROSSI, B. B., and GREISEN, K., 1941, Rev. Mod. Phys., 13, 240.
- SAGANE, R., GARDNER, W. L., and HUCEPAED, H. W., 1951, Phys. Rev., 82, 557.
- SCHMEISER, K., and BOTHE, W., 1938, Ann. Phys. Lpz., 32, 161.
- SUGARMAN, R., and de BENEDETTI, S., 1956, Phys. Rev., 102, 857.
- TANAKA, Y., 1961, J. Phys. Soc. Japan, 16, 866.
- TOYODA, Y., 1962, J. Phys. Soc. Japan, 17, 415.
- TUKISH, E. I., and NIKOLSKIJ, S. I., 1962, J. Phys. Soc. Japan, 17, Suppl. A3, 206.
- UEDA, A., 1960, Progr. Theor. Phys. 24, 1231.
- VERNOV, S. N., DMITRIEV, V. A., SOLOVIEVA, V. I., and KRISTIANSEN, G. B., 1959, Zh. Eksp. Teor. Fiz., 37, 1481 (1960, Soviet Phys., JETP, 10, 1050).
- VISWANATHAN, S. P., MACE, R., and PALMATIER, E. D., 1963, Nuovo Cimento, 28, 850.
- WEI, J., and MONTGOMERY, G. C., 1949, Phys. Rev., 76, 1488.

WILLS,R.D, 1961, Ph.D. Thesis, University of London.

ZATSEPIN,G.T., 1960, Proc.Moscow Cosmic-Ray Conf. (IUPAP), 2, 192.